

KADIR HAS UNIVERSITY  
GRADUATE SCHOOL OF SCIENCE AND ENGINEERING



CLASSIFICATION OF DISTINCT CONFORMERS OF BETA-2  
ADRENERGIC RECEPTOR BASED ON BINDING AFFINITY OF  
LIGANDS THROUGH DOCKING STUDIES

GRADUATE THESIS

GONCA DİLCAN

May, 2017

Gonca Dilcan

M.S. Thesis

2017

CLASSIFICATION OF DISTINCT CONFORMERS OF BETA-2  
ADRENERGIC RECEPTOR BASED ON BINDING AFFINITY OF  
LIGANDS THROUGH DOCKING STUDIES

GONCA DİLCAN

Submitted to the Graduate School of Science and Engineering  
in partial fulfillment of the requirements for the degree of  
Master of Science in  
COMPUTATIONAL BIOLOGY AND BIOINFORMATICS

KADIR HAS UNIVERSITY

May, 2017

KADIR HAS UNIVERSITY  
GRADUATE SCHOOL OF SCIENCE AND ENGINEERING

CLASSIFICATION OF DISTINCT CONFORMERS OF BETA-2  
ADRENERGIC RECEPTOR BASED ON BINDING AFFINITY OF  
LIGANDS THROUGH DOCKING STUDIES

GONCA DİLCAN

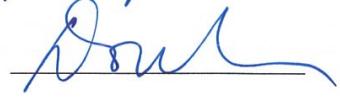
APPROVED BY:

Assoc. Prof. Dr. E. Demet Akten

(Thesis Supervisor)

Prof. Dr. Kemal Yelekçi

Prof. Dr. Pemra Doruker



APPROVAL DATE: 01/06/2017



“I, Gonca Dilcan, confirm that the work presented in this thesis is my own.  
Where information has been derived from other sources, I confirm that this  
has been indicated in the thesis.”



---

GONCA DILCAN

## CLASSIFICATION OF DISTINCT CONFORMERS OF BETA-2 ADRENERGIC RECEPTOR BASED ON BINDING AFFINITY OF LIGANDS THROUGH DOCKING STUDIES

### **Abstract**

$\beta_2$ AR is an important drug target and plays a critical role in the relaxation of pulmonary tissues and cardiovascular physiology. We have developed a strategy for classifying various  $\beta_2$ AR conformers as active or inactive states, based on binding mode of selected ligands with known activities. Previously, distinct conformational states of the ligand's binding pocket were obtained from a 2.8  $\mu$ s MD simulation. Snapshots were clustered based on RMSD value of five key residues at the binding site. Clustering analysis yielded a total of 13 distinct conformers to which five agonists, four inverse agonists, and four antagonists were docked separately, using seven different scoring functions. Best ligand poses with the highest score value were selected and evaluated based on their vicinity to five key residues. Poses that were not in this neighborhood were discarded and remaining ones were sorted based on their score. Before treating MD conformers, this classification scheme was applied first to both active/inactive state crystal structures for critical assessment. MD conformers found in top five in all scoring functions were selected and assigned to be either active or inactive. Finally, selected MD conformers were used to screen a small database to further investigate their discriminatory power. As a result, MD conformers performed more selective screening than inactive state crystal structure for antagonists/inverse agonists. Generating alternative conformations of the receptor and classifying them as active or inactive is an important practice in the drug design studies that were often limited to one snapshot obtained from X-ray studies.

## BETA-2 ADRENERJİK RESEPTÖRÜNÜN FARKLI KONFORMASYONLARININ DOCKİNG ÇALIŞMALARI İLE TEŞHİS EDİLMESİ

### Özet

$\beta_2$ AR reseptörü, akciğerlerin rahatlamasında ve kardiyovasküler fizyolojide rol oynamasıyla önemli bir ilaç hedefidir. Bu çalışmada, çeşitli  $\beta_2$ AR konformasyonlarını aktif veya inaktif olarak sınıflandırmak amacıyla, aktivitesi bilinen ligantlar seçilerek onların bağlanma şekillerine göre bir sınıflandırma stratejisi oluşturulmuştur. Önceki bir çalışmada gerçekleştirilen, reseptörün inaktif halinin 2.8  $\mu$ s'lik MD simülasyonunda, ligandın bağlanma bölgesinin farklı konformasyonları elde edilmiştir. Snapshotlar derlenerek bağlanma bölgesindeki beş anahtar rezidünün RMSD değerlerine göre gruplandırılmıştır. Toplamda 13 farklı konformasyon elde edilmiş ve 5 agonist, 4 ters agonist ve 4 antagonist molekülü her bir konformasyona ayrı ayrı ve 7 farklı skor fonksiyonu kullanılarak dock edilmiştir. En iyi yerleşen konformasyonlar bağlanma bölgesindeki anahtar rezidüleriyle olan yakınlığına göre seçilmiş ve hesaplanmıştır. Anahtar bölgeye yaklaşamayanlar elenmiş, kalanlar ise skor değerlerine göre sıralanmıştır. Bu sınıflandırma, kritik değerlendirme yapabilmek için MD konformasyonlarından önce aktivitesi bilinen aktif/inaktif kristal yapılara uygulanmıştır. Her skor fonksiyonu tarafından seçilen ve ilk 5'te bulunan MD konformasyonları aktif ve inaktif olarak sınıflandırılmıştır. Son olarak, MD konformasyonlarının ayırt ediciliğini analiz edebilmek için, seçilen bu konformasyonlar ile küçük bir dataset kullanılarak sanal tarama yapılmıştır. MD konformasyonlarının inaktif kristal yapıya göre antagonist/ters agonistler için daha seçici olduğu gözlemlenmiştir. Reseptörün alternatif konformasyonlarını üretmek ve onları sınıflandırmak, genellikle tek bir snapshot X-ray örneği ile sınırlandırılmış ilaç tasarımı çalışmalarında önemli rol oynamaktadır.

## **Acknowledgements**

I would like to present my intimate thanks to my thesis advisor Assoc. Prof. Demet Akten who helped me throughout this work in all possible ways. I am very grateful to have the opportunity to work with her, it was intellectually rewarding and fulfilling.

I also want to mention my gratitude for graduate scholarship ensured by TÜBİTAK for my M.S. studies via the project number 213M544.

I would like to thank to my family for their trust in me and support all the time. Lastly, I want to thank to my friends Yiğit Durdağ, Teodora Djikic, Erdi Durmuş, Abdullahi İbrahim Uba and Deniz Hız for their support and believing in my work throughout my thesis. This thesis is dedicated to them.

## Table of Contents

<b>Abstract</b>	<b>i</b>
<b>Özet</b>	<b>ii</b>
<b>Acknowledgements</b>	<b>iii</b>
<b>List of Tables</b>	<b>vi</b>
<b>List of Figures</b>	<b>vii</b>
<b>List of Abbreviations</b>	<b>x</b>
<b>1 Introduction</b>	<b>1</b>
<b>2 Human Beta-2-Adrenergic Receptor: Structure, Function and Dynamics</b>	<b>4</b>
2.1 G-Protein Coupled Receptors.....	4
2.2 X-ray Crystal Structures of $\beta_2$ AR.....	7
2.3 Interactions and Signaling Pathways in $\beta_2$ AR.....	8
2.4 Structural Dynamics of $\beta_2$ AR.....	13
<b>3 Materials and Methods</b>	<b>17</b>
3.1 Generation of the Target Conformers.....	17
3.2 Scoring Functions and Docking Studies.....	21
3.2.1 AutoDock.....	22
3.2.2 GOLD.....	24
3.2.3 DSX.....	26
3.2.4 GLIDE.....	27
3.3 Docking-Based Virtual Screening.....	28
3.4 Receiver Operating Characteristic (ROC) Curves.....	29
<b>4 Results and Discussion</b>	<b>32</b>
4.1 Key Residues at the Ligand-Binding Site.....	32
4.2 Evaluation of the Classification Protocol.....	35
4.3 Docking Experiments of MD Conformers.....	40
4.3.1 Salbutamol Binding.....	50

4.3.2 Alprenolol Binding.....	51
4.3.3 Carazolol Binding.....	52
4.4 Virtual Screening Experiments.....	55
<b>5 Conclusions</b>	<b>62</b>
<b>References</b>	<b>65</b>
<b>Appendix A Representation of 57 compounds that used for virtual screening</b>	<b>70</b>
<b>Appendix B Distance values of 13 MD conformers</b>	<b>79</b>
<b>Appendix C Binding results of the crystal structures</b>	<b>80</b>
<b>Appendix D Interactions table of ligands</b>	<b>84</b>
<b>Appendix E Binding results of the ligands with their score values</b>	<b>86</b>
<b>Appendix F ROC curves of MD frames</b>	<b>99</b>

## List of Tables

Table 4.1	Binding results of inverse agonist carazolol with crystal structures .....	39
Table 4.2	Binding results of the eight ligands with crystal structures ...	40
Table 4.3	Docking results of the crystal structures with all the ligands	42
Table 4.4	Docking results of the crystal structures .....	43
Table 4.5	Docking results of MD conformers with agonists .....	44
Table 4.6	Docking results of MD conformers with inverse agonists.....	45
Table 4.7	Docking results of MD conformers with antagonists .....	45
Table 4.8	Docking summary of the 9 successful MD conformers .....	46
Table 4.9	Binding results of a novel inverse agonist molecule .....	50

## List of Figures

Figure 2.1 Schematic representation of GPCRs.....	5
Figure 2.2 Transmembrane domains of GPCRs.....	6
Figure 2.3 $\beta_2$ AR activation/inactivation cycle .....	11
Figure 2.4 Two different signaling pathways of GPCRs .....	13
Figure 3.1 Five key residues at the binding site and 13 different MD snapshots .....	18
Figure 3.2 Cluster profile of 2800 ns MD trajectory.....	19
Figure 3.3 13 MD snapshots .....	20
Figure 3.4 ROC curve model .....	31
Figure 4.1. The key residues at the ligand-binding site and the distance restraints between these seven residues .....	33
Figure 4.2. The distance plot of the MD conformers between key residues at the ligand binding site .....	34



Figure 4.3. X-ray snapshots of inactive/active states aligned and seven transmembrane helices .....	36
Figure 4.4. Molecular schemes of the ligand molecules that are known and used in crystal structures. ....	37
Figure 4.5. The binding protocol used for classification .....	38
Figure 4.6. Ligand interactions at the binding site.....	38
Figure 4.7. Molecular schemes of the additional ligands with known activities .....	41
Figure 4.8 Ligand interactions of frame1648 .....	47-48
Figure 4.9. Extracellular view of active crystal structure 3SN6 and frame210. ....	51
Figure 4.10. Extracellular view of inactive crystal structure 3NYA, frame585 and frame1648 .....	53
Figure 4.11. Extracellular view of inactive crystal structure 2RH1, frames 715 and 1648.....	54
Figure 4.12. ROC curves of the inactive structure PDB id: 2RH1 .....	56
Figure 4.13. ROC curves of the active structure PDB id: 4QKX .....	56
Figure 4.14. ROC curves of frame715 .....	57

Figure 4.15. ROC curves of frame1618.....	58
Figure 4.16. ROC curves of frame210 and frame1365.....	59
Figure 4.17. ROC curves for all frames and crystals that have been used.....	61

## List of Abbreviations

Å	Angstrom
Asn	Asparagine
Asp	Aspartic Acid
AUC	Area Under Curve
β <sub>2</sub> AR	Human Beta-2 Adrenergic Receptor
G <sub>s</sub>	Alpha Subunit of G-protein
GPCR	G-protein Coupled Receptor
ICL3	Intracellular Loop 3
MD	Molecular Dynamics
NMR	Nuclear Magnetic Resonance
PDB	Protein Data Bank
RMSD	Root Mean Square Deviation
Ser	Serine
TM	Transmembrane
ROC	Receiver Operating Characteristic

## Chapter 1

### Introduction

G protein-coupled receptors (GPCRs) are the largest family of eukaryotic membrane proteins. They are also known as seven transmembrane domain receptors (7TM), and involved in signal transduction across membranes in many different physiological pathways. GPCRs control many cellular responses to hormones, neurotransmitters, peptides, ions, photons, proteins and small molecules. Many diseases are related to the functioning of GPCRs and making them important targets for drug design. Today, more than 50% of the marketed drugs act on these receptors. Human  $\beta_2$ -adrenergic receptors ( $\beta_2$ AR) belong to the class A GPCRs responding to hormones adrenaline and noradrenaline and are the targets of current asthma and cardiac drugs which comprise the mainstream of research (Rosenbaum, Rasmussen and Kobilka, 2009; Li and III, 2010).

In 2007, after the discovery of the first explained X-ray crystal structures of human  $\beta_2$ AR in the inactive states by Rasmussen and his coworkers, one with the anchor protein T4-lysozyme and inverse agonist carazolol (PDB id: 2RH1; Cherezov *et al.*, 2007) and two with the Fab5 complex (PDB ids: 2R4R, 2R4S, Rasmussen *et al.*, 2007), a new gate has opened for drug design studies. In the following years, the active states of the receptor were also revealed with X-ray crystallography studies,

however, the conformational transition between active and inactive states is still not fully understood (Dror *et al.*, 2011).

In order to understand the effect of intracellular loop 3 (ICL3) on the intrinsic dynamics of the receptor, Ozcan *et al.* performed MD simulations using the inactive crystal structure of human  $\beta_2$ AR which was found in complex with the inverse agonist carazolol and T4-lysozyme (PDB id: 2RH1) as the initial conformation. Carazolol and T4-lysozyme were removed prior to the MD simulations and two different models called *loop* and *clipped* were performed. In the *loop* model, the missing ICL3 region was added, while in the *clipped* model the transmembrane helices 5 (H5) and 6 (H6) were covalently bonded to each other. Both models were subjected to 1  $\mu$ s MD simulation, as a result, the *loop* model was found in a very inactive conformation after around 600 ns which is characterized by a further movement of the H6 towards to receptor's core region, and a close packing of ICL3 underneath the membrane blocking the G-protein binding site. The Ser207-Asp113 distance at the binding pocket was found to increase from 11 Å to 18 Å showing that there is a strong coupling between the extracellular and intracellular regions of the receptor (Ozcan *et al.*, 2013).

In this thesis, a total of 13 distinct conformations of  $\beta_2$ AR that has been obtained from the *loop* model of Ozcan *et al.*'s work after clustering the MD trajectory based on RMSD value of the binding site region, were used for a series of molecular docking experiments to bring out the distinctiveness of each conformer interacting

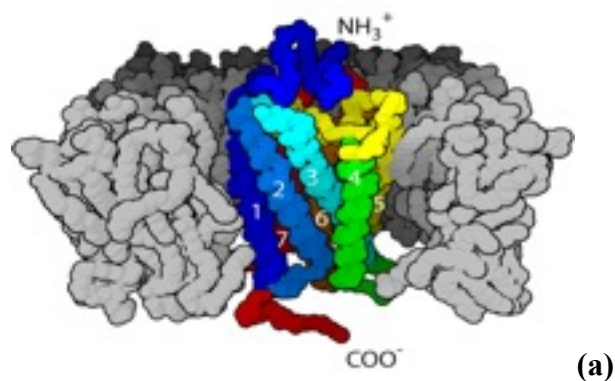
with different ligands with various efficacies (Ozcan *et al.*, 2013). In addition, the presence of ICL3 region in all these conformers provides a more realistic model, which takes into account the allosteric effect between intracellular (G-protein binding site and ICL3) and extracellular (ligand-binding site) region for the first time. Using a classification protocol developed in this study, these conformations were classified as active or inactive states, which were then used in virtual screening experiments and were found to be more selective over antagonists/inverse agonists than any known inactive state crystal structures.

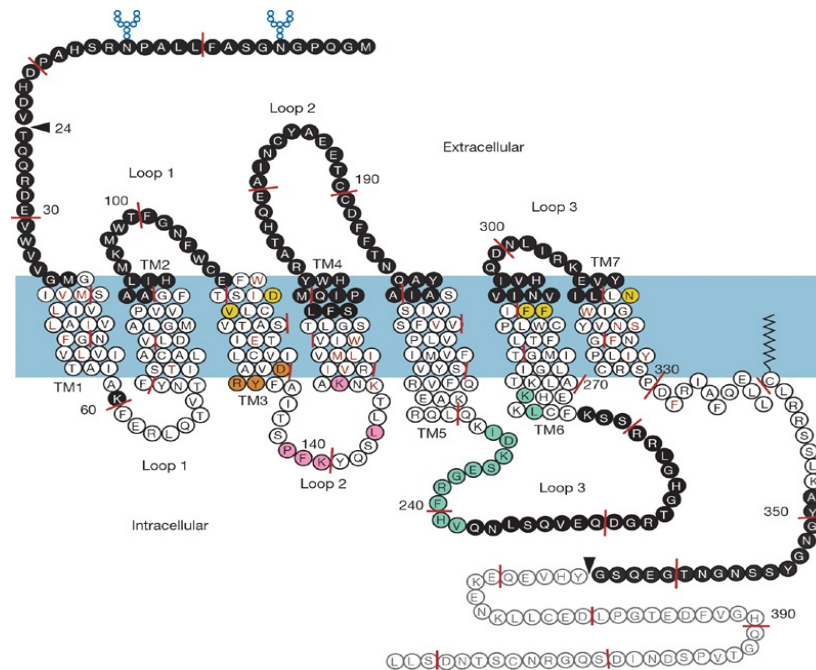
## Chapter 2

### Human Beta-2 Adrenergic Receptor ( $\beta_2$ AR): Structure, Function and Dynamics

#### 2.1. G-Protein Coupled Receptors

Human  $\beta_2$ AR is a member of the G protein coupled receptors (GPCRs) superfamily which has a critical role in cell and tissue communication. All GPCRs have seven membrane-spanning helices, thus they are known as seven transmembrane (7TM) receptors (Nygaard *et al.*, 2009). These helices are separated by three extracellular loops and three intracellular loops as shown in Figure 2.1 (Johnson, 2006). Composed of 400 to 500 amino acids, GPCRs initiate the signaling pathway through binding of extracellular ligands such as neurotransmitters, hormones, or peptides, which trigger specific conformational changes in the ligand-binding site. Most physiological processes such as olfaction, taste, smell, vision, cardiovascular and pulmonary functions mostly depend on GPCRs (Latek *et al.*, 2012).





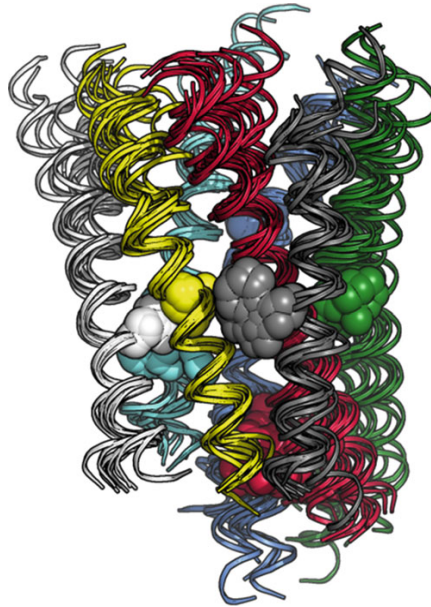
(b)

Figure 2.1. Schematic representation of GPCRs. (a) The seven-transmembrane  $\alpha$ -helix structure of a G protein-coupled receptor (b) 2D representation of  $\beta_2$ AR embedded in the membrane (Wikipedia, 2016; Rasmussen *et al.*, 2007).

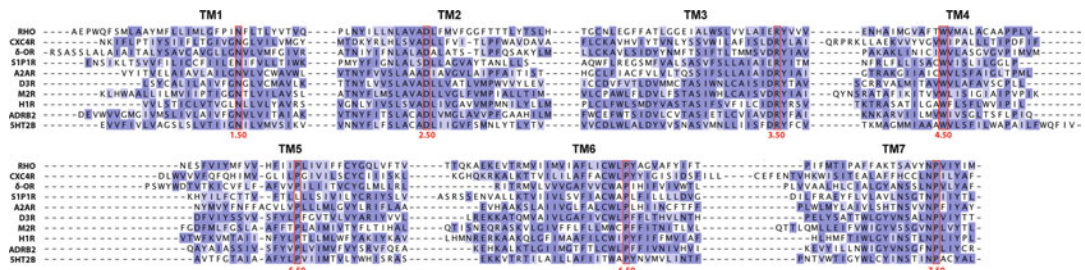
GPCR members share more than 20% sequence identity and have been classified into five families according to their conserved sequence regions and their structure. These families are rhodopsin (family A), secretin (family B), glutamate (family C), adhesion and Frizzled/Taste2 (family O). Family A receptors, which are the most studied one, are also divided into subgroups called opsin, amine, peptide, cannabinoid and olfactory receptors. Furthermore, according to localization and ligand specificity, the amine subgroup diverges into subfamilies as  $\alpha$  and  $\beta$ .  $\beta_2$ -adrenergic receptor ( $\beta_2$ AR) is the member of rhodopsin-like A family, amine group  $\beta$  subfamily (Vauquelin, 2007; Rosenbaum *et al.*, 2009).



The overall sequence identity within the members of class A is low and limited to a few highly conserved key residues as highlighted in Figure 2.2.



(a)



(b)

Figure 2.2. Transmembrane domains of GPCRs. (a) Superimposition of the TM domains. TM1 (white), TM2 (yellow), TM3 (red), TM4 (grey), TM5 (green), TM6 (dark blue), and TM7 (light blue). The highly conserved N1.50 (white), D2.50 (yellow), R3.50 (red), W4.50 (grey), P5.50 (green), P6.50 (dark blue), and P7.50 (light blue) are shown as spheres. (b) Sequence alignments of TMs. Structure conservation of GPCR family is associated with the highly conserved amino acid in each helix (shown in red) (Filizola, 2014).

## 2.2. X-ray Crystal Structures of $\beta_2$ AR

Previous studies on GPCRs were based on a low-resolution model of bovine rhodopsin, which was expected to share a conserved structure with other GPCRs (Unger and Schertler, 1995). Later in 2000, the first crystal structure of rhodopsin was visualized by Palczewski *et al.* in complex with 11-cis-retinal, representing an inactive conformation (Palczewski *et al.*, 2000). This structure has been extensively used as a template for homology modeling for other GPCRs such as  $\beta_2$ AR (Ballesteros, Shi and Javitch, 2001; Stenkamp *et al.*, 2002; Montero *et al.*, 2005).

Afterwards in 2007, the first X-ray crystal structure of the inactive form of human  $\beta_2$ AR GPCR bound to inverse agonist carazolol was revealed; one bound to a monoclonal antibody (Fab5) (PDB ids: 2R4R, 2R4S, Rasmussen *et al.*, 2007) and one with the anchor protein T4 lysozyme (PDB id: 2RH1; Cherezov *et al.*, 2007). Since  $\beta_2$ AR has a flexible and unstable structure, Fab5 and T4 lysozyme molecules have been used to help for crystallization in order to provide conformational stability (Cherezov *et al.*, 2007; Rasmussen *et al.*, 2007). Cherezov *et al.* identified that the poorly structured intracellular loop 3 (ICL3) was obstructive for crystallization, thus, T4-lysozyme (T4L) has been inserted in place of ICL3.

After the identification of the first crystal structures, other inactive conformations of  $\beta_2$ -AR have been reported in complex with a partial inverse agonist timolol (Hanson *et al.*, 2008) and antagonist alprenolol (Wacker *et al.*, 2010). While the hydrogen

bonding with Ser203, Ser204, Ser207, Asp113, Asn312 and Tyr316 was conserved for carazolol, timolol and alprenolol, additional hydrogen bonds and hydrophobic interactions were observed for each ligand with different binding affinities. Although these specific interactions define the pharmacological response, they have a minor impact on the overall structure of the receptor (Dror *et al.*, 2011).

In 2011, Rasmussen and his coworkers have determined two active structures of  $\beta_2$ AR bound to full agonist BI-167107 in complex with a nanobody (Søren G F Rasmussen *et al.*, 2011) and Gs-protein (Soren G F Rasmussen *et al.*, 2011). Comparison of the active and inactive states has revealed minor differences on the ligand binding site region of the receptor. The key change was the interaction with Ser203, Ser204 and Ser207 residues on TM5. The hydrogen bond between the ligand and serines causes an inward movement of TM5 followed by an outward swing of the lower half of TM6. This outward displacement of TM6 upon activation is the largest change observed in  $\beta_2$ AR and is around 11 Å in nanobody bound structure and 14 Å in Gs-protein bound structure (Rasmussen *et al.*, 2011; Chung *et al.*, 2012; Liapakis *et al.* 2000).

### **2.3. Interactions and Signaling Pathways in $\beta_2$ AR**

$\beta_2$ AR has a rich variety of ligands classified according to their effect on basal activity; full agonists maximize the activity by promoting the binding of G-proteins, inverse agonists suppress the basal activity by closing the G-protein binding cavity,

partial agonists cause partial activation and neutral antagonists do not affect the activity while blocking the binding site for other ligands (Rosenbaum *et al.*, 2009).

When it is not stimulated, the receptor tends to stay in an inactive state. Binding of an agonist lowers the energy barrier between the inactive and active states and enables the interaction with G-protein. Heterotrimeric G-protein binding enables the signaling from extracellular ligand-binding site to intracellular region by changing the receptor conformation from inactive to active state. Studies have shown that the presence of an agonist molecule is not sufficient by itself to shift the equilibrium from an inactive to an active state in the absence of a G-protein (Galandrin and Bouvier, 2006; Dror *et al.*, 2011).

The active receptor conformation is defined by limited access to ligand binding site. DeVree *et al.* have provided functional evidence that nucleotide free G-protein coupling of  $\beta_2$ AR stabilizes closed receptor conformation by inducing the transition of ligands to the orthosteric binding site. G-protein activation blockades the association with other ligands while hindering the dissociation of the bound ligand. On the other hand, agonist or hormone binding enhances G-protein coupling via active formation of the receptor and loss of nucleotide from G-protein (DeVree *et al.*, 2016).

In order to understand the effect of different ligand types on the dynamics of  $\beta_2$ AR and Gs protein, Bai *et al.* performed 800 ns long MD simulations  $\beta_2$ AR-Gs protein

complex bound to agonist (BI-167107), antagonist (alprenolol), inverse agonist (ICI 118,551) and their unliganded form. The results showed that binding of different types of ligands to  $\beta_2$ AR has different effect on the behavior of  $G\alpha$  and  $G\beta\gamma$  domain. The inverse agonist ICI 118,551 has triggered the dissociation of  $G\alpha$  and  $G\beta\gamma$  domain by changing the conformation of the receptor. On the other hand,  $G\alpha$  and  $G\beta\gamma$  domain kept the stable distance if agonist, antagonist or no ligand was bound to  $\beta_2$ AR. Also, each ligand had different hydrogen bonding with the receptor; the inverse agonist ICI 118,551 formed hydrogen bonds with Asp113 and Asn312, while the antagonist alprenolol had similar hydrogen bonding except lower bonding with Tyr308. The agonist BI-167107 had hydrogen bonds with Ser203, Ser207 and Asn293 besides Asp113 and Asn312. These different binding modes effect the conformation of the receptor by effecting the binding pocket's volume (Bai *et al.*, 2013).

G-proteins function as a switch inside the cell and belong to GTPase family of enzymes. Heterotrimeric G-proteins consist of three subunits, alpha ( $\alpha$ ), beta ( $\beta$ ) and gamma ( $\gamma$ ).  $\beta_2$ AR activates itself by binding of an agonist molecule from the extracellular region that enables the interaction with the G-protein heterotrimer. Following this interaction, guanosine diphosphate (GDP) leaves the  $G\alpha$  subunit while guanosine triphosphate (GTP) enters the same pocket and activates  $G\alpha$  protein. The binding of GTP to the subunit causes dissociation of the complex, releasing  $G\alpha$  and  $G\beta\gamma$  from the receptor. The activated  $G\alpha$  subunit binds to and activates adenylyl cyclase enzyme, which in turn catalyzes the conversion of ATP into cyclic adenosine

monophosphate (cAMP). The  $G\beta\gamma$  subunits can regulate different types of effector proteins like  $Ca^{2+}$  channels, kinases and other enzymes. Hydrolysis of GTP to GDP in  $\alpha$  subunit causes reassembling of heterotrimeric G-protein and inactivation of  $G\alpha$  protein (Figure 2.3) (Soren G F Rasmussen *et al.*, 2011).

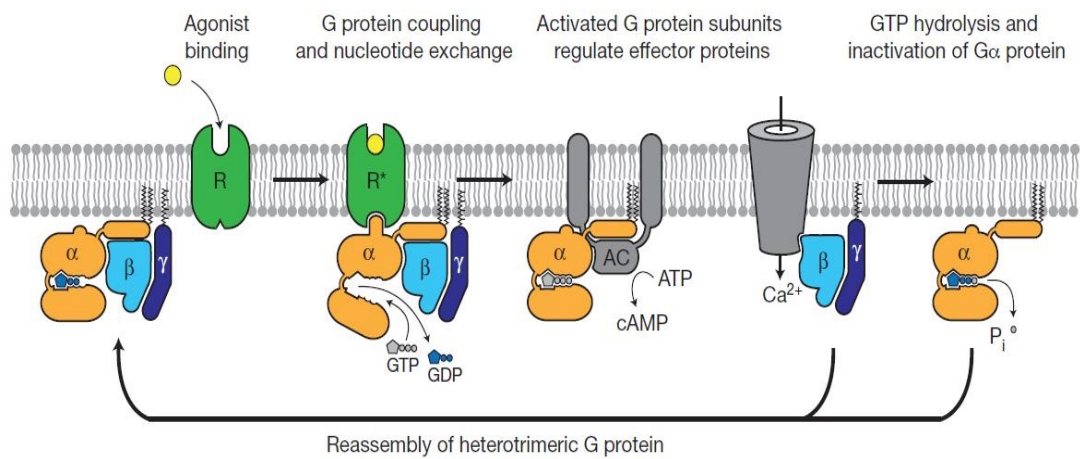


Figure 2.3.  $\beta_2$ AR activation/inactivation cycle.

Another major signaling pathway of  $\beta_2$ AR is through beta-arrestins. The activated receptors are also substrates for G-protein coupled receptor kinases (GRKs). Phosphorylation of the GRKs, trigger the binding of beta-arrestins to the receptor. Beta-arrestins can limit the G-protein signaling and trigger a parallel set of signals. Inverse agonists for G-protein pathway, such as ICI 118;551 and propranolol, have shown positive agonist activity for beta-arrestin GRK. This indicates G-protein and beta-arrestin efficacies can differ and beta-arrestins can be completely independent from G-protein signaling pathway (Figure 2.4) (Violin and Lefkowitz, 2007; Kenakin, 2007).

The coupling of the receptor with beta-arrestins and G-proteins trigger selective modulation of the downstream effects. Biased ligands selectively choose to couple either beta-arrestins or G-proteins. This indicates a difference in the receptor core that allows coupling with only one of these effectors and prevent coupling with the other effector (Shukla, Singh and Ghosh, 2014). <sup>19</sup>F-labeled NMR spectroscopy studies of  $\beta_2$ AR with biased ligands have shown unique conformational changes and different signaling in G-protein and beta-arrestin pathways. Binding of full agonists induced a conformational change on TM6 and TM7 whereas beta-arrestin biased ligands such as carvedilol and isoetharine had shown to have a strong impact on shifting the conformational equilibrium of TM7 towards the active state. While the conformational changes in TM7 did not directly effect the G-protein binding and signaling, it has a crucial role in the beta-arrestin signaling pathway (Liu *et al.*, 2012).

Another conserved interactions in  $\beta_2$ AR are the ionic lock and the rotamer toggle switches. These switches stabilize the movements of helices and thereby help the intracellular part of the receptor to be accessible for G-protein binding, in other words to turn the receptor into an active state. Rather than two state on and off switches, they are able to maintain the continuity of conformations (Rosenbaum *et al.*, 2009). The ionic lock is the salt bridge between Asp130/Arg131 pair on TM3 and Glu268 residues on TM6, whereas the rotamer switch is the bending of TM6 resulting from the interactions between aromatic ring of the ligand and aromatic residues Trp286 and Phe290. The activation of receptor through micro-switches

varies from different ligands to different GPCRs (Kobilka and Deupi, 2007; Katritch, Cherezov and Stevens, 2013). Studies have shown that catechol binding activates the toggle switch whereas ionic lock is not activated. Also, salbutamol binding activates ionic lock but does not activate toggle switch, suggesting that these micro-switches are not coupled (Kobilka, 2007).

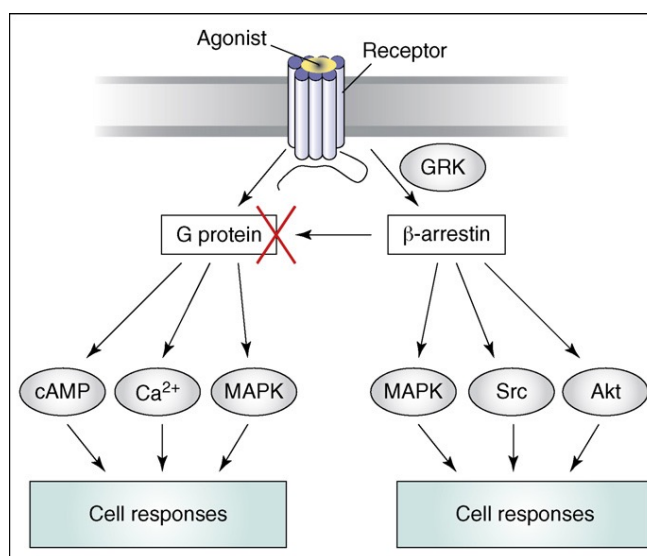


Figure 2.4. Two different signaling pathways of GPCRs. While G-proteins trigger second messengers such as calcium, cyclic adenosine monophosphate (cAMP) and mitogen activated kinases (MAPK); beta-arrestins which phosphorylated by GRKs terminate G-protein signaling pathway. Beta-arrestins also trigger another signaling such as activation of Src, Akt and MAPK. These signaling pathways can stimulate by classical agonists and each of them couples with different signaling pathway (Violin and Lefkowitz, 2007).

## 2.4. Structural Dynamics of $\beta_2$ AR

The structural dynamics of active to inactive transitions of GPCRs is still not fully understood. While agonists shift the existing equilibrium to more active states, the dynamic equilibrium of the receptors remains heterogeneous and even in the high concentrations of agonists, receptor can still adopt an inactive state. On application



of muscarinic  $M_2$  receptor all-atom MD simulations, Bock et al. suggested that an ensemble of active and inactive agonist-receptor complexes in which agonists adopt multiple binding modes indicates different agonist efficacies and that agonists can stabilize inactive agonist-receptor complexes (Bock *et al.*, 2016).

Since the binding site of the receptor is located away from G-protein binding site, key residues in the TM domain mediate the allosteric communication between extracellular and intracellular regions. Although the sequence similarity is low among GPCRs, high structural similarity results to a common mode of activation. Bhattacharya et al. suggested that similar residues were involved in the activation mode of class A GPCRs and their MD simulation studies have shown that allosteric communication pipelines were conserved among the six biogenic amine receptors. Also, among the receptors studied,  $\beta_2$ AR showed the highest level of fluctuation in TM6 and TM7 due to its basal activity (Bhattacharya *et al.*, 2016).

To investigate how agonists with different efficacies modulate  $\beta_2$ AR's active and inactive conformations, Staus et al. have used positive allosteric nanobody Nb80 stabilizing the active state and a negative allosteric nanobody Nb60 stabilizing the inactive state of the receptor. They found out that in the presence of Nb80 the agonist isoprenaline has 15,000-fold higher affinity to  $\beta_2$ AR than in the presence of Nb60. Also Nb60-bound  $\beta_2$ AR has affinity approximately 100-fold lower than the previously described low-affinity inactive state. In other words, there exist an average of multiple, rapidly interconverting inactive and active states. 17 ligands

with varying efficacy to  $\beta_2$ AR have been used in the absence and presence of Nb80 and Nb60 and showed a wide range of efficacies (downstream response) indicating that the receptor has at least three different equilibrium states (Staus *et al.*, 2016). Another MD simulation performed by Shan et al. have showed that binding of full agonist, partial agonist and inverse agonist induces distinct conformational changes and different responses (Shan *et al.*, 2012).

The structural dynamics of  $\beta_2$ AR has been studied by Manglik et al. and showed that unliganded and inverse-agonist-bound  $\beta_2$ AR conformations exist predominantly as two distinct inactive states that can be exchanged within hundreds of microseconds. On the other hand, agonists shift the equilibrium toward a conformation capable of engaging cytoplasmic G proteins and this results in increased conformational heterogeneity and the coexistence of inactive, intermediate, and active states. This findings indicates a loose allosteric coupling between the binding pocket and G-protein binding site that might be responsible for the complex signaling behavior observed for GPCRs (Manglik *et al.*, 2015).

To investigate GPCRs activation mechanism, Dror et al. performed MD simulation of  $\beta_2$ AR that deactivates itself upon the removal of G-protein or its mimetic nanobody. This shows that the agonist is not sufficient enough to keep the receptor in the active state, further indicating the loose coupling between ligand binding site and G protein binding site. Simulations also revealed that receptor adopts an intermediate conformation during the deactivation process (Dror *et al.*, 2011).

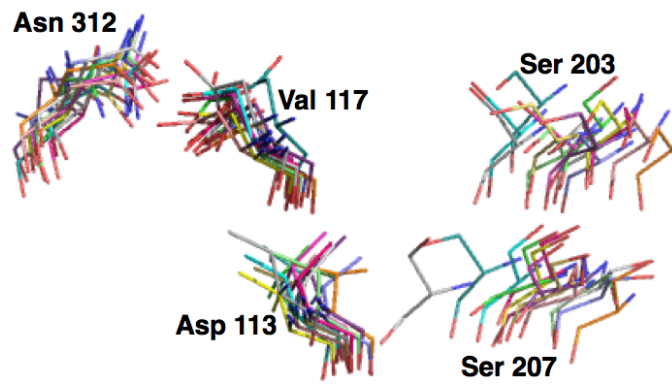
Kohlhoff et al.'s MD simulation studies revealed that  $\beta_2$ AR has multiple activation pathways and that agonists and inverse agonists interact distinctively with these pathways, which can be an important finding for drug design. Results have shown that binding of agonist molecule BI-167107 stabilizes the active-like conformations by strengthening the extra and intracellular interactions; while the inverse agonist carazolol and apo simulations do not show active state conformations and deactivating the receptor rapidly. The apo receptor simulation showed uncoupled interactions while carazolol disconnects the coupling between the extra and intracellular regions indicating that ligands trigger the receptor dynamics through different signaling pathways (Kohlhoff *et al.*, 2014).

## Chapter 3

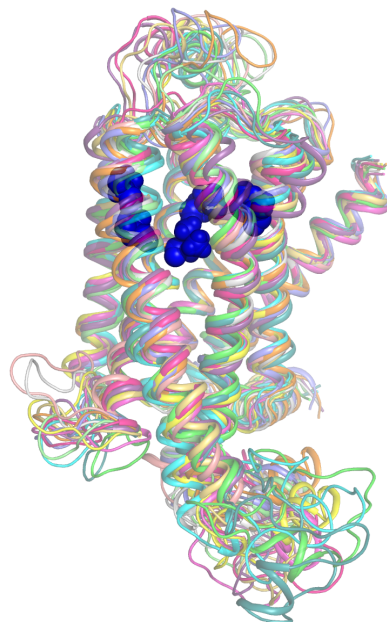
### Methods and Materials

#### 3.1. Generation of the Target Conformers

In this study, the trajectory of 2.8  $\mu$ s long MD simulation of  $\beta_2$ AR conducted by Ozcan *et al.* was used for determining the target conformations. In Ozcan's work, MD simulations were performed using the inactive crystal structure of the receptor obtained from the complex with partial inverse agonist carazolol and the anchor protein T4 lysozyme (PDB id: 2RH1) as the initial conformation. After removal of carazolol and T4L, the ICL3 region has been modeled between residues 230 and 266 in place of T4L. A total of 2800 snapshots were collected from MD simulations at every 1 ns and clustered based on their RMSD value of five key residues shown in Figure 3.1a (Asp113, Val117, Ser203, Ser207 and Asn312) at the binding site using *kClust* algorithm (Wolf and Kirschner, 2013). Clustering goes through each snapshot of the MD trajectory and repeatedly places each conformation to a cluster based on its RMSD value with respect to that cluster's centroid (average structure) and updates the centroid for that cluster. After all frames were assigned to a cluster, the conformation that is closest to the centroid is selected as the representative snapshot for that cluster. The clustering analysis in Ozcan's work yielded a total of 13 distinct conformers for an RMSD cut-off value 1.5 Å Figure 3.2 (Ozcan *et al.*, 2013).



(a)



(b)

Figure 3.1. Five key residues at the binding site (a) and 13 different MD snapshots (frame9, frame210, frame531, frame585, frame715, frame844, frame1365, frame1479, frame1648, frame2311, frame2231, frame2661 and frame2370) aligned to each other based on transmembrane region (b). Blue spheres represent the key residues at ligand-binding site (Serines, Asn312 and Asp113).

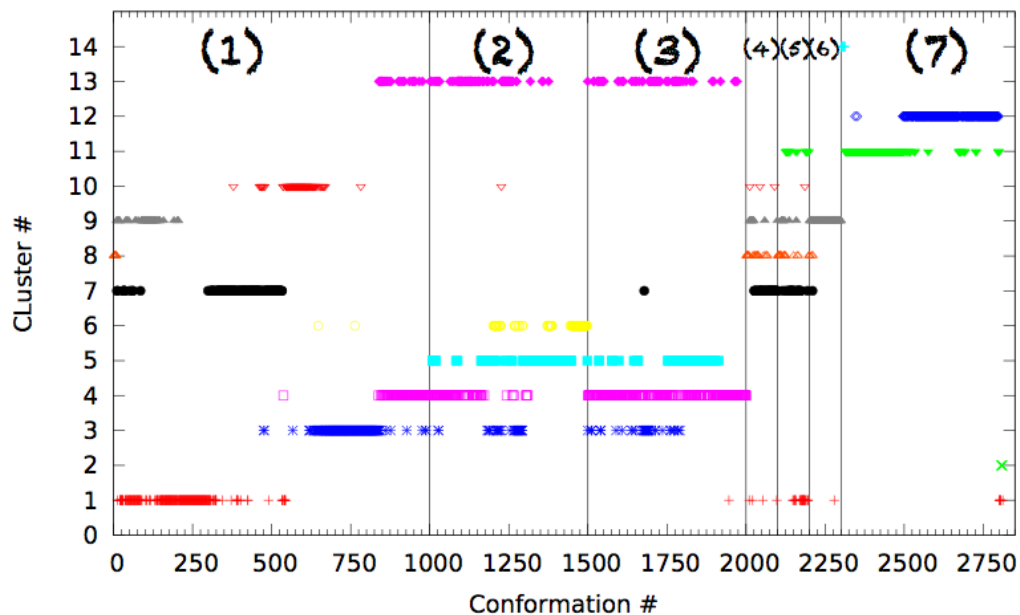


Figure 3.2. Cluster profile of 2800 ns MD trajectory (1): 0-999: Original 1  $\mu$ s MD run, (2): 1000-1499: 1st continued MD run (same initial velocity), (3): 1500-1999: 2nd continued MD run (different initial velocity), (4-5-6): 2000-2299: Short 100 ns MD runs, (7): 2300-2799: Constrained released MD run, 2800-2810: 11 crystal structures.

According to MD simulation, ICL3 starts to pack under the receptor at around 600ns and keep a stationary state until the end of 1  $\mu$ s. After that, in order to observe how long ICL3 region would remain in this packed state, two independent 500 ns long simulations were performed representing the very inactive state of the receptor. In this continuation runs no restrains were applied. The first continued run starts with the same velocity of the previous 1  $\mu$ s long simulation and carries out 500 ns which ICL3 does not change its packed form. The second continued 500 ns run starts with a different velocity, resulting ICL3 to move away from the receptor at around 220 ns before returning back to its packed position. In order to see the effect of restraints on the dynamics of ICL3 and receptor, a total of five independent MD runs performed which were different sets of constraints applied. And one 500 ns long MD run were performed which all distance restraints are released (see Figure 3.2) (Ozgur, Doruker

and Akten, 2016). The 13 frames from MD runs were named according to their MD trajectories, for example frame9 is the snapshot from the original 1  $\mu$ s long simulation at around 9 ns or frame1648 is the 148th frame of the second continued MD run. These 13 frames and the position of ICL3 is shown in Figure 3.3.

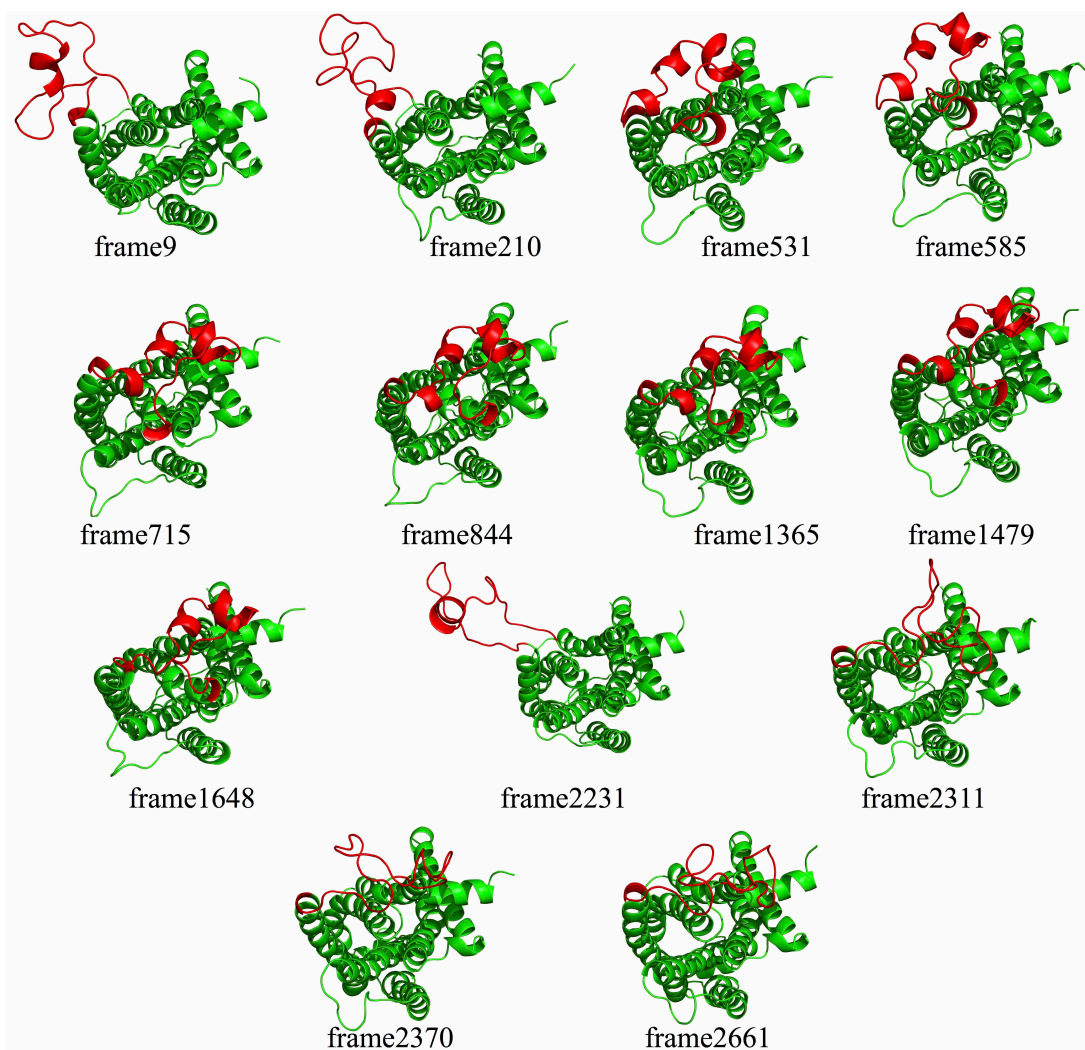


Figure 3.3. 13 MD snapshots. ICL3 region is shown in red color.

### 3.2. Scoring Functions and Docking Studies

Molecular docking aims to predict the most favorable conformation of a ligand bound to a target receptor, which is evaluated by a scoring function. This process begins with a search algorithm that tries to generate all possible ligand poses in the binding cavity accompanied by calculating the score value of each pose that simply predicts the binding affinity of that ligand for the receptor. In general, scoring functions are divided into three categories; physics-based (force-field based), empirical and knowledge based. Each of them uses different parameter sets to end up with a reasonable result. Some docking tools combines different parameters from different scoring function categories. They usually consider the short-range interactions between the ligand and the protein while disregarding the long-range interactions in order to save time.

In general, physics based scoring functions are designed to compute potential energy in the gas phase and some of them were improved by solvation energy terms like Poisson–Boltzmann (PB) or Generalized Born (GB) models. Most of the physics-based scoring functions are based on or composed of molecular mechanics force-fields such as AMBER, CHARMM, GROMOS and OPLS-AA. Interactions between ligand and receptor are computed using noncovalent energy terms, van der Waals and the electrostatic energy terms. While the van der Waals term is given by Lennard-Jones potential function, Coulombic formulation is used for electrostatic terms. Advantage of this method is that, they are applicable on modern force fields, quantum mechanics and solvation models.



Empirical scoring functions compute the final binding energies by summing up the individual uncorrelated energy terms. It relies on regression analysis to derive the weight factors for each term. For the regression analysis protein-ligand complexes with known structures and binding affinity data is required. Unlike the physics based methods that depend on theoretical framework, empirical scoring functions are more intuitive.

Knowledge-based scoring functions compute the energetic factors by summing up pairwise statistical potentials between protein and ligand. Their derivation is based on statistical analysis of the resolved structures of the protein-ligand complexes. They are computationally simple and effective to reproduce protein-ligand binding poses rather than binding energy (Kitchen *et al.*, 2004; Liu and Wang, 2014).

Throughout this thesis, docking experiments were performed with AutoDock, GOLD with ChemPLP scoring function, DSX-CSD and DSX-PDB rescoring functions and Glide molecular docking tool. Their detail algorithm and scoring functions are discussed in the following sections.

### **3.2.1. AutoDock**

AutoDock 4.0 is a free software tool that uses a physics-based scoring function that is derived from AMBER force-field and a genetic algorithm to explore the conformational space. In this so-called Lamarckian Genetic Algorithm (LGA) used by AutoDock, the pose of a ligand is defined as a chromosome, which is made up of genes. The genes are defined as ligand's torsional angles of all possible rotatable

bonds, overall rotation and translation in space. The genetic algorithm starts by generating a population that is composed of 200 different ligand conformations with randomly assigned rotatable bonds, which are used to produce new generations through crossover and mutation events. Crossover is the combination of torsion angles from two randomly selected ligand conformations, and mutation is simply a change in one of the torsion angles. AutoDock's scoring function is as given in the following equation 1.

$$\begin{aligned}
 \Delta G = & \\
 & \Delta G_{vdW} \sum_{i,j} \left( \frac{A_{ij}}{r_{ij}^{12}} - \frac{B_{ij}}{r_{ij}^6} \right) + \\
 & \Delta G_{hbond} \sum_{i,j} \Delta G_{hbond} \sum_{i,j} E(t) \left( \frac{C_{ij}}{r_{ij}^{12}} - \frac{D_{ij}}{r_{ij}^{10}} + E_{hbond} \right) + \Delta G_{elec} \sum_{i,j} \frac{q_i q_j}{\epsilon(r_{ij}) r_{ij}} + \Delta G_{tor} N_{tor} + \\
 & \Delta G_{sol} \sum_{i,j} S_i V_j e^{-\frac{r_{ij}^2}{2\sigma^2}}
 \end{aligned} \tag{3.1}$$

The first term of the equation is the 12-6 Lennard-Jones potential, while the second term is 12-10 Lennard-Jones potential.  $r_{ij}$  indicates the distance between protein atom  $i$  and ligand atom  $j$ ,  $A_{ij}$  and  $B_{ij}$  are the vdW parameters.  $E(t)$  function provides directionality based on the angle  $t$  from ideal hydrogen bonding geometry. The third term is the Coulomb formulation for electrostatic interactions while  $\epsilon(r_{ij})$  represents distance-dependent dielectric constant,  $q_i$  and  $q_j$  are the atomic charges. Last term is the desolvation potential that  $V$  represents the volume of the atoms and  $S$  represents the solvation parameter (Huey *et al.*, 2007).

In this thesis, docking experiments were performed selecting Lamarckian genetic algorithm and a total of 20 runs were performed for each docking experiment. Grid box size was set to 44 x 44 x 44 with a spacing of 0.375 Å and the number of energy evaluations was set to 30 millions. For each docking experiment, the pose with the lowest  $\Delta G$  (or the highest score) was selected as the most probable solution for that complex.

### 3.2.2. GOLD

GOLD (Genetic Optimization for Ligand Docking) is a molecular docking program provided by the Cambridge Crystallographic Data Centre (CCDC). It uses a genetic search algorithm to determine favorable binding poses. A population of chromosomes is manipulated and assigned to a fitness score value (Jones *et al.*, 1997). GOLD has four different fitness functions. The GoldScore molecular mechanics-like function is the original scoring function provided with GOLD. It takes into account H-bonding, van der Waals, metal interactions and ligand torsion strain as shown in equation 2, where  $S_{hb\_ext}$  stands for the protein-ligand hydrogen bond score and  $S_{vdW\_ext}$  stands for the protein-ligand van der Waals score.  $S_{hb\_int}$  and  $S_{vdW\_int}$  stand for the internal hydrogen bonding and van der Waals scores of the ligand (Verdonk *et al.*, 2003).

$$GOLD\ Fitness = S_{hb\_ext} - S_{vdW\_ext} - S_{hb\_int} - S_{vdW\_int} \quad (3.2)$$

Chemscore is one of the oldest scoring functions parameterized from 82 complexes of known binding affinities. It incorporates a protein-ligand atom clash term and an

internal energy term as shown in the equations 3 and 4. It includes terms for loss of covalent bonding, hydrophobic contact area, hydrogen bonding, acceptor-metal and lipophilic interactions (Verdonk *et al.*, 2003).

$$\Delta G_{binding} = \Delta G_0 + \Delta G_{hbond} S_{hbond} + \Delta G_{metal} S_{metal} + \Delta G_{lipo} S_{lipo} + \Delta G_{rot} S_{rot} \quad (3.3)$$

$$\Delta G'_{binding} = \Delta G_{binding} - E_{clash} - E_{int} - E_{cov} \quad (3.4)$$

The Astex Statistical Potential (ASP) fitness function is a knowledge based scoring function provided with GOLD and is based on atom-atom distance potentials derived from a database of protein-ligand complexes. It uses some of the Chemscore terms such as clash term, hydrogen bonding and internal energy term.

ChemPLP fitness function is the default empirical scoring function provided with GOLD that uses Chemscore hydrogen bonding term. It treats van der Waals and repulsive interactions with a piecewise linear potential (PLP). It is faster to calculate ChemPLP than Chemscore and Goldscore. Overall, ChemPLP is generally more effective in pose prediction and virtual screening.

$$f_{PLANTS_{CHEMPLP}} = f_{plp} + f_{hb} + f_{hb-ch} + f_{hb-CHO} + f_{met} + f_{met-coord} + f_{met-ch} + f_{met-coord-ch} + f_{clash} + f_{tors} + c_{site} \quad (3.5)$$

The scoring function is shown as in equation 5, where  $f_{plp}$  stands for piecewise repulsive/attractive interactions and  $f_{hb}$ ,  $f_{hb-ch}$ ,  $f_{hb-CHO}$  stand for distance and angle dependent hydrogen bonding terms. Metal interactions were considered with  $f_{met}$ ,

$f_{met-coord}$ ,  $f_{met-ch}$ ,  $f_{met-coord-ch}$  terms.  $f_{clash}$  stands for empirical heavy-atom potential, to avoid from internal ligand clashes.  $f_{tor}$  is the torsional potential while  $c_{site}$  is for additional contributions outside the binding site (Korb, Stu and Exner, 2009).

In this thesis, GOLD/ChemPLP scoring function was used to perform docking experiments. The binding site is defined as a spherical region with a radius of 10 Å that covers key residues in the cavity. A total of 20 runs were selected for each complex.

### 3.2.3. DSX

DSX (**D**rug**S**core **e**Xtended) is a knowledge-based scoring function that is used to re-evaluate the existing docked poses. In knowledge-based scoring functions, crystallographic data of protein-ligand complexes are required to determine pair distribution functions in order to extract pairwise potentials. Protein Data Bank (PDB) and Cambridge Structural Database (CSD) are used to derive these pairwise potentials for DSX (Neudert and Klebe, 2011). Drugscore calculates binding scores between the protein I and the ligand J as the sum of all existing atom-atom interactions as shown in equation 6, where  $\Delta W_{i,j}$  stands for specific interactions between atoms of type  $i$  and  $j$ , located at a distance  $r$ .

$$\Delta W_{I,J} = \sum_{i \in I} \sum_{j \in J} \Delta W_{i,j}(r) \quad (3.6)$$

In this thesis, the DSX-online webserver was used to perform the rescoring. 20 binding poses generated by AutoDock were rescored using both DSX-CSD and DSX-PDB scoring functions for each protein-ligand complex.

### 3.2.4. GLIDE

GLIDE (Grid-based Ligand Docking with Energetics) is a molecular docking program provided by the Schrödinger Suite which uses an empirical scoring function and an OPLS-AA force-field. To find the best binding pose of the ligand, GLIDE uses a series of hierarchical filters. It represents the shape and properties of the receptor on a grid by several different sets of fields in order to find the most accurate binding poses. These filters are; distance matching on a 2 Å spaced grid, clash test for ligand atoms, prescreening of the initial set of ligands, greedy scoring and refinement. The prescreening process reduces computationally expensive energy and gradient evaluations. GLIDE has two scoring functions GlideScore Standard Precision (SP) and GlideScore Extra Precision (XP) and both functions are based on ChemScore, with differences in the hydrogen-bonding term, metal-ligand interaction term and additional solvation terms as shown in the equation 7 (Friesner *et al.*, 2004, 2006).

$$XP \text{ GlideScore} = E_{coul} + E_{vdW} + E_{bind} + E_{penalty}$$

$$E_{bind} = E_{hyd\_enclosure} + E_{hb\_nn\_motif} + E_{hb\_cc\_motif} + E_{PI} + E_{hb\_pair} \\ + E_{phobic\_pair}$$

$$E_{penalty} = E_{desolv} + E_{ligand\_strain} \quad (3.7)$$

In this thesis, GlideScore XP was selected to perform the docking experiments for higher accuracy. Inner box was set to 15 x 15 x 15 and outer box was set to 35 x 35 x 35 size, where the inner box defines the volume that the ligand center explores during the exhaustive site-point search and outer box defines the volume in which the grid potentials are computed. Other parameters were set to default features and 20 runs were selected for each protein-ligand complex.

### **3.3. Docking-Based Virtual Screening**

With the developments in genomics projects, NMR and crystallographic studies, docking based virtual screening approach (DBVS) become a very important first step in lengthy drug discovery process. DBVS is the rapid evaluation of large chemical compound libraries in order to select the best candidates using a docking program. To achieve an optimal complementarity, docking program virtually docks each compound in the library to the target protein. Using a search algorithm, it predicts the possible binding poses and ranks these docking results with a scoring function. At the end of screening, a small group of top-ranked compounds are selected as candidate (hit) molecules for later experimental assays (Tuccinardi, 2009; Cheng *et al.*, 2012).

In this thesis, GOLD with ChemPLP scoring function was selected to perform virtual screening. The same classification protocol with the binding test was applied (Figure 3.8), but this time only the conformers found in top five in all four docking results for at least one ligand molecule were selected for virtual screening and these are

frame9, frame210, frame531, frame585, frame715, frame844, frame1365, frame1479 and frame1648, a total of nine conformers. For comparison, one active crystal structure (PDBid: 2RH1) and two inactive crystal structures (PDBids: 3SN6, 4QKX) were also selected for screening. Default features were used and radius spacing was selected to be 10 Å for the grid box. For each compound, number of runs was selected to be 20. The small compound dataset used for the screening was composed of 26 antagonists and 31 agonists for  $\beta_2$ AR. These 57 ligands were generated from ChEMBL (Gaulton *et al.*, 2012) and GPCR Ligand and Decoy Sets (Gatica and Cavasotto, 2012) databases. MarvinSketch program was used to transform these molecules into 3D mol2 format (Marvin 15.1.26, 2015, ChemAxon). These molecules were depicted in Appendix A.

### 3.4. Receiver Operating Characteristic (ROC) Curve

Receiver Operating Characteristic (ROC) curve is a common method used to evaluate the performance of virtual screening tools. Also it provides a way to compare the selectivity of different target molecules; the one with steeper slope curve has better discriminatory power for ligands with desired activities over the others in the database. ROC curves were obtained using the sensitivity ( $Se$ ) value on y-axis, and the specificity ( $1-Sp$ ) on x-axis.  $Se$  is the true positive rate and gives the ratio of the selected active molecules over the number of all active molecules;

$$Se = \frac{\text{Selected actives}}{\text{All actives}} = \frac{TP}{TP+FN} \quad (3.8)$$



where TP represents true positives and FN represents false negatives.  $Sp$  is the false positive rate and gives the ratio of the inactive molecules that is not selected by target over all inactive molecules;

$$Sp = \frac{\text{Discarded inactives}}{\text{All inactives}} = \frac{TN}{TN+FP} \quad (3.9)$$

where TN represents true negatives and FP represents false positives. Therefore,  $1-Sp$  is;

$$1 - Sp = \frac{FP}{TN+FP} \quad (3.10)$$

ROC curves starts with the top scored molecule on the hit list and continues according to their score values. While a curve between the ideal and the random curve represents a better performance, a curve under the random curve represents ineffective performance (see Figure 3.4) (Sottriffer, 2006).

In this thesis, the results were analyzed through ROC curves based on both ChemPLP score values and its normalized forms using number of heavy atoms (N) to prevent biasing towards large molecules,

$$S_{normalized} = \frac{S}{N^a} \quad (3.11)$$

where the power  $a$  is taken as 1/10, 1/3, 1/2, 3/4 and 1 as shown in the equation 11 (Pan *et al.*, 2003).

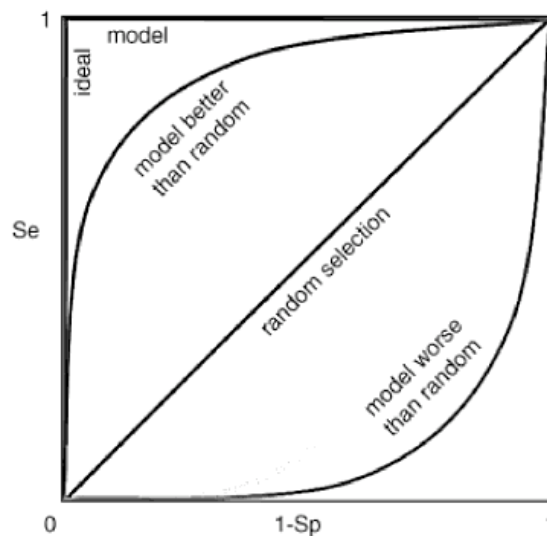


Figure 3.4. ROC curve model (Sottriffer, 2006).

In order to provide a value for enrichment comparison than the visual analysis, for each ROC curve, AUC (Area Under the ROC Curve) values were also calculated. The AUC value can be calculated by the following equation 12;

$$AUC = \sum_i [(Se_{i+1})(Sp_i - Sp_{i+1})] \quad (3.12)$$

The AUC value is limited between 0 and 1. An AUC value of 0.5 represents a random prediction, thus, an AUC value of > 0.5 indicates predictions better than random. The higher AUC value means a higher early recognition of active compounds. The AUC values of 0.5-0.7 are considered to represent poor model performance while values of 0.7-0.9 are considered moderate.

## Chapter 4

### Results and Discussions

#### 4.1. Key Residues at the Ligand-Binding Site

As the intracellular loop 3 (ICL3) links the transmembrane helices V and VI (TM5 and TM6), and the size of the ligand-binding site is identified by the positioning of the TM5, TM6 and TM7, ICL3 has an important role in the allosteric mechanism of the receptor which was previously revealed in a simulation study conducted by Ozgur *et al.* (Ozgur, Doruker and Akten, 2016) through applying specific distance restraints between key residues at the ligand-binding site. These restraints helped us to understand the correlation between the changes at the extracellular ligand-binding site and its effect on the conformational change of the lower half (intracellular) of the receptor, which consists of ICL3 and the G protein-binding site. These restrained distances between Asp113 located on TM3 and Ser203, Ser204, Ser207 located on TM5, Phe289 and Asn293 located on TM6 and Asn312 located on TM7 were shown as in Figure 4.1 adopted from the work by Ozgur *et al.* (Ozgur, Doruker and Akten, 2016).

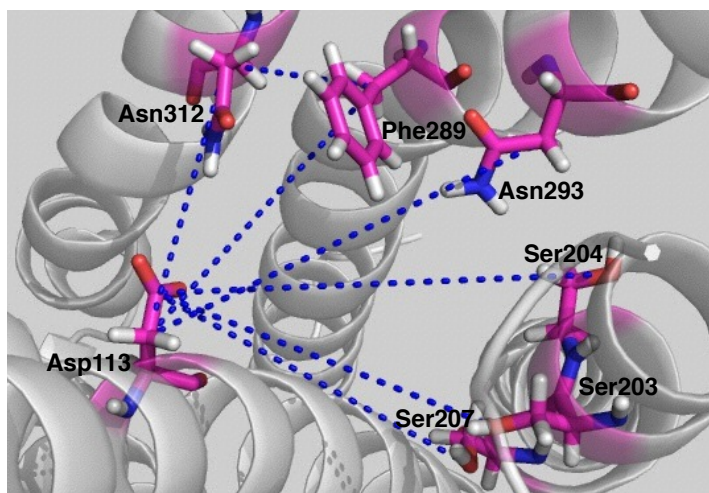


Figure 4.1. The key residues at the ligand-binding site and the distance restraints between these seven residues (Ozgur, Doruker and Akten, 2016).

Especially, Asp113 on TM3 and Ser207 on TM5 are the two important residues at the ligand-binding site, due to the fact that the distance between these residues greatly influences the binding capability of the ligand. They form multiple hydrogen bonds and/or close contacts with ligands where Ser207 interacts with the ligand's aromatic ring and Asp113 with the polar end of the ligand. The distance range of experimental measurements between the two side chain atoms, O $\gamma$  atom of Ser207 and C $\gamma$  atom of Asp113 is 8 Å to 10 Å when the receptor is in its active state, while the receptor changes its conformation to inactive state the distance is around 11 Å to 12 Å (Simpson *et al.*, 2011).

The very inactive state of the receptor was characterized by a further movement of the lower half of TM6 towards the receptor core, and simultaneous close packing of ICL3 underneath the membrane completely blocking the G-protein binding site. All together, the extracellular ligand-binding site expands with the increasing distance between Ser207 and Asp113. In the MD conformers this distance varies from 8.3 Å up to 16.7 Å as shown in Figure 4.2 and more detailed results are provided in Appendix B. Most of the MD snapshots have higher distances than the experimentally known inactive structures.

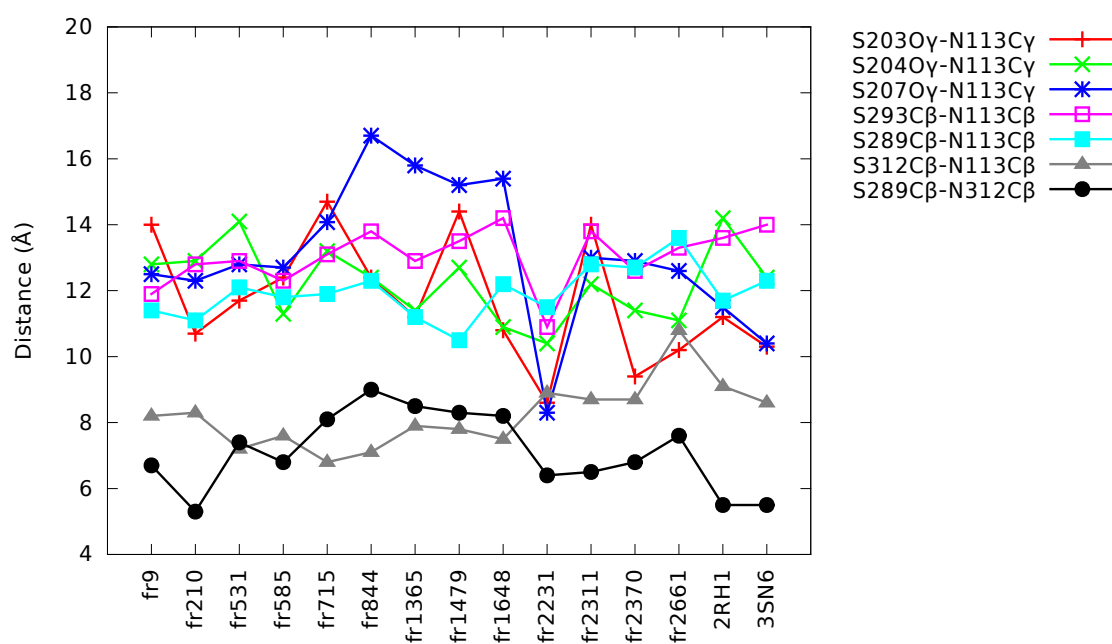
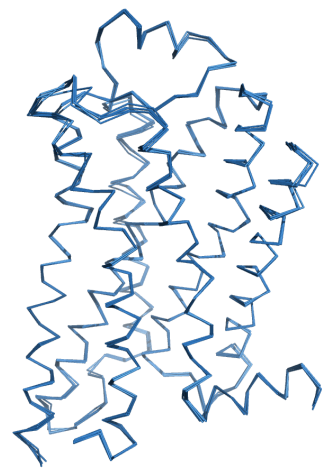


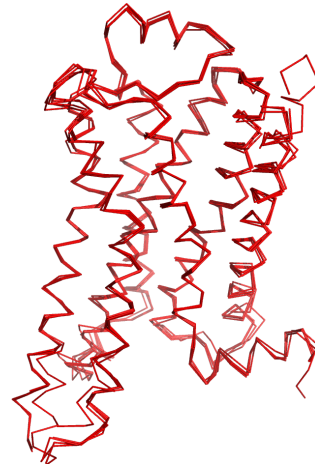
Figure 4.2. The distance plot of the MD conformers between key residues at the ligand binding site. Both inactive and active x-ray structures (PDB ids: 2RH1 and 3SN6) also added for comparison.

## 4.2. Evaluation of the Classification Protocol

A total of eleven crystal structures of  $\beta_2$ AR of which five represent inactive (PDBids: 2RH1, 3D4S, 3NYA, 3NY8, 3NY9) (Figure 4.3) and six represent active states (PDBids: 3POG, 3SN6, 4LDE, 4LDL, 4LDO, 4QKX) (Figure 4.3) were used as targets to their experimentally known ligands carazolol, ICI 118;551, a novel compound (JSZ), alprenolol, timolol, BI-167107 (POG), hydroxybenzylisoproterenol (XQC) and epinephrine (see Figure 4.4) in order to bring out the ability of scoring functions to distinguish active states from inactive states. AutoDock, GOLD with three scoring functions ChemPLP, GoldScore and ChemScore, two rescoring functions DSX-CSD and DSX-PDB and finally the Glide software tool with Glide XP (extra precision) scoring function were selected to perform the dockings.



**5 superimposed inactive X-ray:**  
*2rh1, 3ny8, 3ny9, 3nya, 3d4s*



**6 superimposed active X-ray:**  
*3p0g, 3sn6, 4ldl, 4ldo, 4ldl, 4qxc*

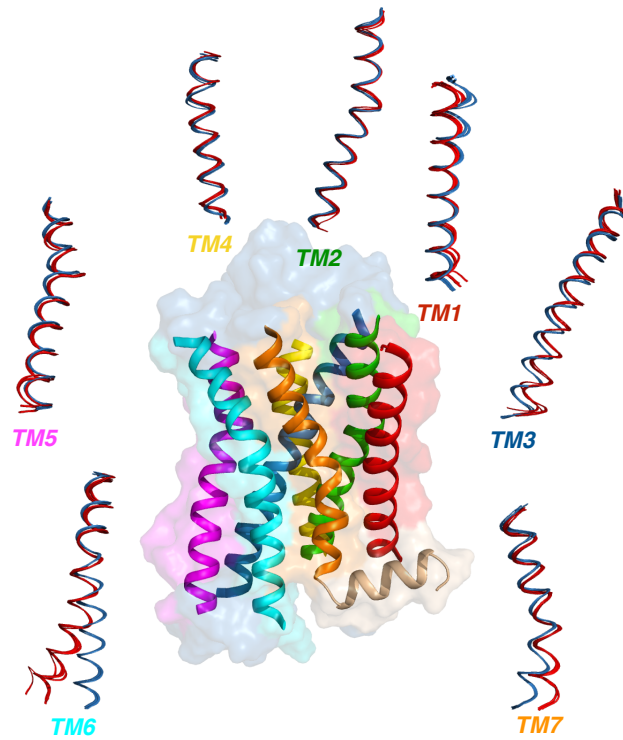


Figure 4.3. X-ray snapshots of inactive (blue) and active (red) states aligned and seven transmembrane helices.

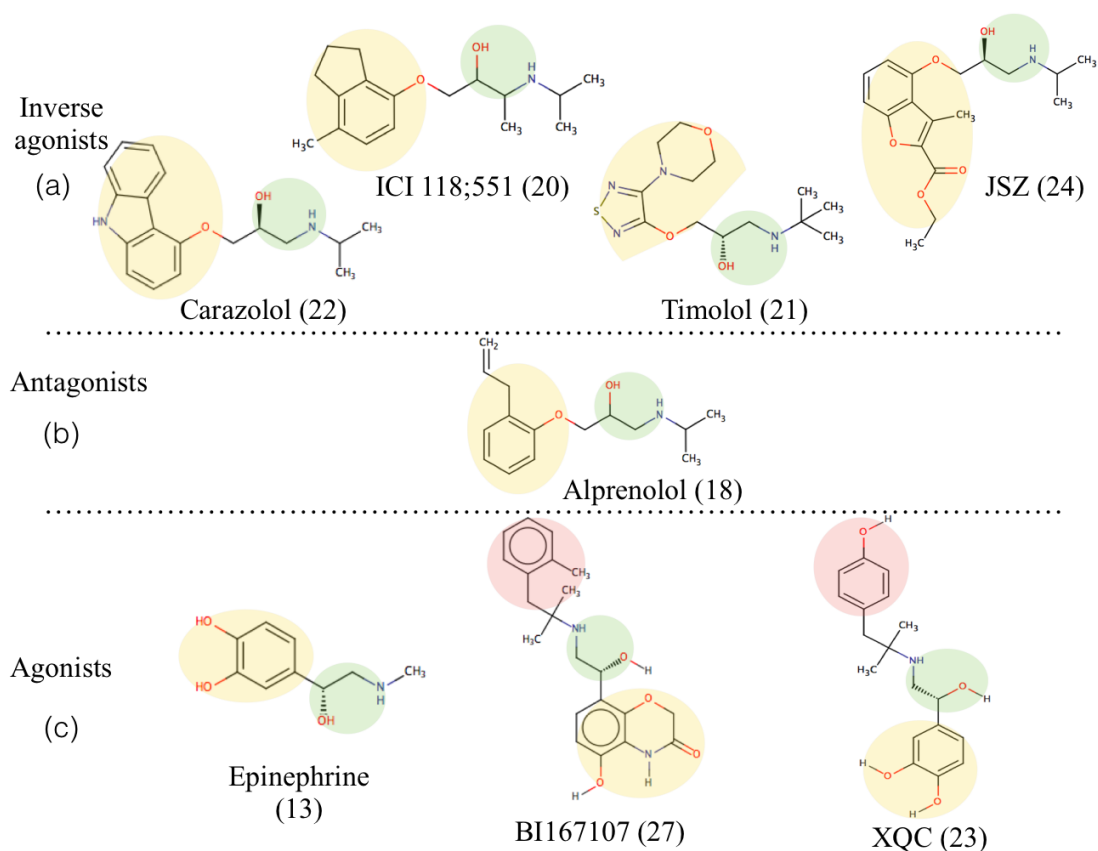


Figure 4.4. Molecular schemes of the ligand molecules that are known and used in crystal structures. (a) Four inverse agonists carazolol (PDB id: 2RH1), ICI 118;551 (PDB id: 3NY8), timolol (PDB id: 3D4S) and a novel molecule (PDB id: 3NY9). (b) Antagonist molecule alprenolol (PDB id: 3NY8). (c) Three agonists epinephrine (PDB id: 4LDO), BI167107 (PDB id: 3P0G) and XQC (hydroxybenzylisoproterenol) (PDB id: 4LDL). Yellow circle: ring (I), Green circle: ethanolamine, Red circle: ring (II). The numbers next to ligand names indicate number of heavy atoms.

Each ligand was docked to its own receptor in the complex crystal structure and also cross-docked to the other ten crystal structures. A classification protocol (see Figure 4.5) was applied for the docking results based on their activity state. The poses with the highest score value (best pose) were selected and evaluated based on their vicinity to five key residues at the ligand-binding site. The best pose should interact with either Asp113 (TM3) or Asn312 (TM7) on one side, and with Ser203 or Ser204



or Ser207 (TM5) on the other side of the binding pocket (See Figure 4.6). The poses that were not in this neighborhood were simply discarded and the remaining ones were sorted based on their score values. Conformers that were found in the top five were evaluated based on their activity state.

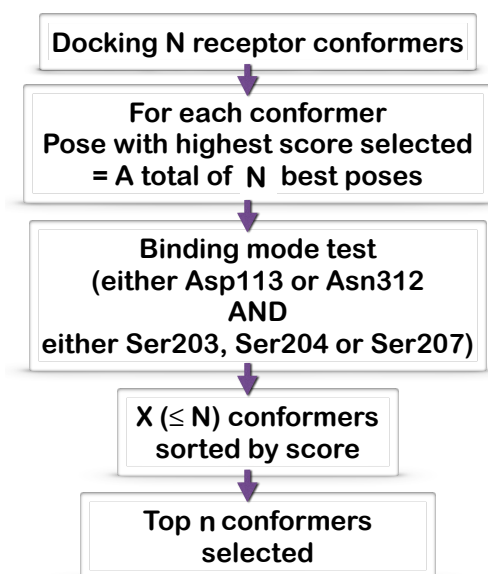


Figure 4.5. The binding protocol used for classification.

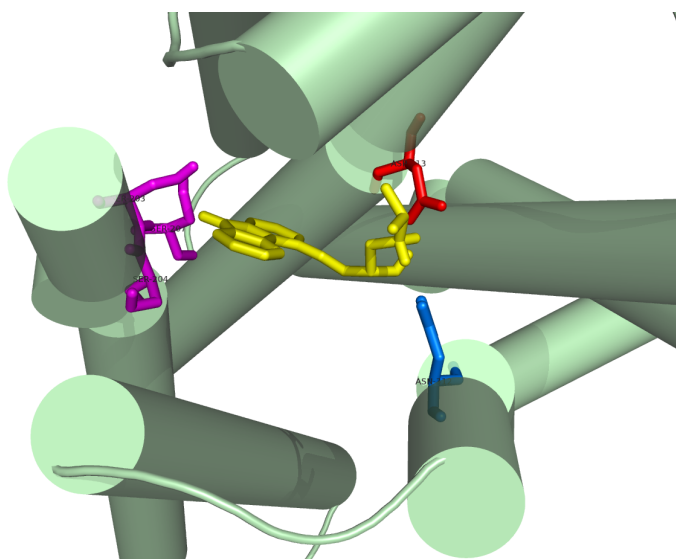


Figure 4.6. Ligand interactions at the binding site. The interactions of inverse agonist carazolol (PDBid: 2RH1) with the five key residues. It fits the binding protocol by interacting with Serines (pink) with the aromatic head group while interacting with Asp312 (blue) and Asp113 (red) on the other side.

Carazolol is one of the experimentally known inverse agonists which preferentially binds to the inactive state of the receptor. The binding results of carazolol were significant as shown in Table 4.1 in which the top five consists solely of inactive states of the receptor in all seven scoring functions. Similar calculations for the remaining ligands (ICI 118;551, a novel compound (JSZ), alprenolol, timolol, BI-167107, XQC, epinephrine) were performed and their corresponding tables with ranked structures were provided in Appendix C.

Table 4.1. Binding results of the inverse agonist carazolol docked to 11 crystal structures sorted by their score values in decreasing order. The active states are shown in red and inactive states are shown in blue.

Rank	Auto Dock	Chem PLP	Gold Score	Chem Score	DSX/ CSD	DSX/ PDB	Glide
1	3D4S	2RH1	3D4S	3NYA	2RH1	3D4S	2RH1
2	2RH1	3D4S	2RH1	2RH1	3D4S	2RH1	3D4S
3	3NY9	3NY9	3NYA	3NY9	3NYA	3NY9	3NYA
4	3NYA	3NYA	3NY8	3D4S	3NY9	3NYA	3NY9
5	3NY8	3NY8	3NY9	3NY8	3NY8	3NY8	3NY8
6	3SN6	4LDL	3SN6	3POG	3SN6	3SN6	
7	3POG	3SN6	4LDE	4LDE	4LDE	4LDE	
8	4LDO	4LDE		3SN6	4QKX	4LDL	
9	4LDE				4LDO	4QKX	
10					3POG	3POG	
11					4LDL	4LDO	

Finally, all docking results were summarized as in Table 4.2 which shows the number of active states found in top five if the ligand is an agonist or if the ligand is an inverse agonist or antagonist, the number of inactive states found in top five. Accordingly, AutoDock and GOLD/ChemPLP were found to be the most successful scoring function with 37 conformers (out of 40) with correct states placed in the top five, while GOLD/GoldScore showed the weakest performance (29 conformers out of 40). On the other hand, when the same docking results were evaluated according

to the docked ligand, ICI 118;551 had the least amount of correct predictions in top five (only 16 out of 35), which might indicate that its specificity is not very strong.

Table 4.2. Binding results of the eight ligands with crystal structures. If the ligand is agonist, results are corresponding to the number of active states found or if the ligand is an inverse agonist or antagonist it corresponds to the number of inactive states.

Efficacy	Ligand	Auto-Dock	Chem PLP	Gold Score	Chem Score	DSX/CSD	DSX/PDB	Glide	Total
Inverse Agonist	Carazolol	5	5	5	5	5	5	5	35
	ICI 118;551	4	3	0	2	1	3	3	16
	JSZ	5	5	5	5	5	5	4	34
	Timolol	4	5	4	3	5	5	4	30
Antagonist	Alprenelol	4	5	1	3	3	4	2	22
Agonist	BI-167107	5	4	5	3	3	3	5	28
	XQC	5	5	4	5	5	5	5	34
	Epinephrine	5	5	5	5	5	5	5	35
	<b>TOTAL</b>	<b>37</b>	<b>37</b>	29	31	32	<b>35</b>	<b>33</b>	

To summarize, among seven different scoring functions, four of them (AutoDock, ChemPLP, DSX-PDB and Glide XP) were relatively successful in ranking the correct state in top five therefore they were selected to proceed further docking analysis of MD conformers.

### 4.3. Docking Experiments of MD Conformers

After the elimination of scoring functions, six new molecules with known activities were also added to the ligand list; four antagonists (nebivolol, carvediolol, esmolol and butaxamine) and two agonists; one of them is long-acting agonist (formoterol), the other is a short-acting agonist (salbutamol) as shown in Figure 4.7. However, these ligands do not have any resolved structures and this enables us to further

evaluate the classification scheme in distinguishing the active states from the inactive ones. These new ligands were docked to eleven crystal structures using only four most successful scoring functions, AutoDock, ChemPLP, DSX-PDB and Glide XP.

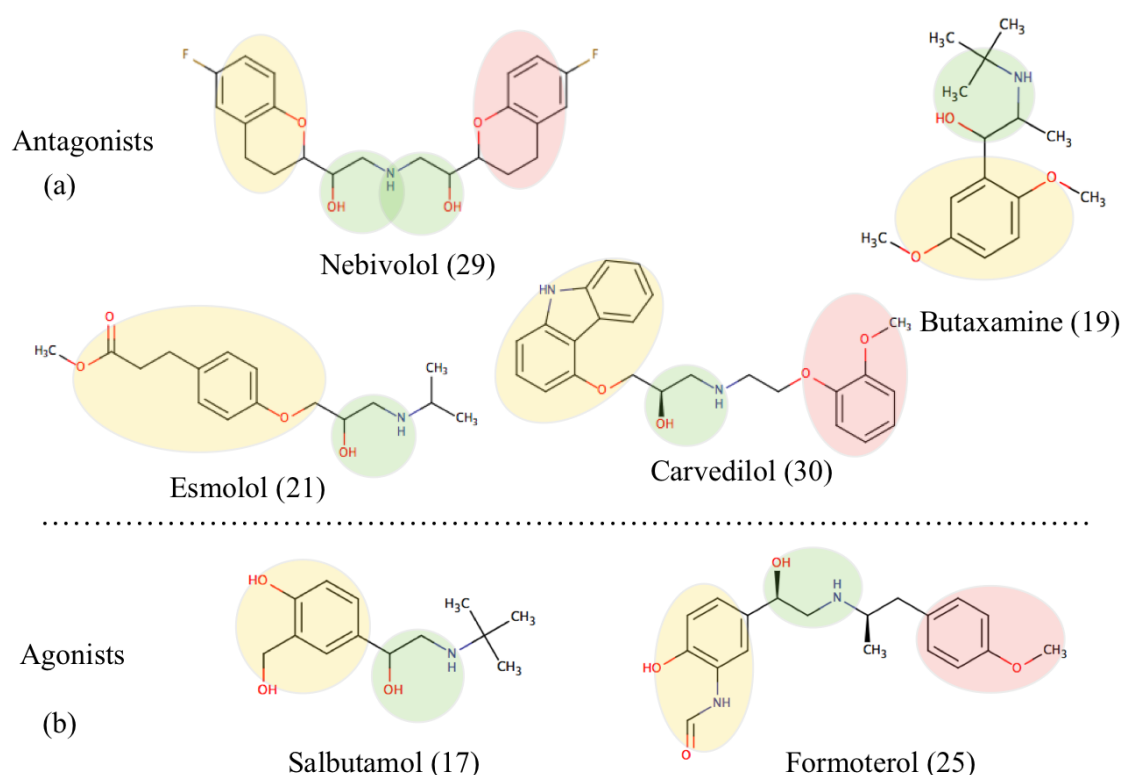


Figure 4.7. Molecular schemes of the additional ligands with known activities. (a) Four antagonists nebivolol, carvedilol, butaxamine and esmolol. (b) Two agonists salbutamol and long acting formoterol. Yellow circle: ring (I), Green circle: ethanolamine, Red circle: ring (II). The numbers next to ligand names indicate number of heavy atoms.

The summary of all the ligands' docking results is given in Table 4.3 which shows the number of states in top five with correct activity state, i.e., active if the ligand is agonist and inactive if the ligand is an inverse agonist and/or antagonist. Accordingly, butaxamine which is one of the antagonists in the list was found to be the least successful in distinguishing inactive states from the active states, and was

discarded from the ligand list for further docking analysis of MD conformers. The most successful case was the inverse agonist carazolol, which predicted all inactive states in top five in all docking experiments. Alternatively, the same docking results were presented using the target structure in the column, which receives a tick mark if that crystal structure was seen in top five in all four docking results (See Table 4.4). Although ICI118;551 only selected one of the inactive crystal structures (3D4S), most of the ligands selected the structure with the activity state that matches the ligand efficacy. On the other hand, in Table 4.4 esmolol was not selected by any crystal structure and was discarded from the ligand list. This results both support the reliability of the classification scheme and the docking tools as well.

Table 4.3. Docking results of the crystal structures with all the ligands.

Biological Effect	Ligand	AutoDock	ChemPLP	DSX/PDB	Glide	Total
Inverse Agonist	Carazolol	5	5	5	5	20
	Timolol	4	5	5	4	18
	ICI	4	3	3	3	13
	JSZ	5	5	5	4	19
Antagonist	Alprenolol	4	5	4	2	15
	Nebivolol	3	4	4	4	15
	Butaxamine	0	3	1	4	8
	Esmolol	4	0	5	5	14
	Carvedilol	5	3	3	4	15
Agonist	Formoterol	5	5	5	3	18
	Salbutamol	5	5	5	4	19
	XQC	5	5	5	5	20
	BI167107	5	4	3	5	17
	Epinephrine	5	5	5	5	20
	TOTAL	59	57	58	57	

Table 4.4. Docking results of the crystal structures. First five (2RH1, 3NY8, 3NY9, 3NYA, 3D4S) are inactive and last six (3P0G, 3SN6, 4LDO, 4LDE, 4LDL, 4QKX) are active conformations of the receptor.

Mechanism of Action	Ligand Name	2RH1	3NY8	3NY9	3NYA	3D4S	3P0G	3SN6	4LDO	4LDE	4LDL	4QKX
Inverse Agonist	Carazolol	✓	✓	✓	✓	✓						
	Timolol	✓		✓	✓	✓						
	JSZ		✓	✓	✓	✓						
	ICI					✓						
Antagonist	Alprenolol	✓				✓						
	Nebivolol			✓		✓						
	Esmolol											
	Carvedilol			✓		✓						
Agonist	Formoterol						✓			✓		
	Salbutamol						✓	✓		✓		
	XQC						✓		✓		✓	✓
	BI167107							✓		✓		
	Epinephrine						✓		✓			✓

Finally, each one of the thirteen ligands was docked to thirteen MD conformers. The same classification protocol was applied to determine the most favorable receptor conformation for each ligand, and the MD conformers that are present in all four scoring functions and in top five were selected to represent the most favorable conformational state for that ligand molecule.

Docking results of agonists were listed in Table 4.5. Since MD conformers represent the inactive state of the receptor, epinephrine showed no preference in any of the MD frames, as expected. On the other hand, frame1365 was selected by three out of five agonists, which might indicate an active-like state of the receptor. Finally, frame210 was favored by the potent selective agonist salbutamol.

Table 4.5. Docking results of MD conformers with agonists.

Efficacy	Ligand	Rank	AutoDock	ChemPLP	DSX/PDB	Glide
Agonist	Salbutamol	1	fr210	fr1479	fr9	fr210
		2	fr531	fr531	fr715	fr715
		3	fr585	fr1365	fr1648	fr2311
		4	fr1648	fr1648	fr1365	fr1365
		5	fr2231	fr210	fr210	fr844
	Formoterol	1	fr210	fr844	fr9	fr844
		2	fr1365	fr1365	fr1365	fr2311
		3	fr715	fr2661	fr844	fr1365
		4	fr2370	fr1648	fr210	fr210
		5	fr531	fr2311	fr715	fr1648
	BI167107	1	fr1648	fr844	fr1365	fr844
		2	fr1365	fr1365	fr1648	fr2311
		3	fr210	fr1479	fr715	fr1365
		4	fr715	fr1648	fr844	fr1479
		5	fr531	fr2311	fr210	fr2661
	XQC	1	fr1365	fr1365	fr1648	fr715
		2	fr210	fr844	fr210	fr2311
		3	fr1648	fr9	fr531	fr844
		4	fr715	fr2370	fr1365	fr1365
		5	fr531	fr1648	fr715	fr1648
	Epinephrine	1	fr210	fr210	fr715	fr531
		2	fr531	fr585	fr2231	fr715
		3	fr2231	fr1365	fr531	fr1365
		4	fr585	fr2661	fr585	fr210
		5	fr715	fr1648	fr1365	fr1648

Among thirteen MD conformers, eight of them were selected by at least one ligand. Frame531 and frame715 were found only in inverse agonists (see Table 4.6), frame844 and frame9 were selected only by antagonists (see Table 4.7), while frame1365 and frame210 were selected only by agonists (see Table 4.5). Also, frame585 was selected both by an inverse agonist and an antagonist. Unexpectedly, frame1648 showed preference to ligands from all three categories; two inverse agonists (carazolol and alprenolol), one antagonist (JTZ) and surprisingly one agonist (XQC). Similar representation of the docking results based on target conformers is provided in Table 4.8.

Table 4.6. Docking results of MD conformers with inverse agonists.

Efficacy	Ligand	Rank	AutoDock	ChemPLP	DSX/PDB	Glide
Inverse Agonist	Carazolol	1	fr1365	fr1365	fr1648	fr715
		2	fr1648	fr715	fr715	fr1648
		3	fr715	fr1648	fr9	fr531
		4	fr531	fr9	fr210	fr1365
		5	fr2231	fr844	fr531	fr2231
	ICI	1	fr531	fr1365	fr1648	fr585
		2	fr9	fr1479	fr585	fr9
		3	fr585	fr1648	fr210	fr2370
		4	fr210	fr585	fr9	fr210
		5	fr1365	fr844	fr844	fr1479
	JSZ	1	fr2231	fr1648	fr1648	fr715
		2	fr1365	fr844	fr210	fr1648
		3	fr1479	fr1479	fr9	fr1479
		4	fr1648	fr9	fr531	fr2311
		5	fr531	fr715	fr1365	fr9
	TIM	1	fr1648	fr1648	fr1648	fr531
		2	fr1365	fr1365	fr531	fr715
		3	fr844	fr844	fr9	fr9
		4	fr531	fr9	fr715	fr2311
		5	fr2231	fr531	fr1365	fr2231

Table 4.7. Docking results of MD conformers with antagonists.

Efficacy	Ligand	Rank	AutoDock	ChemPLP	DSX/PDB	Glide
Antagonist	JTZ	1	fr210	fr1648	fr1648	fr715
		2	fr585	fr531	fr210	fr1648
		3	fr1648	fr210	fr585	fr1365
		4	fr715	fr585	fr1365	fr585
		5	fr9		fr9	fr9
	Nebivolol	1	fr210	fr1648	fr844	fr2311
		2	fr9	fr844	fr715	fr844
		3	fr844	fr2311	fr2370	fr1365
		4	fr2370	fr2231	fr531	fr1648
		5	fr715	fr1479	fr9	fr2370
	Carvedilol	1	fr1648	fr1365	fr1648	fr2661
		2	fr844	fr1648	fr9	fr844
		3	fr1365	fr2231	fr585	fr9
		4	fr2231	fr844	fr844	fr1365
		5	fr9	fr9	fr210	fr2311



Table 4.8. Docking summary of the 9 successful MD conformers. Blue ones were selected by at least one inverse agonist, yellow ones were selected by only antagonists while orange ones were selected by only agonists. Green one was selected from all categories.

Mechanism of Action	Ligand Name	Frame531	Frame585	Frame715	Frame1648	Frame9	Frame844	Frame210	Frame1365
Inverse Agonist	Carazolol			✓	✓				
	Timolol	✓							
	JSZ				✓				
	ICI		✓						
Antagonist	Alprenolol		✓		✓				
	Nebivolol			✓			✓		
	Carvedilol					✓	✓		
Agonist	Formoterol								✓
	Salbutamol							✓	
	XQC				✓				✓
	BI167107								✓
	Epinephrine								

If we take a closer look at frame1648 as shown in Figure 4.8, only agonist molecule hydroxybenzylisoproterenol (XQC) interact with hydrogen bonds between Ser203 on TM5 and its aromatic head group, whereas inverse agonists and antagonists only interact via close contacts with three Serines (S203, S204 and S207) on TM5. On the other hand, only inverse agonists have made close contacts with both Trp286 and Phe289 residues on TM6, as this is a common behavior for inverse agonists. All ligands have formed hydrogen bonds at least with one of the Asp113 or Asn312 residues in frame1648. Moreover, if we compare their binding scores, carazolol (Figure 4.4a) has the highest affinity with the -9.46 kcal/mol AutoDock score value. Remaining ones have the following score values; -9.19 kcal/mol for XQC (Figure 4.4c), -8.64 kcal/mol for JSZ (Figure 4.4a), -7.42 kcal/mol for alprenolol (Figure

4.4b). The number next to the ligand names is the number of heavy atoms in that ligand.

The chemical structure of a ligand defines its interactions with the receptor, i.e., it defines its pharmacological properties and also affects the overall dynamics of the receptor. For example, polar interactions with Ser203 and Ser207 located on TM5 are important to maintain the active state of the receptor, and it's specific to agonist molecules. Generally, agonists form hydrogen bonds with TM5 and rarely interact through hydrophobic interactions. However, antagonists mostly have non-polar, hydrophobic interactions with TM5 and TM6 while inverse agonists have non-polar interactions with TM6. These interactions stabilize the extracellular core of the receptor while resulting in a smaller intracellular ligand-binding pocket with less water. Even though we have frames that are close to the inactive state, agonist molecules can strongly bind to residues on TM5 since they form hydrogen bonds with Ser203 and Ser207 residues with their aromatic rings. Details of the interactions are provided in Appendix D.

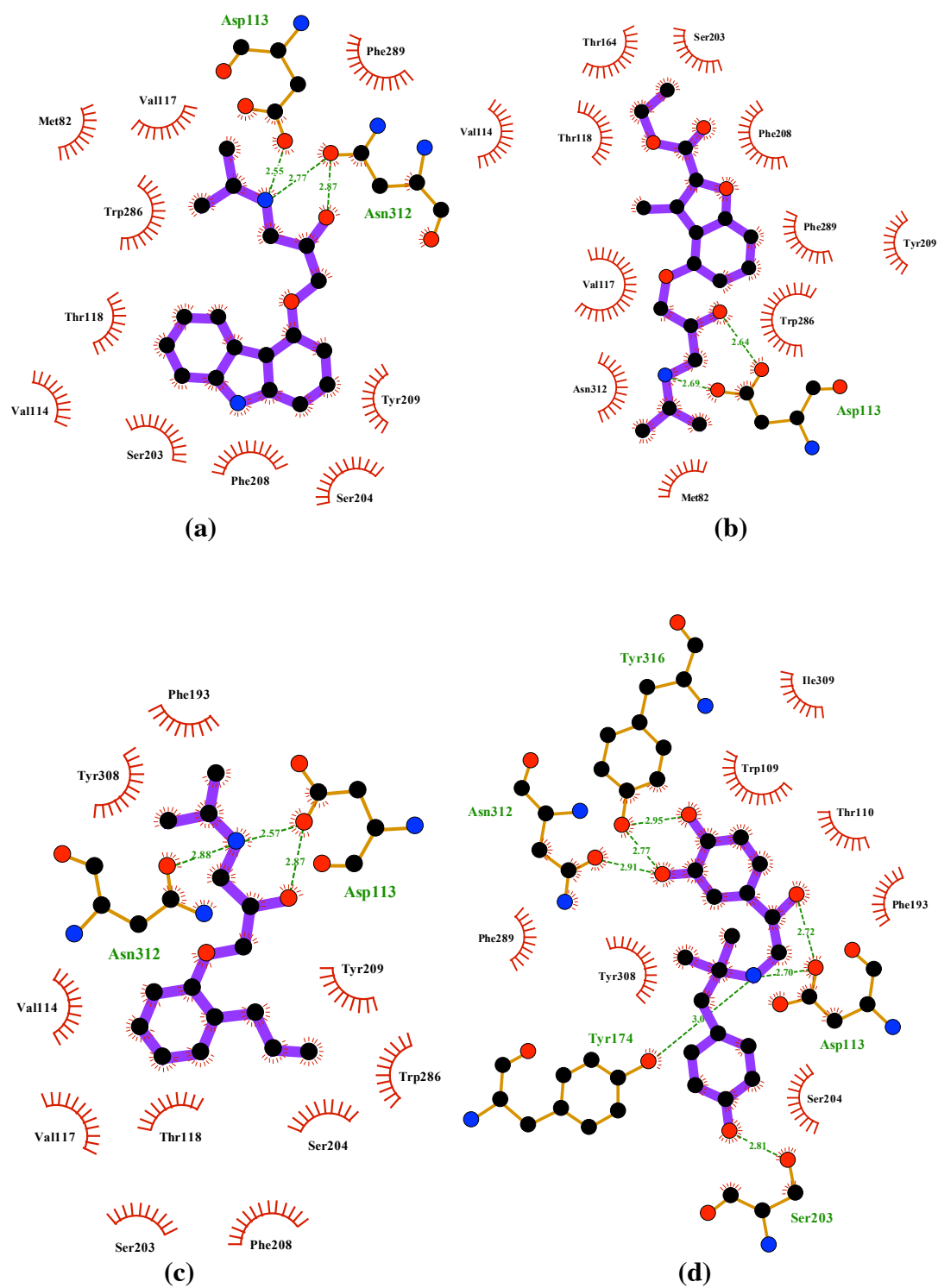


Figure 4.8 Ligand interactions of frame1648. The poses are from AutoDock results for (a) carazolol, (b) JSZ, (c) alprenolol, (d) XQC. Ligands are shown in purple and hydrogen bonds are shown in green connecting dots.

When we compare the binding score values of MD conformers and crystal structures, frames had lower score values than crystal structures with a few exceptions. Detailed score table of the inverse agonist JSZ is shown in Table 4.9 and the same tables were also created for each ligand and provided in Appendix E. In Table 4.9, if we look at the top eleven since we have 11 crystal structures, we can see that frame1648 and frame1479 were placed within top eleven in at least three of the scoring functions. Moreover, these two MD frames had higher ranks than active state structures in most of the docking experiments.

The reason that crystal structures higher score values than most of the MD conformers in docking experiments is that the crystal structures represent the most thermodynamically stable state induced by a ligand molecule. However, MD frames are optimized without any ligand molecule, therefore its side chains are not found at their most optimum orientation for interacting with a ligand.

Table 4.9. Binding results of a novel inverse agonist molecule (JSZ). Bold characters representing the active states of the receptor, italic characters representing the MD frames. MD conformers that are found in top 11 are colored.

Rank	ChemPLP	AutoDock	DSX/PDB	Glide
1	3D4S 93.64	3NY9 -10.66	2RH1 -143.3	3NY8 -11.91
2	3NY9 92.74	2RH1 -10.62	3NYA -140.7	3NY9 -10.85
3	3NYA 89.53	3D4S -10.53	3NY9 -139.0	<b>3SN6</b> -10.75
4	2RH1 83.36	3NYA -10.36	3D4S -138.6	3NYA -10.74
5	3NY8 83.30	3NY8 -10.13	3NY8 -134.2	3D4S -10.66
6	<i>fr1648</i> 81.68	<i>fr2231</i> -8.94	<i>fr1648</i> -125.2	2RH1 -10.48
7	<i>fr844</i> 79.97	<i>fr1365</i> -8.83	<i>fr210</i> -116.7	<i>fr715</i> -10.47
8	<i>fr1479</i> 78.18	<i>fr1479</i> -8.68	<i>fr9</i> -116.7	<i>fr1648</i> -9.48
9	<i>fr9</i> 77.68	<i>fr1648</i> -8.64	<b>4QKX</b> -111.6	<i>fr1479</i> -8.73
10	<i>fr715</i> 74.34	<i>fr531</i> -8.60	<b>4LDO</b> -110.9	<b>4LDE</b> -7.71
11	<i>fr1365</i> 71.28	<b>4LDO</b> -8.39	<b>3SN6</b> -110.6	<b>4LDL</b> -7.66
12	<i>fr2311</i> 62.86	<i>fr844</i> -8.38	<i>fr531</i> -109.0	<i>fr2311</i> -7.30
13	<i>fr531</i> 62.84	<i>fr585</i> -8.34	<i>fr1365</i> -108.3	<i>fr9</i> -7.28
14	<i>fr2661</i> 57.44	<i>fr2311</i> -8.21	<i>fr2231</i> -103.7	<i>fr2370</i> -7.16
15	<i>fr585</i> 56.40	<i>fr210</i> -8.18	<i>fr715</i> -103.4	<i>fr2231</i> -6.26
16	<i>fr210</i> 51.49	<i>fr715</i> -8.18	<i>fr2370</i> -102.7	<i>fr585</i> -6.19
17		<b>3POG</b> -8.17	<i>fr2311</i> -100.6	<i>fr210</i> -3.76
18		<i>fr9</i> -8.16	<b>3POG</b> -99.25	<i>fr531</i> -3.55
19		<b>4LDL</b> -8.13	<i>fr585</i> -94.94	
20		<b>3SN6</b> -8.01	<i>fr2661</i> -90.89	
21		<i>fr2661</i> -7.46		

#### 4.3.1. Salbutamol Binding

Salbutamol is a known short-acting agonist and is used to treat asthma. In Figure 4.9, it perfectly binds to active state crystal structure 3SN6 with -8.33 kcal/mol AutoDock score value forming hydrogen bonds with four of the key residues (Ser203, Ser207, Asn312 and Asp113) and additionally making close contacts with nine residues. On the other hand, frame210, which was selected by salbutamol as the most preferred conformation has -7.34 kcal/mol AutoDock score value and forms hydrogen bonds with two residues only, Asp113 and Thr118 located on TM3, while making close contacts with nine residues including S207.

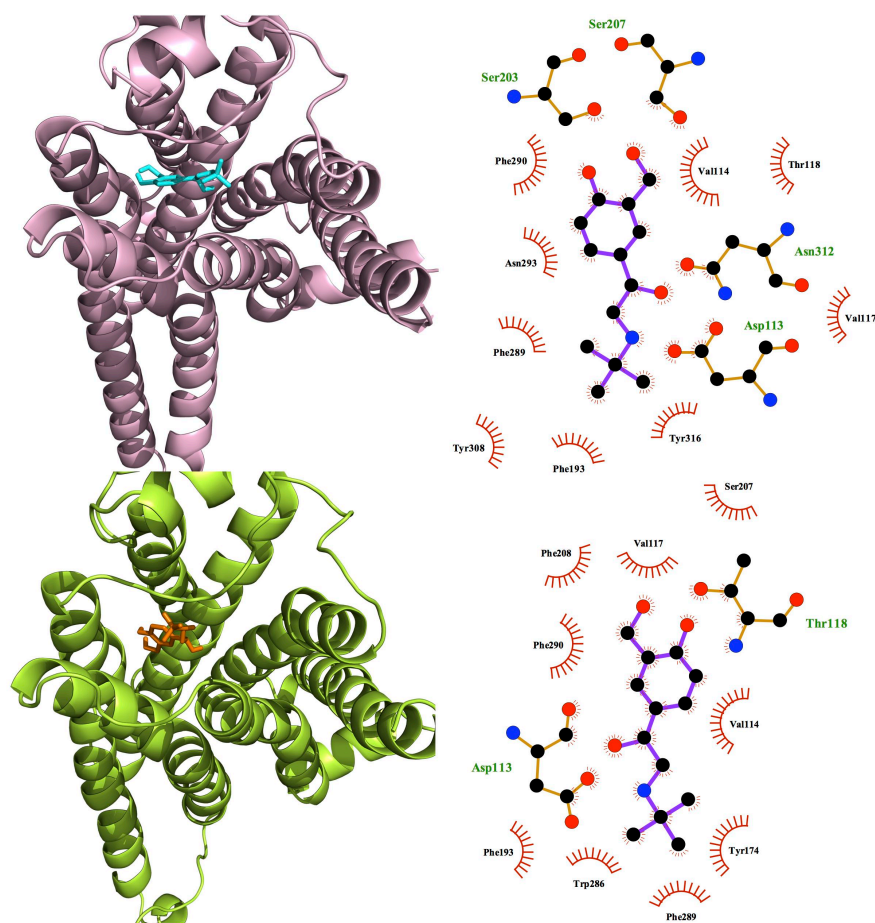


Figure 4.9. Extracellular view of active crystal structure 3SN6 (pink), frame210 (green) with the best poses of short-acting agonist salbutamol from AutoDock results. The residue interactions have shown right next to each figure.

### 4.3.2. Alprenolol Binding

Alprenolol is one of the antagonists used as anti-arrhythmic agent with a minor effect on  $\beta_2$ ARs. In figure 4.10, best poses are shown and their AutoDock scores are -8.59 kcal/mol for 3NYA, -7.61 kcal/mol for frame585 and -7.42 kcal/mol for frame1648. However, in comparison with inactive structure 3NYA, frame1648 has more hydrogen bonds at the binding site (with Asp113 and Asn312). Frame585 has one hydrogen bond with one of the key residues (Asp113), as in the inactive structure. All of them have a common interaction on TM3, TM5 and TM6.

### 4.3.3. Carazolol Binding

When we take a closer look into the docked state of the partial inverse agonist carazolol in the inactive crystal structure (PDB id: 2RH1) and in the two preferred MD frames (frame715 and frame1648), we see some differences in the interaction network. With the inactive crystal state (PDB id: 2RH1), carazolol forms hydrogen bonds with two of the key residues Asn312 and Asp113 with its polar end and Ser203 with its aromatic ring end while making a close contact with Ser207 having -11.00 kcal/mol AutoDock score value and 12 close contacts in total (Figure 4.11). Frame1648 has -9.46 kcal/mol score value and it is binding almost similarly to this initial pose while having a very close score value. It forms hydrogen bonds with two of the key residues Asn312 and Asp113 as in the crystal structure while making a close contact with both Ser203 and Ser204 with its aromatic end. It makes 10 close contacts in total. Lastly frame715 has -9.37 kcal/mol AutoDock score and forms hydrogen bond with one of the key residues Asp113 while making a close contact with Asn312 and with Ser204 on the other side (see Figure 4.11). It has the highest number of close contacts which is 14.

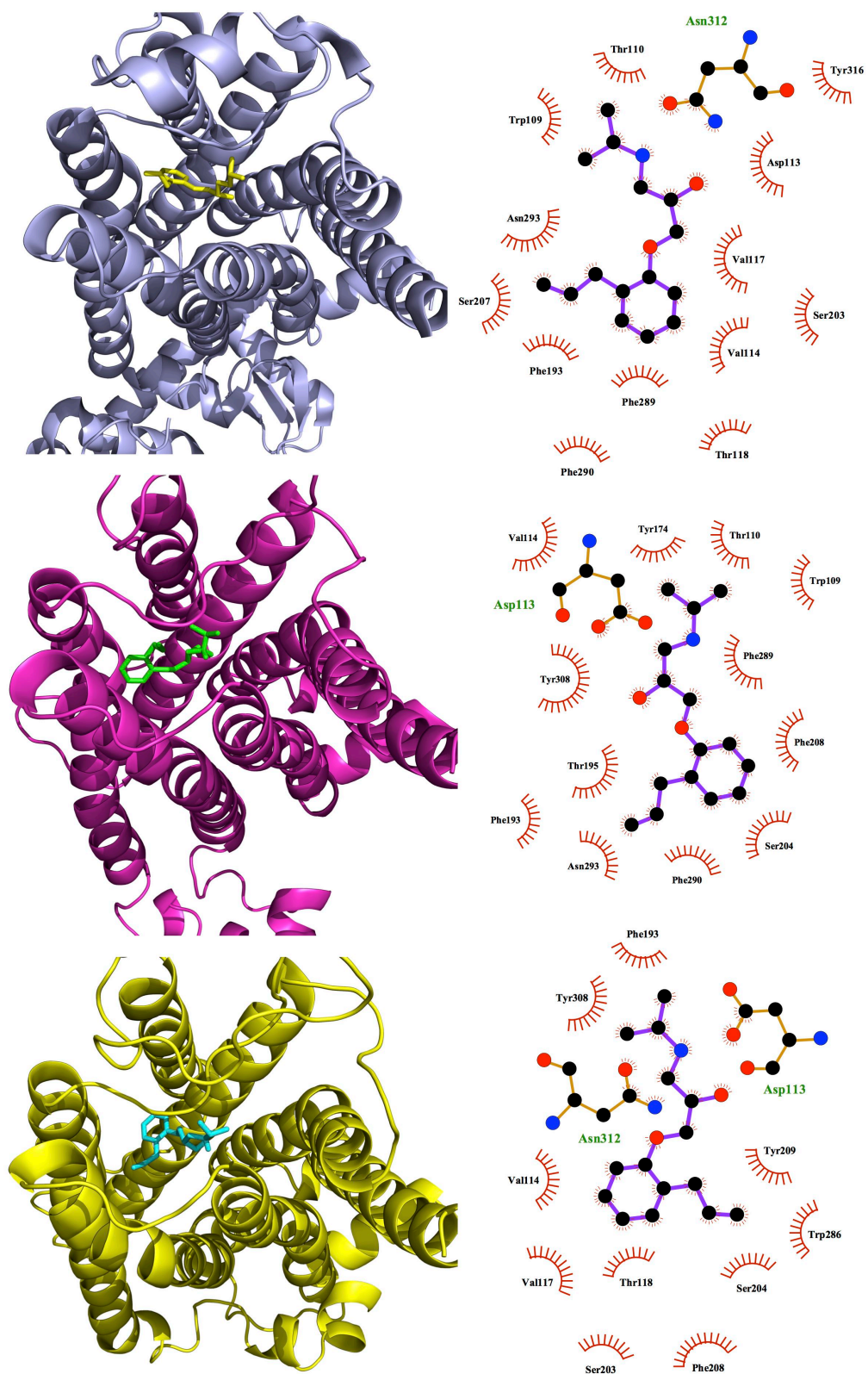


Figure 4.10. Extracellular view of inactive crystal structure 3NYA (purple), frame585 (pink) and frame1648 (yellow) with the best poses of antagonist alprenolol from AutoDock results. The residue interactions have shown right next to each figure.



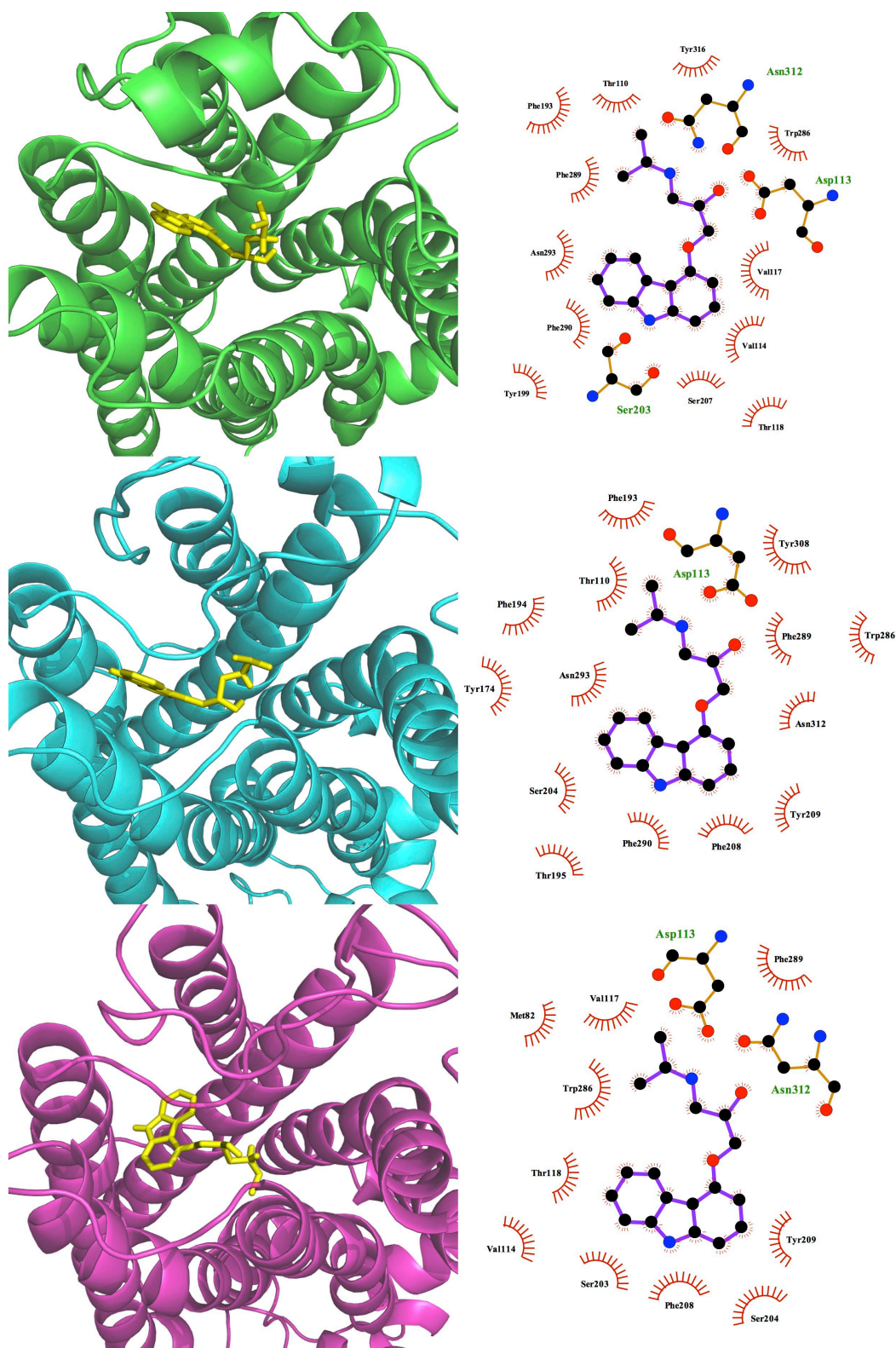


Figure 4.11. Extracellular view of inactive crystal structure 2RH1 (green), MD frames 715 (blue) and 1648 (pink) with the best poses of inverse agonist carazolol from AutoDock results. The residue interactions have shown right next to each figure.

#### 4.4. Virtual Screening Experiments

In order to validate how well our eight MD frames in discriminating antagonists and inverse agonists from agonists, a small database composed of 31 agonists and 26 antagonists/inverse agonists was screened using GOLD/ChemPLP scoring function. ROC (Receiver Operating Characteristic) curves for each screening were determined and AUC (Area Under ROC Curve) values were calculated for each normalized score value. Here the *x*-axis indicates the percentage of false positives, which represent the percentage of agonists selected in the list, and *y*-axis indicates the percentage of true positives, which represent the percentage of antagonists and/or agonists.

In order to compare the results with the crystal structures, two active (PDB ids: 4QKX and 3SN6) and one inactive (PDB id: 2RH1) crystal structures were also used as target conformers for screening. The corresponding ROC curves are illustrated in Figures 4.12 and 4.13 and AUC values are given inside the caption. The predictions that are better than random must have AUC value higher than 0.5. In Figure 4.12, inactive crystal structure 2RH1 has all the curves very near the diagonal indicating that the predictions were not better than random.

ROC curves and AUC values are shown for frame715 in Figure 4.14 and for frame1648 in Figure 4.15. Even though the scoring values of MD conformers with the selected ligands were not as high as those of the crystal structures, they showed

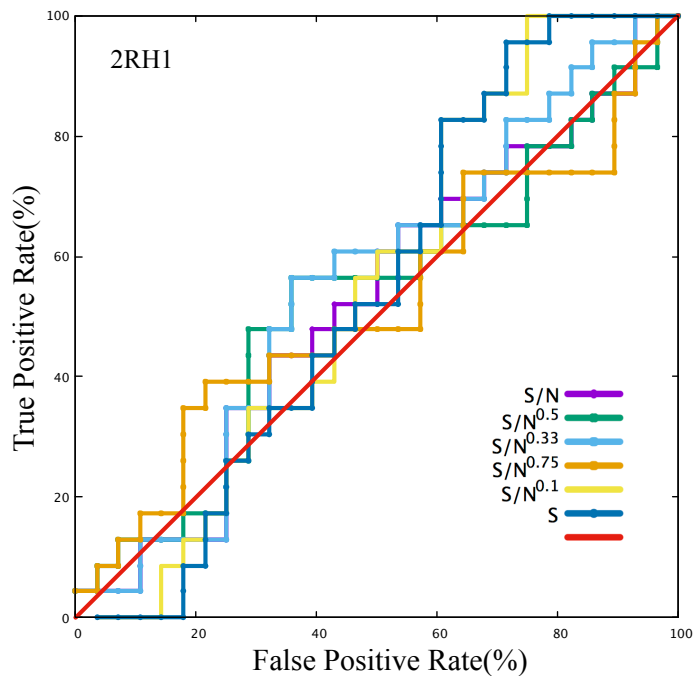
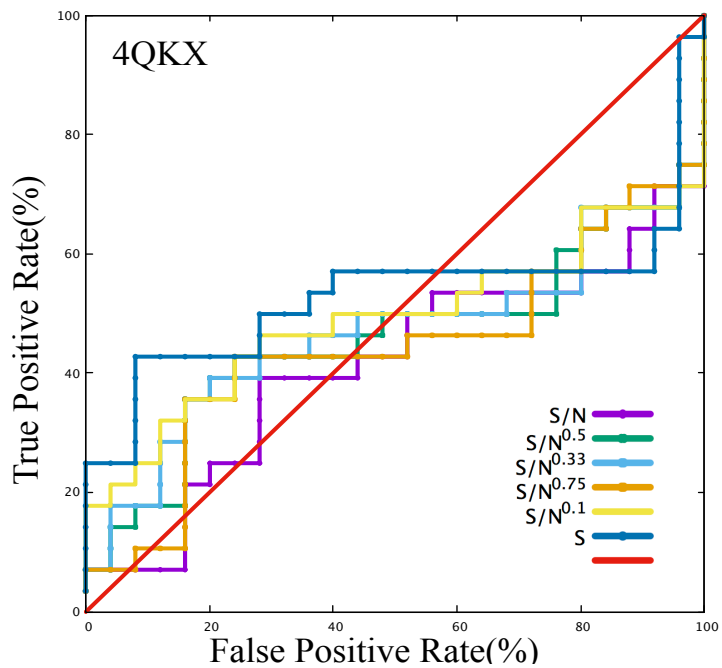
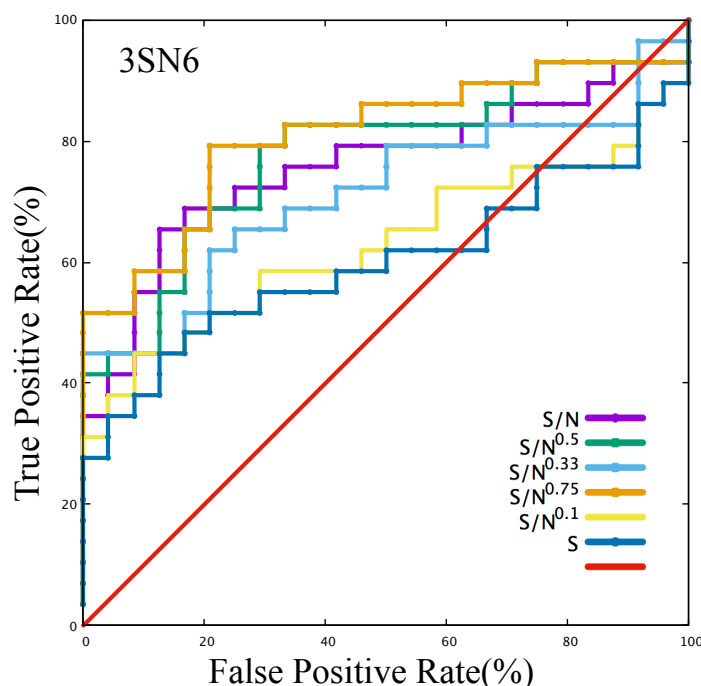


Figure 4.12. ROC curves of the inactive structure PDB id: 2RH1. AUC values are  $S=0.54$ ,  $S/N^{0.1}=0.54$ ,  $S/N^{0.75}=0.52$ ,  $S/N^{0.33}=0.55$ ,  $S/N^{0.5}=0.52$ ,  $S/N=0.52$ .



(a)



(b)

Figure 4.13. ROC curves of the active structures (a) PDB id: 4QKX and (b) PDB id: 3SN6. AUC values of 4QKX are  $S=0.53$ ,  $S/N^{0.1}=0.49$ ,  $S/N^{0.75}=0.45$ ,  $S/N^{0.33}=0.47$ ,  $S/N^{0.5}=0.46$ ,  $S/N=0.42$ . AUC values of 3SN6 are  $S=0.60$ ,  $S/N^{0.1}=0.63$ ,  $S/N^{0.75}=0.81$ ,  $S/N^{0.33}=0.72$ ,  $S/N^{0.5}=0.78$ ,  $S/N=0.76$ .

higher discriminatory power than crystal structures. In some of the curves ( $S/N^{0.1}$ ,  $S/N^{0.5}$  and  $S$ ), antagonists were almost not at the beginning of the list for frame715, however the overall ROC curve has an AUC value around 0.7, which is considered as moderate (see Figure 4.14). On the other hand, in frame1648 ROC curve was initially above the diagonal line, which indicates a preference of antagonists over agonists and the whole curve yielded AUC values between 0.59 and 0.69, which can be considered as moderate (see Figure 4.15).

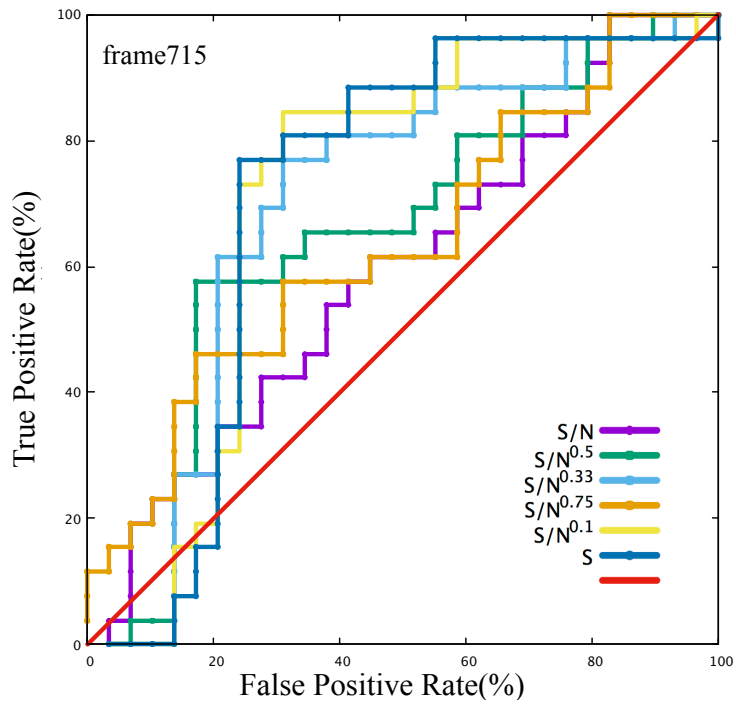


Figure 4.14. ROC curves of frame715. AUC values are  $S=0.70$ ,  $S/N^{0.1}=0.70$ ,  $S/N^{0.75}=0.63$ ,  $S/N^{0.33}=0.69$ ,  $S/N^{0.5}=0.65$ ,  $S/N=0.59$ .

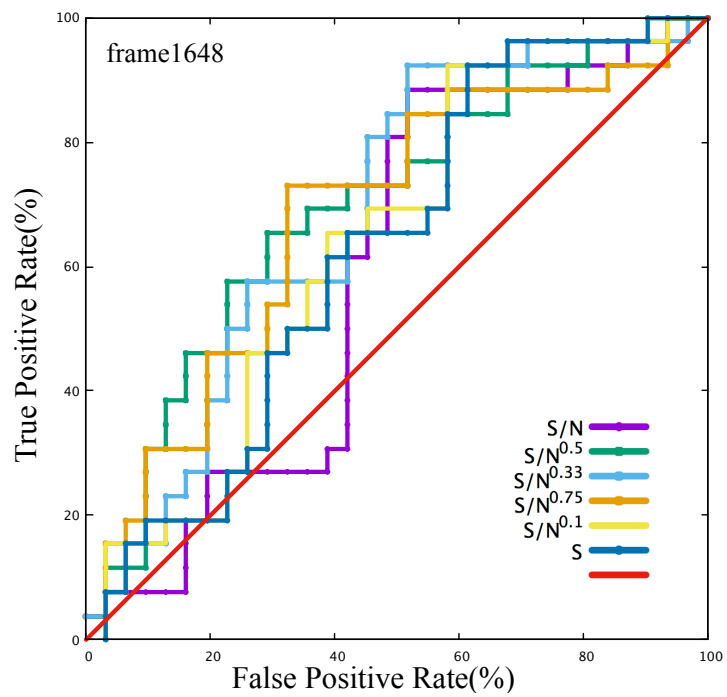
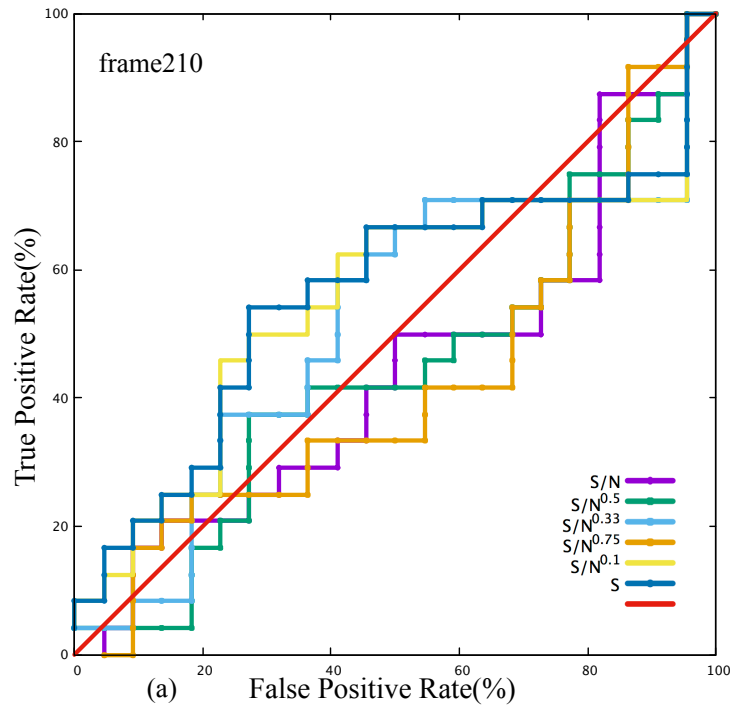
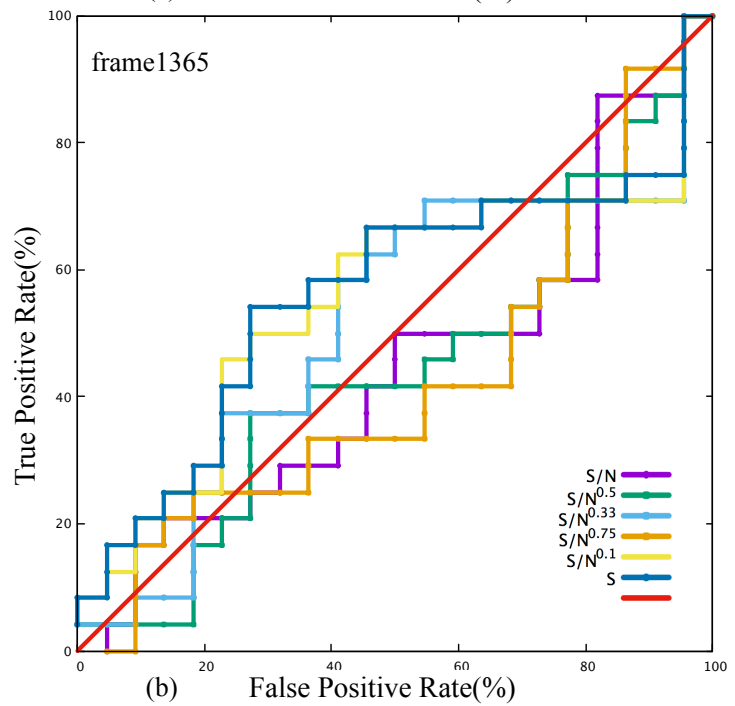


Figure 4.15. ROC curves of frame1648. AUC values are  $S=0.62$ ,  $S/N^{0.1}=0.64$ ,  $S/N^{0.75}=0.68$ ,  $S/N^{0.33}=0.68$ ,  $S/N^{0.5}=0.69$ ,  $S/N=0.59$ .



(a)



(b)

Figure 4.16. ROC curves of the (a) frame210 and (b) frame1365. AUC values of fr210 are  $S=0.47$ ,  $S/N^{0.1}=0.48$ ,  $S/N^{0.75}=0.60$ ,  $S/N^{0.33}=0.54$ ,  $S/N^{0.5}=0.59$ ,  $S/N=0.57$ . AUC values of fr1365 are  $S=0.56$ ,  $S/N^{0.1}=0.55$ ,  $S/N^{0.75}=0.42$ ,  $S/N^{0.33}=0.51$ ,  $S/N^{0.5}=0.44$ ,  $S/N=0.44$ .

Frame210 and frame1365 were selected by only agonist molecules, therefore, they were assigned as active states. As shown in Figure 4.16, their ROC curves for agonists are comparable with active state crystal 4QKX.

When we summarized all ROC curves, at least five MD frames had ROC curves higher than those of crystal structure (2RH1), which are frames 531, 585, 715 and 1648 (see Figure 4.17). When we look at the previous docking results, we see that all these successful conformers were selected at least by one inverse agonist as the most favored conformer in top five for all scoring functions.

The crystal active structures (3SN6 and 4QKX) select agonists over antagonists and therefore in Figure 4.17 their curves are fall under the diagonal line. For both normalized and unnormalized scores, the curves for frame1365 were also found under the diagonal, which complements the previous docking results where frame1365 was found to be the most favored conformer by three out of five agonists. Similarly, frame210 was selected only by one agonist on the list and produced a ROC curve under the diagonal, which indicates a preference for agonists.

On the other hand, frame844 was selected to be the most favored conformer by two antagonists, however its ROC curve was observed under the diagonal line, which indicates a preference for agonists. We speculate that this contradictory result shows that antagonists may not be a strong indicator for determining the activity state of the receptor and eventually the performance of that receptor in screening experiments.

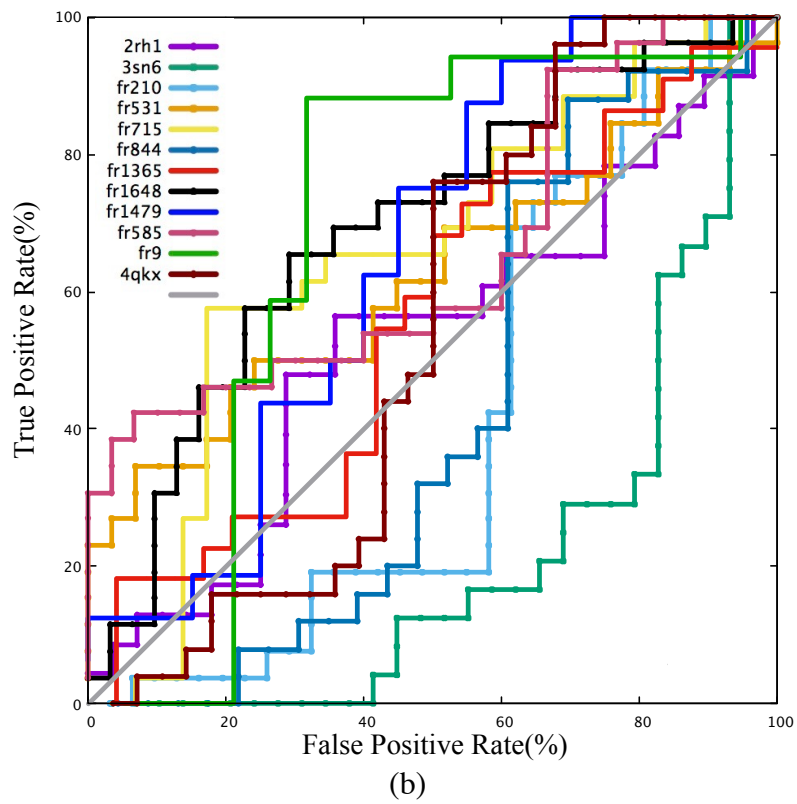
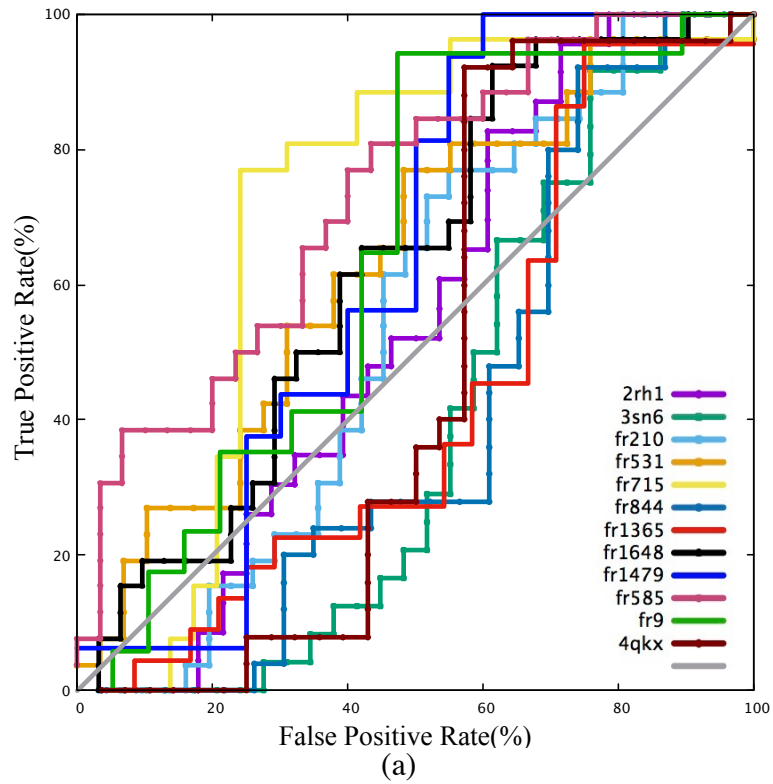


Figure 4.17. ROC curves for all frames and crystals that have been used. The curves that were generated without normalizing the scores on top (a) and were normalized with  $S/N^{0.5}$  on bottom (b).



An exceptional case is presented by frame1648 which was found to be the most favored conformer by ligands from all three categories (two inverse agonists carazolol and JSZ, one antagonist alprenolol, one agonist isoproterenol), and produced a much better performance than most of the MD frames and the crystal structure 2RH1, especially for the normalized for of  $S/N^{0.5}$ . Detailed ROC curves of the MD frames are provided in Appendix F.

Crystal structures only represent only one snapshot, thus, they certainly miss the whole information about the conformational dynamics of the receptor. Furthermore, the flexible regions have a fundamental role in reflecting the dynamics of a protein and the flexible ICL3 region was missing in those crystal structures. But in native conditions, receptor-ligand interactions would be influenced by the presence of ICL3. MD simulations provide a detailed information about the fluctuations and conformational changes of the receptor. These are important factors for a protein to be selective in drug design. As we see in our virtual screening results, MD conformers were much more selective than the inactive state crystal structure and therefore would be potential targets to be used in the initial phase of drug screening experiments.

## Chapter 5

### Conclusion

As a member of the seven-transmembrane GPCR superfamily,  $\beta_2$ AR is one of the most important drug targets in human's respiratory tract. In this thesis, a strategy has been developed in order to classify various  $\beta_2$ AR conformers obtained from an MD simulation trajectory, as active or inactive state based on the efficacy of the favorably bound ligand. For the first time, the receptor consisted of the frequently neglected intracellular loop 3 (ICL3), which significantly affects the dynamic character of the receptor.

First, 13 distinct conformations have been obtained from the previously studied 2.8  $\mu$ s long MD simulation. For critical assessment, eight ligands (carazolol, ICI118;551, timolol, JSZ, alprenolol, epinephrine, BI167107 and XQC) which were extracted from the x-ray ligand-receptor complex structures, were individually docked to 11 crystal structures using AutoDock, GOLD/ChemPLP, GOLD/ChemScore, GOLD/GoldScore, DSX/PDB, DSX/CSD and Glide/XP scoring functions. The poses with the highest score value were selected and evaluated based on their vicinity to five key residues (Ser203, Ser204, Ser207, Asp133 and Asn312) at the ligand-binding site. The best poses that were not in this neighborhood were simply discarded and remaining ones were sorted based on their score value. The successful

scoring functions were selected based on their performance to distinguish active state crystal structures from the inactive ones and have been used for further analysis of MD frames. The most successful ones were AutoDock, GOLD/ChemPLP, DSX/PDB and Glide/XP.

Next, six ligands (butaxamine, esmolol, nebivolol, carvedilol formoterol and salbutamol) with known activities were added to the ligands list. These ligands do not have any experimentally solved structure and have been selected to further evaluate the classification scheme. In total, five agonists, four inverse agonists and five antagonists have been docked to 11 crystal structures. Except butaxamine, the remaining thirteen ligands have been successful in distinguishing active crystal structures from the inactive ones. Next, a total thirteen MD snapshots were evaluated using the same classification scheme after docking thirteen ligands separately. As a result, eight out of thirteen MD frames were selected to be the most favored conformation for the docked ligand.

Based on the efficacy of the ligand, the classification scheme yielded two active and six inactive states. Frame 210 was assigned to be active as it was favored by the agonist salbutamol. The other active state was assigned to frame 1365, which was selected by three agonists, formoterol, isoproterenol and BI167107. The remaining MD frames were found in top five for either one antagonist and/or one inverse agonist, except frame 1648. Frame 1648 presented an unusual case as it was preferred by all three ligands category. Overall, the score values for MD frames were

smaller than crystal structures as the crystal structures represent the optimized bound states, whereas MD frames were optimized as apo form.

Finally, the selected eight MD conformers were used to screen a small database composed of 31 agonists and 26 antagonists to further investigate their discriminatory power between agonists and antagonists/inverse agonists. As a result, MD conformers who were assigned as inactive (frame531, frame715, frame585, frame1648) showed a better performance for distinguishing antagonist/inverse agonists from agonists than the inactive state crystal structure (PDB id: 2RH1). Also, frame 210 classified as an active state selected agonists over antagonists/inverse agonists, which was not better but comparable to the performance of the known active crystal structure (PDB id: 3SN6).

## References

Bai, Q., Zhang, Y., Ban, Y., Liu, H. and Yao, X. (2013) “Computational Study on the Different Ligands Induced Conformation Change of  $\beta$ 2 Adrenergic Receptor-Gs Protein Complex,” *PLoS ONE*. Edited by F. Salsbury Jr. San Francisco, USA: Public Library of Science, 8(7), p. e68138. doi: 10.1371/journal.pone.0068138.

Ballesteros, J. A., Shi, L. and Javitch, J. A. (2001) “Structural Mimicry in G Protein-Coupled Receptors: Implications of the High-Resolution Structure of Rhodopsin for Structure-Function Analysis of Rhodopsin-Like Receptors,” *Molecular Pharmacology*, 60(1), p. 1 LP-19.

Bhattacharya, S., Salomon-Ferrer, R., Lee, S. and Vaidehi, N. (2016) “Conserved Mechanism of Conformational Stability and Dynamics in G-Protein-Coupled Receptors,” *Journal of Chemical Theory and Computation*, 12(11), pp. 5575–5584. doi: 10.1021/acs.jctc.6b00618.

Bock, A., Bermudez, M., Krebs, F., Matera, C., Chirinda, B., Sydow, D., Dallanocce, C., Holzgrabe, U., De Amici, M., Lohse, M. J., Wolber, G. and Mohr, K. (2016) “Ligand binding ensembles determine graded agonist efficacies at a G protein-coupled receptor,” *Journal of Biological Chemistry*, 291(31), pp. 16375–16389. doi: 10.1074/jbc.M116.735431.

Cheng, T., Li, Q., Zhou, Z., Wang, Y. and Bryant, S. H. (2012) “Structure-Based Virtual Screening for Drug Discovery: a Problem-Centric Review,” *The AAPS Journal*, 14(1), pp. 133–141. doi: 10.1208/s12248-012-9322-0.

Cherezov, V., Rosenbaum, D. M., Hanson, M. A., Rasmussen, S. G. F., Thian, F. S., Kobilka, T. S., Choi, H., Kuhn, P., Weis, W. I., Kobilka, B. K. and Stevens, R. C. (2007) “High-Resolution Crystal Structure of an Engineered Human  $\beta$ 2-Adrenergic,” *Science*, 318(November), pp. 1258–1266. doi: 10.1126/science.1150577.

Chung, Y., Kobilka, T. S., Thian, F. S., Chae, P. S., Pardon, E., Mathiesen, J. M., Shah, S. T. a, Lyons, J. a, Caffrey, M., Gellman, S. H., Steyaert, J., Skiniotis, G., Weis, W. I., Roger, K. and Kobilka, B. K. (2012) “Crystal Structure of the B2 Adrenergic Receptor-Gs protein complex,” *Nature*, 477(7366), pp. 549–555. doi: 10.1038/nature10361.Crystal.

DeVree, B. T., Mahoney, J. P., Vélez-Ruiz, G. A., Rasmussen, S. G. F., Kuszak, A. J., Edwald, E., Fung, J.-J., Manglik, A., Masureel, M., Du, Y., Matt, R. A., Pardon, E., Steyaert, J., Kobilka, B. K. and Sunahara, R. K. (2016) “Allosteric coupling from G protein to the agonist-binding pocket in GPCRs,” *Nature*, 535(7610), pp. 182–6. doi: 10.1038/nature18324.

Dror, R. O., Arlow, D. H., Maragakis, P., Mildorf, T. J., Pan, A. C., Xu, H., Borhani, D. W. and Shaw, D. E. (2011) “Activation mechanism of the  $\beta_2$  -adrenergic receptor,” *Proceedings of the National academy of sciences of the USA*, 108(46), pp. 18684–18689. doi: 10.1073/pnas.1110499108/-/DCSupplemental.www.pnas.org/cgi/doi/10.1073/pnas.1110499108.

Friesner, R. A., Banks, J. L., Murphy, R. B., Halgren, T. A., Klicic, J. J., Mainz, D. T., Repasky, M. P., Knoll, E. H., Shelley, M., Perry, J. K., Shaw, D. E., Francis, P. and Shenkin, P. S. (2004) “Glide : A New Approach for Rapid , Accurate Docking and Scoring . 1 . Method and Assessment of Docking Accuracy,” pp. 1739–1749.

Friesner, R. A., Murphy, R. B., Repasky, M. P., Frye, L. L., Greenwood, J. R., Halgren, T. A., Sanschagrin, P. C. and Mainz, D. T. (2006) “Extra Precision Glide: Docking and Scoring Incorporating a Model of Hydrophobic Enclosure for Protein - Ligand Complexes,” pp. 6177–6196.

Galandrin, S. and Bouvier, M. (2006) “Distinct Signaling Profiles of  $\beta_1$  and  $\beta_2$  Adrenergic Receptor Ligands toward Adenylyl Cyclase and Mitogen-Activated Protein Kinase Reveals the Pluridimensionality of Efficacy,” *Molecular Pharmacology*, 70(5), p. 1575 LP-1584. Available at: <http://molpharm.aspetjournals.org/content/70/5/1575.abstract>.

Gatica, E. A. and Cavasotto, C. N. (2012) “Ligand and decoy sets for docking to G protein-coupled receptors,” *Journal of Chemical Information and Modeling*, 52(1), pp. 1–6. doi: 10.1021/ci200412p.

Gaulton, A., Bellis, L. J., Bento, A. P., Chambers, J., Davies, M., Hersey, A., Light, Y., McGlinchey, S., Michalovich, D., Al-Lazikani, B. and Overington, J. P. (2012) "ChEMBL: a large-scale bioactivity database for drug discovery," *Nucleic Acids Research*. Oxford University Press, 40(Database issue), pp. D1100–D1107. doi: 10.1093/nar/gkr777.

Hanson, M. A., Cherezov, V., Roth, C. B., Griffith, M. T., Jaakola, V.-P., Chien, E. Y. T., Velasquez, J., Kuhn, P. and Stevens, R. C. (2008) "A specific cholesterol binding site is established by the 2.8 Å structure of the human  $\beta(2)$ -adrenergic receptor in an alternate crystal form," *Structure (London, England : 1993)*, 16(6), pp. 897–905. doi: 10.1016/j.str.2008.05.001.

Huey, R., Morris, G. M., Olson, A. J. and Goodsell, D. S. (2007) "Software News and Update A Semiempirical Free Energy Force Field with Charge-Based Desolvation." doi: 10.1002/jcc.

Johnson, M. (2006) "Molecular mechanisms of Beta-2-adrenergic receptor function, response, and regulation," *Journal of Allergy and Clinical Immunology*, 117(1), pp. 18–24. doi: 10.1016/j.jaci.2005.11.012.

Jones, G., Willett, P., Glen, R. C., Leach, A. R., Taylor, R. and Uk, K. B. R. (1997) "Development and Validation of a Genetic Algorithm for Flexible Docking."

Kenakin, T. (2016) "Collateral efficacy in drug discovery: taking advantage of the good (allosteric) nature of 7TM receptors," *Trends in Pharmacological Sciences*. Elsevier, 28(8), pp. 407–415. doi: 10.1016/j.tips.2007.06.009.

Kitchen, D. B., Decornez, H., Furr, J. R. and Bajorath, J. (2004) "Docking and Scoring in Virtual Screening for Drug Discovery: Methods and Applications," *Nat. Rev. Drug Disc.*, 3(11), pp. 935–949. doi: 10.1038/nrd1549.

Korb, O., Stu, T. and Exner, T. E. (2009) "Empirical Scoring Functions for Advanced Protein - Ligand Docking with PLANTS," pp. 84–96.

Latek, D., Modzelewska, A., Trzaskowski, B., Krzysztof, P. and Filipek, S. (2012) “G protein-coupled receptors — recent advances,” *Acta Biochim Pol*, 59(4), pp. 515–529. doi: 10.1016/j.surg.2006.10.010.Use.

Li, Y. Y. and III, T. J. H. and W. A. G. (2010) “Computational Modeling of Structure-Function of G Protein-Coupled Receptors with Applications for Drug Design,” *Current Medicinal Chemistry*, pp. 1167–1180. doi: <http://dx.doi.org/10.2174/092986710790827807>.

Liu, J. J., Horst, R., Katritch, V., Stevens, R. C. and Wüthrich, K. (2012) “Biased signaling pathways in  $\beta$ 2-adrenergic receptor characterized by 19F-NMR.,” *Science (New York, N.Y.)*, 335(6072), pp. 1106–10. doi: 10.1126/science.1215802.

Liu, J. and Wang, R. (2014) “Classification of Current Scoring Functions.” doi: 10.1021/ci500731a.

Manglik, A., Kim, T. H., Masureel, M., Altenbach, C., Yang, Z., Hilger, D., Lerch, M. T., Kobilka, T. S., Thian, F. S., Hubbell, W. L., Prosser, R. S. and Kobilka, B. K. (2015) “Structural Insights into the Dynamic Process of  $\beta$ 2-Adrenergic Receptor Signaling,” *Cell*, 161(5), pp. 1101–1111. doi: 10.1016/j.cell.2015.04.043.

Montero, C., Campillo, N. E., Goya, P. and Pérez, J. A. (2005) “Homology models of the cannabinoid CB1 and CB2 receptors. A docking analysis study,” *European Journal of Medicinal Chemistry*, 40(1), pp. 75–83. doi: 10.1016/j.ejmech.2004.10.002.

Neudert, G. and Klebe, G. (2011) “DSX : A Knowledge-Based Scoring Function for the Assessment of Protein À Ligand Complexes,” pp. 2731–2745.

Nygaard, R., Frimurer, T. M., Holst, B., Rosenkilde, M. M. and Schwartz, T. W. (2009) “Ligand binding and micro-switches in 7TM receptor structures,” *Trends in Pharmacological Sciences*, 30(5), pp. 249–259. doi: 10.1016/j.tips.2009.02.006.



Ozcan, O., Uyar, A., Doruker, P. and Akten, E. D. (2013) “Effect of intracellular loop 3 on intrinsic dynamics of human  $\beta$ 2-adrenergic receptor.,” *BMC structural biology*, 13(1), p. 29. doi: 10.1186/1472-6807-13-29.

Ozgun, C., Doruker, P. and Akten, E. D. (2016) “Investigation of allosteric coupling in human  $\beta$  2 -adrenergic receptor in the presence of intracellular loop 3,” pp. 1–13. doi: 10.1186/s12900-016-0061-9.

Pan, Y., Huang, N., Cho, S. and MacKerell, A. D. (2003) “Consideration of molecular weight during compound selection in virtual target-based database screening,” *Journal of Chemical Information and Computer Sciences*, 43(1), pp. 267–272. doi: 10.1021/ci020055f.

Rasmussen, S. G. F., Choi, H.-J., Fung, J. J., Pardon, E., Casarosa, P., Chae, P. S., Devree, B. T., Rosenbaum, D. M., Thian, F. S., Kobilka, T. S., Schnapp, A., Konetzki, I., Sunahara, R. K., Gellman, S. H., Pautsch, A., Steyaert, J., Weis, W. I. and Kobilka, B. K. (2011) “Structure of a nanobody-stabilized active state of the  $\beta$ (2) adrenoceptor.,” *Nature*. Nature Publishing Group, 469(7329), pp. 175–80. doi: 10.1038/nature09648.

Rasmussen, S. G. F., Choi, H.-J., Rosenbaum, D. M., Kobilka, T. S., Thian, F. S., Edwards, P. C., Burghammer, M., Ratnala, V. R. P., Sanishvili, R., Fischetti, R. F., Schertler, G. F. X., Weis, W. I. and Kobilka, B. K. (2007) “Crystal structure of the human [bgr]2 adrenergic G-protein-coupled receptor,” *Nature*. Nature Publishing Group, 450(7168), pp. 383–387. Available at: <http://dx.doi.org/10.1038/nature06325>.

Rasmussen, S. G. F., DeVree, B. T., Zou, Y., Kruse, A. C., Chung, K. Y., Kobilka, T. S., Thian, F. S., Chae, P. S., Pardon, E., Calinski, D., Mathiesen, J. M., Shah, S. T. A., Lyons, J. A., Caffrey, M., Gellman, S. H., Steyaert, J., Skiniotis, G., Weis, W. I., Sunahara, R. K. and Kobilka, B. K. (2011) “Crystal structure of the [bgr]2 adrenergic receptor-Gs protein complex,” *Nature*. Nature Publishing Group, a division of Macmillan Publishers Limited. All Rights Reserved., 477(7366), pp. 549–555. Available at: <http://dx.doi.org/10.1038/nature10361>.

Rosenbaum, D. M., Rasmussen, S. G. F. and Kobilka, B. K. (2009) “The structure and function of G-protein-coupled receptors,” *Nature*, 459(7245), pp. 356–363. doi: 10.1038/nature08144.

Shan, J., Khelashvili, G., Mondal, S., Mehler, E. L. and Weinstein, H. (2012) “Ligand-Dependent Conformations and Dynamics of the Serotonin 5-HT(2A) Receptor Determine Its Activation and Membrane-Driven Oligomerization Properties,” *PLoS Computational Biology*. Edited by D. R. Livesay. San Francisco, USA: Public Library of Science, 8(4), p. e1002473. doi: 10.1371/journal.pcbi.1002473.

Shukla, A. K., Singh, G. and Ghosh, E. (2014) “Emerging structural insights into biased GPCR signaling,” *Trends in Biochemical Sciences*. Elsevier Ltd, 39(12), pp. 594–602. doi: 10.1016/j.tibs.2014.10.001.

Simpson, L. M., Wall, I. D., Blaney, F. E. and Reynolds, C. A. (2011) “Modeling GPCR active state conformations: The  $\beta$  2-adrenergic receptor,” *Proteins: Structure, Function and Bioinformatics*, 79(5), pp. 1441–1457. doi: 10.1002/prot.22974.

Staus, D. P., Strachan, R. T., Manglik, A., Pani, B., Kahsai, A. W., Kim, T. H., Wingler, L. M., Ahn, S., Chatterjee, A., Masoudi, A., Kruse, A. C., Pardon, E., Steyaert, J., Weis, W. I., Prosser, R. S., Kobilka, B. K., Costa, T. and Lefkowitz, R. J. (2016) “Allosteric nanobodies reveal the dynamic range and diverse mechanisms of G-protein-coupled receptor activation,” *Nature*, 535(7612), pp. 448–52. doi: 10.1038/nature18636.

Stenkamp, R. E., Filipek, S., Driessen, C. A. G. G., Teller, D. C. and Palczewski, K. (2002) “Crystal structure of rhodopsin: A template for cone visual pigments and other G protein-coupled receptors,” *Biochimica et Biophysica Acta - Biomembranes*, 1565(2), pp. 168–182. doi: 10.1016/S0005-2736(02)00567-9.

Sottriffer, C., “Virtual Screening: Principles, Challenges and Practical Guidelines”, Volume 32, 2006

Tuccinardi, T. (2009) “Docking-Based Virtual Screening : Recent Developments,” (1), pp. 303–314.

Unger, V. M. and Schertler, G. F. (1995) “Low resolution structure of bovine rhodopsin determined by electron cryo-microscopy,” *Biophysical Journal*, 68(5), pp. 1776–1786. Available at: <http://www.ncbi.nlm.nih.gov/pmc/articles/PMC1282080/>.

Verdonk, M. L., Cole, J. C., Hartshorn, M. J., Murray, C. W. and Taylor, R. D. (2003) "Improved Protein – Ligand Docking Using GOLD," 623(November 2002), pp. 609–623.

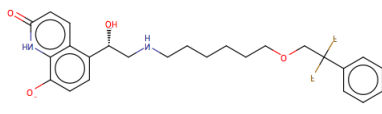
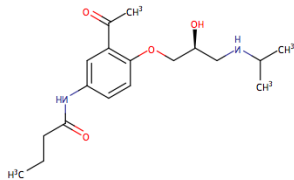
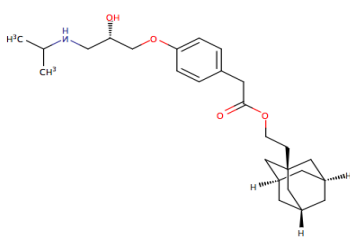
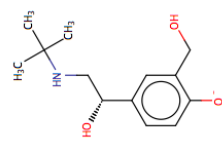
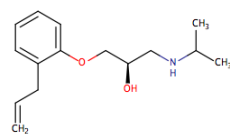
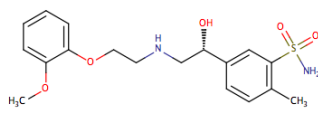
Violin, J. D. and Lefkowitz, R. J. (2007) "Beta-Arrestin-biased ligands at seven-transmembrane receptors," *Trends in Pharmacological Sciences*, 28(8), pp. 416–422. doi: 10.1016/j.tips.2007.06.006.

Wolf, A. and Kirschner, K. N. (2013) "Principal component and clustering analysis on molecular dynamics data of the ribosomal L11·23S subdomain," *Journal of Molecular Modeling*. Berlin/Heidelberg: Springer-Verlag, 19(2), pp. 539–549. doi: 10.1007/s00894-012-1563-4.

Wacker, D., Fenalti, G., Brown, M. A., Katritch, V., Abagyan, R., Cherezov, V. and Stevens, R. C. (2010) "Conserved Binding Mode of Human  $\beta$ 2 Adrenergic Receptor Inverse Agonists and Antagonist Revealed by X-ray Crystallography," *Journal of the American Chemical Society*. American Chemical Society, 132(33), pp. 11443–11445. doi: 10.1021/ja105108q.

## APPENDIX A

### Representation of 57 compounds that used for virtual screening

Compound Number	Compound Name	Chemical Formula	Chemical Sketches
1	Abediterol	$C_{25}H_{30}F_2N_2O_4$	
2	Acebutolol	$C_{18}H_{28}N_2O_4$	
3	Adaprolol	$C_{26}H_{39}NO_4$	
4	Albuterol	$C_{13}H_{21}NO_3$	
5	Alprenolol	$C_{15}H_{23}NO_2$	
6	Amosulalol	$C_{18}H_{24}N_2O_5S$	

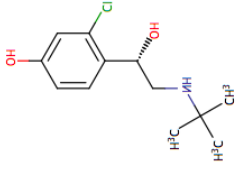
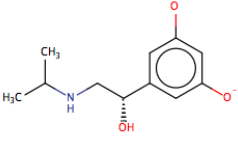
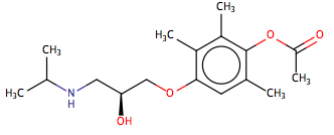
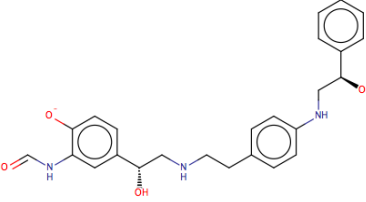
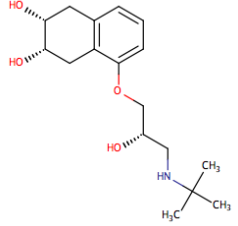
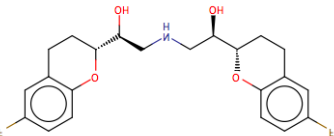
Compound Number	Compound Name	Chemical Formula	Chemical Sketches
7	Arformoterol	$C_{19}H_{24}N_2O_4$	
8	Arotinolol	$C_{15}H_{21}N_3O_2S_3$	
9	Atenolol	$C_{14}H_{22}N_2O_3$	
10	Bambuterol	$C_{18}H_{29}N_3O_5$	
11	Batefenterol	$C_{40}H_{42}ClN_5O_7$	
12	Bedoadrine	$C_{24}H_{32}N_2O_5$	
13	Betaxalol	$C_{18}H_{29}NO_3$	

Compound Number	Compound Name	Chemical Formula	Chemical Sketches
14	Bevantolol	$C_{20}H_{27}NO_4$	
15	Bisoprolol	$C_{18}H_{31}NO_4$	
16	Bitolterol	$C_{28}H_{31}NO_5$	
17	Broncholine	$C_{13}H_{19}Cl_2F_3N_2O$	
18	Bucindolol	$C_{22}H_{25}N_3O_2$	
19	Carazolol	$C_{18}H_{22}N_2O_2$	

Compound Number	Compound Name	Chemical Formula	Chemical Sketches
20	Carmoterol	$C_{21}H_{24}N_2O_4$	
21	Carteolol	$C_{16}H_{24}N_2O_3$	
22	Carvedilol	$C_{24}H_{26}N_2O_4$	
23	Celiprolol	$C_{20}H_{33}N_3O_4$	
24	Desipramine	$C_{18}H_{22}N_2$	
25	Dobutamine	$C_{18}H_{23}NO_3$	
26	Dopaxamine	$C_{22}H_{32}N_2O_2$	

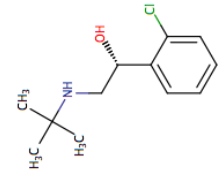
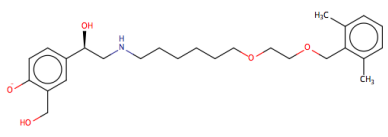
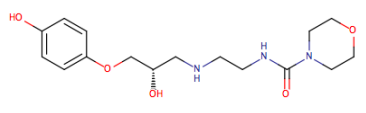
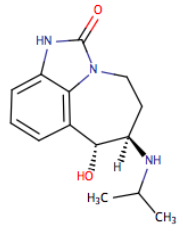
Compound Number	Compound Name	Chemical Formula	Chemical Sketches
27	Esmolol	$C_{16}H_{25}NO_4$	
28	Fenoterol	$C_{17}H_{21}NO_4$	
29	Formoterol	$C_{19}H_{24}N_2O_4$	
30	Indacaterol	$C_{24}H_{28}N_2O_3$	
31	Isoetarine	$C_{13}H_{21}NO_3$	
32	Levalbuterol	$C_{13}H_{21}NO_3$	
33	Levobunolol	$C_{17}H_{25}NO_3$	



Compound Number	Compound Name	Chemical Formula	Chemical Sketches
34	Meluadrine	$C_{12}H_{18}ClNO_2$	
35	Metaproterenol	$C_{11}H_{17}NO_3$	
36	Metipranolol	$C_{17}H_{27}NO_4$	
37	Milveterol	$C_{25}H_{30}ClN_3O_4$	
38	Nadolol	$C_{17}H_{27}NO_4$	
39	Nebivolol	$C_{22}H_{25}F_2NO_4$	

Compound Number	Compound Name	Chemical Formula	Chemical Sketches
40	Olodaterol	$C_{21}H_{26}N_2O_5$	
41	Oxprenolol	$C_{15}H_{23}NO_3$	
42	Penbutolol	$C_{18}H_{29}NO_2$	
43	Pindolol	$C_{14}H_{20}N_2O_2$	
44	Pirbuterol	$C_{12}H_{20}N_2O_3$	
45	Procaterol	$C_{16}H_{22}N_2O_3$	
46	Protokylol	$C_{18}H_{21}NO_5$	



Compound Number	Compound Name	Chemical Formula	Chemical Sketches
54	Tulobuterol	$C_{12}H_{18}ClNO$	
55	Vilanterol	$C_{24}H_{33}Cl_2NO_5$	
56	Xamoterol	$C_{16}H_{25}N_3O_5$	
57	Zilpaterol	$C_{14}H_{19}N_3O_2$	



## APPENDIX C

### Binding Results of the Crystal Structures

Table C.1. Binding results of the inverse agonist ICI 118,551 docked to 11 crystal structures. Blue ones are inactive, red ones are active states.

	Auto Dock	Chem PLP	Gold Score	Chem Score	DSX/ CSD	DSX/ PDB	Glide
1	4LDO	4LDL	4QKX	3NYA	3SN6	3D4S	3NY8
2	2RH1	4LDE	4LDO	4LDL	4LDO	4LDL	3SN6
3	3NYA	3D4S	3P0G	3P0G	3D4S	2RH1	4LDO
4	3D4S	3NYA	3SN6	4LDE	4LDL	4LDE	3NYA
5	3NY8	3NY9	4LDL	3NY9	3P0G	3NY8	3D4S
6	4LDL	3NY8		4LDO	4LDE	3SN6	3NY9
7	4LDE	3P0G		3SN6	3NYA	3P0G	4LDL
8	3SN6	3SN6		2RH1	2RH1	3NYA	3P0G
9	3P0G	2RH1			4QKX	4LDO	4QKX
10	4QKX				3NY9	3NY9	2RH1
11	3NY9				3NY8	4QKX	4LDE

Table C.2. Binding results of the inverse agonist JSZ (a novel molecule) docked to 11 crystal structures. Blue ones are inactive, red ones are active states.

	Auto Dock	Chem PLP	Gold Score	Chem Score	DSX/ CSD	DSX/ PDB	Glide
1	3NY9	3D4S	3NY9	3D4S	2RH1	2RH1	3NY8
2	2RH1	3NY9	3NYA	3NYA	3NY9	3NYA	3NY9
3	3D4S	3NYA	2RH1	3NY9	3D4S	3NY9	3SN6
4	3NYA	2RH1	3NY8	3NY8	3NY9	3D4S	3NYA
5	3NY8	3NY8	3D4S	2RH1	3NY8	3NY8	3D4S
6	4LDO		4LDL		4QKX	3SN6	2RH1
7	3P0G				3SN6	3P0G	4LDE
8	4LDOL				4LDE	3NYA	4LDL
9	3SN6				4QKX	4LDO	
10					3P0G	3NY9	
11						4QKX	

Table C.3. Binding results of the antagonist alprenolol docked to 11 crystal structures. Blue ones are inactive, red ones are active states.

	<b>Auto Dock</b>	<b>Chem PLP</b>	<b>Gold Score</b>	<b>Chem Score</b>	<b>DSX/ CSD</b>	<b>DSX/ PDB</b>	<b>Glide</b>
1	2RH1	3NYA	4LDO	4LDL	3D4S	3D4S	2RH1
2	3D4S	3NY9	3NYA	2RH1	4LDE	4LDL	3P0G
3	4LDO	3D4S	3SN6	3SN6	3NY8	3NY8	3SN6
4	3NYA	3NY8	4QKX	3NYA	4LDL	2RH1	3D4S
5	3NY9	2RH1	3P0G	3NY9	2RH1	3NYA	4LDE
6	4LDL		2RH1	4LDE	3NYA	4LDO	3NY9
7	3NY8			4QKX	3NY9	3P0G	3NYA
8	3P0G			3NY8	4QKX	4LDE	4LDO
9	4LDE			3D4S	4LDO	3NY9	3NY8
10	3SN6				3SN6	4QKX	4LDL
11	4QKX					3SN6	4QKX

Table C.4. Binding results of the inverse agonist timolol docked to 11 crystal structures. Blue ones are inactive, red ones are active states.

	<b>Auto Dock</b>	<b>Chem PLP</b>	<b>Gold Score</b>	<b>Chem Score</b>	<b>DSX/ CSD</b>	<b>DSX/ PDB</b>	<b>Glide</b>
1	3NYA	3D4S	3D4S	3D4S	3D4S	3NY9	2RH1
2	3D4S	3NY9	3NYA	3NY9	2RH1	3D4S	3D4S
3	3NY9	2RH1	3NY9	3NY8	3NYA	2RH1	3NYA
4	2RH1	3NYA	4LDL		3NY9	3NYA	3NY9
5	4LDL	3NY8	2RH1		3NY8	3NY8	3NY8
6	4LDO		3NY8		4LDL	4LDL	
7	4LDE				4QKX	4LDE	
8	3SN6				4LDE	4QKX	
9	3NY8					3P0G	
10	4QKX						
11	3P0G						

Table C.5. Binding results of the agonist BI167107 docked to 11 crystal structures. Blue ones are inactive, red ones are active states.

	<b>Auto Dock</b>	<b>Chem PLP</b>	<b>Gold Score</b>	<b>Chem Score</b>	<b>DSX/ CSD</b>	<b>DSX/ PDB</b>	<b>Glide</b>
1	4LDE	4LDE	4LDO	4LDE	4LDE	4LDE	4LDE
2	4LDL	3P0G	4QKX	3SN6	4LDL	3NY9	4LDO
3	3SN6	4LDL	4LDE	3P0G	3SN6	3SN6	3P0G
4	4QKX	3SN6	4LDL	3NYA	3NYA	3NYA	3SN6
5	4LDO	3NYA	3P0G	3NY9	3NY9	4LDL	4QKX
6	3NYA	3D4S	3NY8	4LDO	4LDO	4QKX	4LDL
7	3D4S	3NY9	3NY9	4LDL	3P0G	3D4S	3NYA
8	3NY9	4QKX	3NYA	3NY8	3D4S	4LDO	3NY8
9	2RH1	4LDO	3D4S	4QKX	4QKX	2RH1	3NY9
10	3P0G	2RH1	3SN6	2RH1	2RH1	3P0G	3D4S
11	3NY8	3NY8		3D4S	3NY8	3NY8	

Table C.6. Binding results of the agonist hydroxybenzyl isoproterenol docked to 11 crystal structures. Blue ones are inactive, red ones are active states.

	<b>Auto Dock</b>	<b>Chem PLP</b>	<b>Gold Score</b>	<b>Chem Score</b>	<b>DSX/ CSD</b>	<b>DSX/ PDB</b>	<b>Glide</b>
1	4LDL	3SN6	4LDE	3P0G	4LDO	4LDO	3P0G
2	3P0G	4LDO	3SN6	4QKX	4LDL	4LDL	4QKX
3	4LDO	4LDL	3P0G	3SN6	4QKX	4QKX	4LDL
4	3SN6	3P0G	4LDL	4LDO	3P0G	3P0G	4LDO
5	4QKX	4QKX	3NYA	3NYA	4LDE	4LDE	4LDE
6	4LDE	4LDE	3NY9	4LDE	3SN6	3NY9	3SN6
7	3NYA	3D4S	4LDO	4LDL	3NYA	3SN6	3NY9
8	3NY9	3NY9	3D4S	2RH1	3NY8	3NYA	3NYA
9	3D4S	3NY8	2RH1	3D4S	3NY9	3NY8	3D4S
10	3NY8		4QKX	3NY9	2RH1	2RH1	2RH1
11							3NY8



Table C.7. Binding results of the agonist epinephrine docked to 11 crystal structures. Blue ones are inactive, red ones are active states.

	<b>Auto Dock</b>	<b>Chem PLP</b>	<b>Gold Score</b>	<b>Chem Score</b>	<b>DSX/ CSD</b>	<b>DSX/ PDB</b>	<b>Glide</b>
<b>1</b>	4LDO	4LDO	4LDO	3P0G	4LDO	4QKX	4LDO
<b>2</b>	4LDE	3SN6	3SN6	4QKX	4QKX	4LDO	4LDE
<b>3</b>	4LDL	4QKX	4QKX	4LDO	4LDL	4LDL	3SN6
<b>4</b>	3P0G	3P0G	3P0G	4LDE	3P0G	3P0G	4QKX
<b>5</b>	4QKX	4LDL	4LDE	4LDL	4LDE	4LDE	3P0G
<b>6</b>	2RH1	4LDE	4LDL	3NYA	3SN6	2RH1	4LDE
<b>7</b>	3SN6	3NY8	3NY8	2RH1	3D4S	3NYA	3NY8
<b>8</b>	3NY9	3D4S	3NY9	3NY9	2RH1	3D4S	3D4S
<b>9</b>	3NY8	3NY9	3NYA	3D4S	3NY9	3SN6	3NYA
<b>10</b>		3NYA	3D4S	3NY8	3NY8	3NY9	3NY9
<b>11</b>						3NY8	2RH1

## APPENDIX D

### Interaction Table of the Ligands with Residues

Ligand/ Receptor	M 8 2	W 1 0 9	T 1 1 0	D 1 1 3	V 1 1 4	V 1 1 7	T 1 1 8	T 1 6 4	Y 1 7 4	F 1 9 3	F 1 9 4	T 1 9 5	F 1 9 9	A 2 0 0	S 2 0 3	S 2 0 4	S 2 0 7	F 2 0 0	Y 2 0 9	W 2 8 6	F 2 8 9	F 2 9 0	N 2 9 3	H 2 9 6	V 2 9 7	Y 3 0 8	N 3 1 2	Y 3 1 6	L 3 1 1	C 2 8 5	G 3 1 5	V 8 6	W 3 1 3	I 3 1 4	I 3 0 9	C 1 0 6	D 1 9 2	C 1 9 1							
CAU/ 2RH1				H B	•	•				•					H B	•												H B	•																
CAU/ fr715				H B						•	•	•				•		•	•	•	•	•						•	•																
CAU/ fr1648	•			H B	•	•									•	•		•	•	•	•							H B																	
ICI11 8,551/ 3NY8		•		H B	•	•									•	•				•	•	•						•	H B																
ICI11 8,551/ fr585		•	•	H B	•						•				•	•		•	•	•	•						•	•																	
JSZ/ 3NY9		•	•	H B	•	•				•		•			•	H B	•			•	•	•	H B					H B	•																
JSZ/ fr1648	•			H B	•	•	•								•			•	•	•	•							•																	
TIM/ 3D4S			•	H B	•	•				•					•					•	•	•	H B				•	H B	H B																
TIM/ fr531				H B	•	•			H B	•	•	•	•	•	•			•		•	•	•		•	•	•	H B																		
JTZ/ 3NYA		•	•	H B	•	•									•	•				•	•	•						•	H B	•															
JTZ/ fr585		•	•	H B	•					•	•	•			•			•		•	•	•						•																	
JTZ/ fr1648				H B	•	•				•					•	•		•	•	•	•						•	H B																	
NBI/ fr844	•			H B	•	•			•						•			•	H B	•	•	•						•	•	•	•														
CVD/ fr9		•	•	H B						•		•								•	•	H B					H B	H B	•						•	•									
CVD/ fr844				H B	•				•		•				•			•	•	•	•	•					H B	H B	•																

Ligand/ Receptor	M 8 2	W 1 0 9	T 1 1 0	D 1 1 3	V 1 1 4	V 1 1 7	T 1 1 8	T 1 6 4	Y 1 7 4	F 1 9 3	F 1 9 4	T 1 9 5	F 1 9 9	A 2 0 0	S 2 0 3	S 2 0 4	S 2 0 7	F 2 0 8	Y 2 0 9	W 2 8 6	F 2 8 9	F 2 9 0	N 2 9 3	H 2 9 6	V 2 9 7	Y 3 0 8	N 3 1 2	Y 3 1 6	L 3 1 1	C 2 8 5	G 3 1 5	V 8 6	W 3 1 3	I 3 1 4	I 3 0 9	C 1 0 6	D 1 9 2	C 1 9 1							
BI167 07/ 3P0G		•	•	H B	•	•				•				•	H B		H B					•																							
BI167 07/ fr1365		•	•	H B	•				•	•									•	•	•	•					•	•												•	•				
XQC/ 4LDL				H B	H B	•	H B			H B					•		H B				•	•					•	H B	•										•		•	•			
XQC/ fr1648		•	•	H B					H B	•					H B	•					•						•	H B	H B											•					
XQC/ fr1365		•	H B	H B	•				•	H B	•	H B				•					•						•	•																	
Formo terol/ 1365			•	H B	•	•			H B	•	•	H B				•		•	•	•	•	•					•	H B																	
Salbut amol/ fr210				H B	•	•	H B		•	•							•	•		•	•	•																							

## APPENDIX E

### Docking Results of the Ligands with Their Score Values

Table E.1. Binding results of antagonist molecule butaxamine. Bold characters representing the active states of the receptor, italic characters representing the MD frames.

<u>Rank</u>	<u>ChemPLP</u>		<u>AutoDock</u>		<u>DSX/PDB</u>		<u>Glide</u>	
1	<b>4LDL</b>	62.88	<i>fr210</i>	-7.02	<b>4LDL</b>	-109.3	3NY9	-7.03
2	<i>fr2311</i>	62.59	<b>3P0G</b>	-6.89	<b>4QKX</b>	-103.7	<b>4LDE</b>	-5.66
3	2RH1	60.80	<b>4LDO</b>	-6.84	3D4S	-101.6	3NYA	-5.52
4	3D4S	60.73	<i>fr1365</i>	-6.65	<b>3P0G</b>	-97.93	<i>fr210</i>	-5.52
5	<b>3SN6</b>	59.84	<b>3SN6</b>	-6.49	<b>3SN6</b>	-97.18	3NY8	-5.12
6	3NYA	59.73	<i>fr585</i>	-6.48	<b>4LDE</b>	-96.95	<i>fr531</i>	-5.02
7	3NY9	59.56	<b>4QKX</b>	-6.43	2RH1	-96.07	<i>fr1365</i>	-5.01
8	<b>4LDE</b>	58.06	<b>4LDL</b>	-6.33	3NY9	-94.68	3D4S	-4.85
9	3NY8	57.71	2RH1	-6.28	3NY8	-94.68	2RH1	-4.62
10	<b>4LDO</b>	56.73	3D4S	-6.25	3NYA	-93.43	<i>fr1648</i>	-4.34
11	<i>fr9</i>	55.15	3NYA	-6.15	<b>4LDO</b>	-92.42	<i>fr844</i>	-3.65
12	<i>fr715</i>	54.32	<b>4LDE</b>	-6.15	<i>fr210</i>	-91.51	<i>fr585</i>	-3.48
13	<i>fr531</i>	53.91	3NY9	-6.14	<i>fr531</i>	-89.72	<i>fr9</i>	-3.37
14	<i>fr210</i>	52.54	<i>fr715</i>	-6.03	<i>fr715</i>	-86.79		
15	<i>fr1648</i>	52.19	<i>fr531</i>	-5.95	<i>fr1648</i>	-84.75		
16	<i>fr1365</i>	50.37	<i>fr2231</i>	-5.89	<i>fr1365</i>	-84.60		
17			3NY8	-5.46	<i>fr585</i>	-80.10		
18			<i>fr2370</i>	-5.27	<i>fr2370</i>	-75.46		
19			<i>fr1648</i>	-5.22	<i>fr2231</i>	-74.98		
20								
21								
22								
23								
24								

Table E.2. Binding results of antagonist molecule esmolol. Bold characters representing the active states of the receptor, italic characters representing the MD frames.

Rank	ChemPLP		AutoDock		DSX/PDB		Glide	
1	<b>4LDL</b>	74.63	3NY9	-8.60	3NY9	-120.6	3D4S	-8.32
2	<b>3P0G</b>	74.31	3NYA	-8.32	2RH1	-116.3	<i>fr1479</i>	-8.22
3	<b>4LDO</b>	73.52	<b>4LDO</b>	-8.28	<i>fr715</i>	-115.6	3NY9	-8.16
4	<i>fr715</i>	72.62	3NY8	-8.07	3NYA	-115.6	3NYA	-7.62
5	<b>4LDE</b>	72.59	2RH1	-7.87	3D4S	-112.1	<i>fr2311</i>	-7.42
6	<i>fr844</i>	72.59	<b>4LDL</b>	-7.65	<i>fr2370</i>	-109.0	2RH1	-7.15
7	<b>4QKX</b>	72.44	<b>4LDE</b>	-7.63	<i>fr1365</i>	-108.7	3NY8	-6.98
8	<i>fr1648</i>	72.22	<i>fr531</i>	-7.57	3NY8	-104.9	<b>3SN6</b>	-6.73
9	<i>fr1479</i>	71.94	<i>fr9</i>	-7.44	<b>4LDE</b>	-104.7	<i>fr1648</i>	-6.72
10	3D4S	71.77	<b>3P0G</b>	-7.43	<b>3SN6</b>	-104.6	<i>fr844</i>	-5.85
11	<i>fr2311</i>	71.61	<i>fr715</i>	-7.40	<i>fr585</i>	-104.6	<b>3P0G</b>	-5.64
12	3NYA	70.74	3D4S	-7.33	<b>4LDL</b>	-104.1	<i>fr1365</i>	-5.56
13	<b>3SN6</b>	68.92	<i>fr210</i>	-7.22	<i>fr1648</i>	-100.2	<b>4QKX</b>	-5.46
14	3NY9	67.96	<b>3SN6</b>	-7.18	<b>4LDO</b>	-99.4	<i>fr210</i>	-5.31
15	3NY8	67.66	<i>fr1648</i>	-6.95	<i>fr210</i>	-99.39	<i>fr2231</i>	-5.11
16	<i>fr1365</i>	66.10	<b>4QKX</b>	-6.76	<b>4QKX</b>	-99.09	<i>fr531</i>	-4.81
17	<i>fr585</i>	62.49	<i>fr585</i>	-6.67	<b>3P0G</b>	-97.42	<i>fr585</i>	-4.35
18	<i>fr2231</i>	62.47	<i>fr2370</i>	-6.58	<i>fr844</i>	-96.56		
19	<i>fr2661</i>	62.18	<i>fr2231</i>	-6.29	<i>fr531</i>	-92.6		
20	<i>fr210</i>	60.94	<i>fr2311</i>	-6.05	<i>fr2231</i>	-88.69		
21	<i>fr531</i>	60.59			<i>fr231</i>	-88.41		
22								
23								
24								

Table E.3. Binding results of agonist molecule formoterol. Bold characters representing the active states of the receptor, italic characters representing the MD frames.

Rank	ChemPLP		AutoDock		DSX/PDB		Glide	
1	<b>3SN6</b>	91.24	<b>3P0G</b>	-9.57	<b>3P0G</b>	-139.5	<b>3P0G</b>	-10.99
2	<b>3P0G</b>	91.23	<b>3SN6</b>	-9.54	<b>4LDE</b>	-130.2	3NY9	-10.83
3	<b>4LDE</b>	85.49	<b>4LDE</b>	-9.51	<b>4LDL</b>	-129.4	<b>4QKX</b>	-10.54
4	<b>4LDL</b>	84.75	<b>4LDO</b>	-9.45	<b>3SN6</b>	-126.3	3D4S	-10.39
5	<b>4LDO</b>	84.48	<i>fr210</i>	-9.19	<b>4QKX</b>	-125.7	<b>4LDE</b>	-10.35
6	<i>fr844</i>	84.35	<b>4LDL</b>	-9.10	3NYA	-125.7	3NYA	-9.52
7	<b>4QKX</b>	81.42	3NY8	-9.09	3D4S	-122.7	2RH1	-9.37
8	3NY8	79.18	<i>fr1365</i>	-8.88	<b>4LDO</b>	-122.3	<b>4LDL</b>	-9.36
9	<i>fr1365</i>	78.19	<i>fr715</i>	-8.87	3NY9	-118.8	<b>4LDO</b>	-9.34
10	3D4S	77.77	3NYA	-8.86	2RH1	-111.0	<b>3SN6</b>	-9.32
11	2RH1	77.08	<b>4QKX</b>	-8.79	<i>fr9</i>	-110.0	3NY8	-9.18
12	3NYA	76.99	<i>fr2370</i>	-8.72	<i>fr1365</i>	-109.8	<i>fr844</i>	-9.00
13	<i>fr2661</i>	76.94	3D4S	-8.61	<i>fr844</i>	-109.0	<i>fr2311</i>	-8.90
14	<i>fr1648</i>	76.56	2RH1	-8.57	<i>fr210</i>	-108.7	<i>fr1365</i>	-8.28
15	3NY9	76.43	<i>fr531</i>	-8.48	<i>fr715</i>	-107.5	<i>fr210</i>	-7.96
16	<i>fr2311</i>	73.40	<i>fr2231</i>	-8.43	<i>fr2231</i>	-106.5	<i>fr1648</i>	-7.89
17	<i>fr2231</i>	69.70	3NY9	-8.39	3NY8	-106.1	<i>fr531</i>	-7.07
18	<i>fr715</i>	67.99	<i>fr9</i>	-8.36	<i>fr1648</i>	-106.1	<i>fr715</i>	-6.90
19	<i>fr531</i>	65.02	<i>fr844</i>	-8.23	<i>fr531</i>	-105.4	<i>fr2231</i>	-6.65
20	<i>fr585</i>	64.24	<i>fr585</i>	-7.98	<i>fr1479</i>	-103.5	<i>fr585</i>	-3.36
21	<i>fr210</i>	63.58	<i>fr1648</i>	-7.93	<i>fr585</i>	-101.9		
22					<i>fr2661</i>	-101.7		
23								
24								

Table E.4. Binding results of inverse agonist molecule ICI 118;551. Bold characters representing the active states of the receptor, italic characters representing the MD frames.

Rank	ChemPLP		AutoDock		DSX/PDB		Glide	
1	<b>4LDL</b>	72.43	<b>4LDO</b>	-9.87	3D4S	-113.1	3NY8	-10.83
2	<b>4LDE</b>	72.14	2RH1	-9.67	<b>4LDL</b>	-113.0	<b>3SN6</b>	-10.74
3	3D4S	68.09	3NYA	-9.62	2RH1	-111.5	<b>4LDO</b>	-10.23
4	<i>fr1365</i>	66.37	3D4S	-9.35	<b>4LDE</b>	-109.9	3NYA	-9.69
5	3NYA	66.36	3NY8	-9.33	3NY8	-109.4	3D4S	-9.67
6	<i>fr1479</i>	66.0	<b>4LDL</b>	-9.29	<b>3SN6</b>	-109.1	3NY9	-9.56
7	<i>fr1648</i>	65.28	<b>4LDE</b>	-9.19	<b>3P0G</b>	-109.0	<b>4LDL</b>	-9.40
8	3NY9	64.96	<b>3SN6</b>	-9.15	3NYA	-106.8	<b>3P0G</b>	-9.03
9	3NY8	64.60	<b>3P0G</b>	-9.05	<b>4LDO</b>	-104.1	<b>4QKX</b>	-8.93
10	<b>3P0G</b>	64.40	<b>4QKX</b>	-9.04	<i>fr1648</i>	-103.0	2RH1	-8.93
11	<b>3SN6</b>	64.04	<i>fr531</i>	-8.72	3NY9	-97.91	<i>fr585</i>	-8.78
12	2RH1	63.58	<i>fr9</i>	-8.52	<b>4QKX</b>	-95.27	<b>4LDE</b>	-8.76
13	<i>fr585</i>	61.68	<i>fr585</i>	-8.49	<i>fr585</i>	-94.58	<i>fr9</i>	-8.14
14	<i>fr844</i>	60.54	<i>fr210</i>	-8.48	<i>fr210</i>	-94.25	<i>fr2370</i>	-7.78
15	<i>fr715</i>	60.36	<i>fr1365</i>	-8.32	<i>fr9</i>	-94.16	<i>fr210</i>	-7.13
16	<i>fr210</i>	51.13	<i>fr2231</i>	-8.30	<i>fr844</i>	-90.94	<i>fr1479</i>	-7.08
17			3NY9	-8.27	<i>fr1365</i>	-90.30	<i>fr1365</i>	-7.07
18			<i>fr844</i>	-8.22	<i>fr715</i>	-87.72	<i>fr715</i>	-4.98
19			<i>fr715</i>	-8.20	<i>fr2231</i>	-78.02	<i>fr531</i>	-4.11
20					<i>fr531</i>	-77.55		
21								
22								
23								
24								

Table E.5. Binding results of antagonist molecule alprenolol. Bold characters representing the active states of the receptor, italic characters representing the MD frames.

Rank	ChemPLP		AutoDock		DSX/PDB		Glide	
1	3NYA	75.06	2RH1	-8.77	3D4S	-119.2	<i>fr715</i>	-9.28
2	3NY9	71.62	3D4S	-8.76	<b>4LDL</b>	-116.7	2RH1	-8.79
3	3D4S	67.85	<b>4LDO</b>	-8.61	3NY8	-114.4	<b>3P0G</b>	-8.69
4	<i>fr1648</i>	67.14	3NYA	-8.59	2RH1	-112.3	<b>3SN6</b>	-8.50
5	3NY8	64.70	3NY9	-8.42	3NYA	-107.0	3D4S	-8.24
6	2RH1	61.42	<b>4LDL</b>	-8.26	<b>4LDO</b>	-106.7	<b>4LDE</b>	-8.04
7	<i>fr531</i>	61.19	3NY8	-8.16	<b>3P0G</b>	-104.7	3NY9	-7.86
8	<i>fr210</i>	58.95	<i>fr210</i>	-7.92	<b>4LDE</b>	-104.5	3NYA	-7.78
9	<i>fr585</i>	58.19	<b>3P0G</b>	-7.72	3NY9	-104.3	<b>4LDO</b>	-7.49
10			<i>fr585</i>	-7.61	<i>fr1648</i>	-98.91	3NY8	-7.29
11			<b>4LDE</b>	-7.55	<i>fr210</i>	-94.13	<i>fr1648</i>	-7.26
12			<b>3SN6</b>	-7.52	<b>4QKX</b>	-93.21	<b>4LDL</b>	-7.23
13			<i>fr1648</i>	-7.42	<i>fr585</i>	-91.82	<b>4QKX</b>	-7.13
14			<b>4QKX</b>	-7.39	<i>fr9</i>	-89.81	<i>fr1365</i>	-6.67
15			<i>fr715</i>	-7.09	<i>fr1365</i>	-89.81	<i>fr585</i>	-6.57
16			<i>fr9</i>	-7.03-	<i>fr844</i>	-87.67	<i>fr9</i>	-6.34
17			<i>fr531</i>	-6.98	<i>fr2231</i>	-86.74	<i>fr531</i>	-6.17
18			<i>fr844</i>	-6.77	<i>fr531</i>	-84.89	<i>fr210</i>	-5.77
19					<i>fr2311</i>	-77.30		
20					<b>3SN6</b>	-70.25		
21								
22								
23								
24								



Table E.6. Binding results of inverse agonist molecule timolol. Bold characters representing the active states of the receptor, italic characters representing the MD frames.

Rank	ChemPLP		AutoDock		DSX/PDB		Glide	
1	3D4S	82.47	3NYA	-9.56	3NY9	-130.4	3D4S	-8.97
2	3NY9	79.78	3D4S	-9.49	3D4S	-129.4	3NYA	-8.83
3	<i>fr1648</i>	72.96	3NY9	-9.45	2RH1	-128.1	2RH1	-8.25
4	2RH1	71.56	2RH1	-9.14	3NYA	-123.6	<i>fr531</i>	-8.23
5	<i>fr1365</i>	70.87	<b>4LDL</b>	-9.09	3NY8	-123.3	3NY9	-8.06
6	3NYA	69.82	<b>4LDO</b>	-8.96	<b>4LDL</b>	-117.7	<i>fr715</i>	-7.51
7	3NY8	66.35	<b>4LDE</b>	-8.77	<b>4LDE</b>	-116.2	<i>fr9</i>	-7.03
8	<i>fr844</i>	64.45	<b>3SN6</b>	-8.69	<b>4QKX</b>	-112.9	<i>fr2311</i>	-7.03
9	<i>fr9</i>	63.45	3NY8	-8.69	<b>3P0G</b>	-112.2	<b>4LDE</b>	-6.74
10	<i>fr531</i>	61.80	<i>fr1648</i>	-8.67	<b>4LDO</b>	-111.0	<i>fr2231</i>	-6.57
11	<i>fr1479</i>	61.43	<b>4QKX</b>	-8.22	<i>fr1648</i>	-109.6	<i>fr1479</i>	-6.30
12	<i>fr715</i>	61.40	<i>fr1365</i>	-8.04	<i>fr531</i>	-103.0	<i>fr585</i>	-6.25
13	<i>fr2231</i>	60.05	<b>3P0G</b>	-7.96	<i>fr9</i>	-101.8	<i>fr210</i>	-6.06
14	<i>fr210</i>	59.08	<i>fr844</i>	-7.93	<i>fr715</i>	-101.3		
15	<i>fr2311</i>	53.69	<i>fr531</i>	-7.88	<i>fr1365</i>	-100.3		
16	<i>fr585</i>	51.89	<i>fr2231</i>	-7.34	<i>fr2231</i>	-99.75		
17			<i>fr9</i>	-7.14	<i>fr210</i>	-97.72		
18			<i>fr210</i>	-6.89	<i>fr844</i>	-97.43		
19			<i>fr585</i>	-6.78	<i>fr585</i>	-95.03		
20					<i>fr2370</i>	-92.81		
21					<i>fr1479</i>	-90.88		
22								
23								
24								

Table E.7. Binding results of agonist molecule BI167107. Bold characters representing the active states of the receptor, italic characters representing the MD frames.

Rank	ChemPLP		AutoDock		DSX/PDB		Glide	
1	<b>4LDE</b>	100.76	<b>4LDE</b>	-12.95	<b>4LDE</b>	-147.2	<b>4LDE</b>	-15.71
2	<b>3P0G</b>	98.17	<b>4LDL</b>	-12.70	3NY9	-139.7	<b>4LDO</b>	-13.36
3	<b>4LDL</b>	96.84	<b>3SN6</b>	-11.80	<b>3SN6</b>	-138.7	<b>3P0G</b>	-13.05
4	<b>3SN6</b>	96.39	<b>4QKX</b>	-11.75	3NYA	-138.5	<b>3SN6</b>	-12.40
5	3NYA	90.13	<b>4LDO</b>	-11.55	<b>4LDL</b>	-134.5	<b>4QKX</b>	-11.62
6	3D4S	90.04	3NYA	-10.98	<b>4QKX</b>	-128.5	<b>4LDL</b>	-11.37
7	3NY9	89.88	3D4S	-10.91	3D4S	-127.6	3NYA	-10.76
8	<b>4QKX</b>	89.25	3NY9	-10.75	<b>4LDO</b>	-126.3	3NY8	-10.66
9	<b>4LDO</b>	86.74	2RH1	-10.54	2RH1	-124.9	3NY9	-10.33
10	2RH1	85.84	<b>3P0G</b>	-10.47	<b>3P0G</b>	-124.2	3D4S	-10.03
11	<i>fr844</i>	85.51	<i>fr1648</i>	-10.21	3NY8	-121.4	<i>fr844</i>	-9.85
12	3NY8	85.07	<i>fr1365</i>	-10.11	<i>fr1365</i>	-115.7	<i>fr2311</i>	-8.96
13	<i>fr1365</i>	72.75	<i>fr210</i>	-10.02	<i>fr1648</i>	-114.3	<i>fr1365</i>	-8.66
14	<i>fr1479</i>	72.22	3NY8	-9.95	<i>fr715</i>	-107.9	<i>fr1479</i>	-8.60
15	<i>fr1648</i>	68.32	<i>fr715</i>	-9.55	<i>fr844</i>	-107.9	<i>fr2661</i>	-8.45
16	<i>fr2311</i>	65.32	<i>fr531</i>	-9.53	<i>fr210</i>	-93.68	<i>fr1648</i>	-8.39
17	<i>fr210</i>	61.26	<i>fr9</i>	-9.42	<i>fr2311</i>	-92.62	<i>fr2231</i>	-7.09
18	<i>fr585</i>	61.20	<i>fr844</i>	-9.13	<i>fr531</i>	-91.83	<i>fr9</i>	-6.59
19	<i>fr715</i>	52.46	<i>fr2311</i>	-8.46	<i>fr2661</i>	-75.74		
20	<i>fr531</i>	42.34	<i>fr585</i>	-6.60	<i>fr585</i>	-69.50		
21								
22								
23								
24								

Table E.8. Binding results of agonist molecule hydroxybenzylisoproterenol. Bold characters representing the active states of the receptor, italic characters representing the MD frames.

Rank	ChemPLP		AutoDock		DSX/PDB		Glide	
1	<b>3SN6</b>	95.89	<b>4LDL</b>	-11.03	<b>4LDO</b>	-124.3	<b>3P0G</b>	-14.41
2	<b>4LDO</b>	94.80	<b>3P0G</b>	-11.00	<b>4LDL</b>	-123.7	<b>4QKX</b>	-13.81
3	<b>4LDL</b>	93.94	<b>4LDO</b>	-10.95	<b>4QKX</b>	-122.1	<b>4LDL</b>	-13.53
4	<b>3P0G</b>	92.90	<b>3SN6</b>	-10.75	<b>3P0G</b>	-118.8	<b>4LDO</b>	-13.05
5	<b>4QKX</b>	92.08	<b>4QKX</b>	-10.56	<b>4LDE</b>	-117.7	<b>4LDE</b>	-12.94
6	<b>4LDE</b>	88.93	<b>4LDE</b>	-10.28	3NY9	-116.8	<b>3SN6</b>	-12.41
7	3D4S	83.84	3NYA	-10.11	<b>3SN6</b>	-116.4	3NY9	-11.35
8	3NY9	82.86	3NY9	-9.81	3NYA	-115.2	3NYA	-10.99
9	3NY8	75.63	<i>fr1365</i>	-9.76	3NY8	-114.5	3D4S	-10.96
10	<i>fr1365</i>	74.06	3D4S	-9.37	2RH1	-112.7	<i>fr715</i>	-10.52
11	<i>fr844</i>	73.67	<i>fr210</i>	-9.36	<i>fr1648</i>	-110.0	2RH1	-10.40
12	<i>fr9</i>	70.82	<i>fr1648</i>	-9.19	<i>fr210</i>	-103.9	3NY8	-10.35
13	<i>fr2370</i>	69.23	<i>fr715</i>	-9.15	<i>fr531</i>	-102.5	<i>fr2311</i>	-9.41
14	<i>fr1648</i>	68.27	<i>fr531</i>	-8.76	<i>fr1365</i>	-95.11	<i>fr844</i>	-9.40
15	<i>fr715</i>	65.54	3NY8	-8.71	<i>fr715</i>	-91.13	<i>fr1365</i>	-9.38
16	<i>fr2661</i>	63.26	<i>fr2231</i>	-8.21	<i>fr9</i>	-88.87	<i>fr1648</i>	-8.67
17	<i>fr585</i>	62.42	<i>fr9</i>	-7.97	<i>fr2231</i>	-84.98	<i>fr2370</i>	-8.41
18	<i>fr210</i>	60.28	<i>fr844</i>	-7.95	<i>fr2661</i>	-79.70	<i>fr585</i>	-7.91
19	<i>fr531</i>	49.68	<i>fr585</i>	-7.09	<i>fr844</i>	-77.46	<i>fr9</i>	-7.74
20			<i>fr2311</i>	-6.96	<i>fr585</i>	-72.00	<i>fr531</i>	-7.34
21								
22								
23								
24								

Table E.9. Binding results of antagonist molecule nebivolol. Bold characters representing the active states of the receptor, italic characters representing the MD frames.

Rank	ChemPLP		AutoDock		DSX/PDB		Glide	
1	3D4S	97.18	3NY9	-10.57	2RH1	-148.4	2RH1	-12.95
2	<b>4LDL</b>	94.89	<b>3SN6</b>	-10.53	3NY9	-144.6	3D4S	-12.32
3	2RH1	93.93	3NYA	-10.50	3NYA	-139.1	3NY8	-12.20
4	3NY9	91.40	3D4S	-10.29	3D4S	-136.1	3NY9	-12.13
5	<i>fr1648</i>	91.19	<b>3P0G</b>	-10.19	<b>3P0G</b>	-136.0	<b>4LDL</b>	-12.00
6	3NYA	90.67	<b>4LDE</b>	-10.00	3NY8	-135.1	<i>fr2311</i>	-11.80
7	<b>4LDO</b>	89.34	2RH1	-9.96	<b>4LDE</b>	-133.9	3NYA	-11.66
8	3NY8	88.40	3NY8	-9.74	<i>fr844</i>	-130.6	<b>4QKX</b>	-10.90
9	<b>4LDE</b>	87.97	<i>fr210</i>	-9.72	<i>fr715</i>	-125.1	<i>fr844</i>	-10.85
10	<i>fr844</i>	87.70	<b>4LDO</b>	-9.66	<i>fr2370</i>	-124.4	<b>4LDE</b>	-10.77
11	<b>4QKX</b>	85.01	<i>fr9</i>	-9.61	<b>3SN6</b>	-123.1	<i>fr1365</i>	-10.56
12	<i>fr2311</i>	82.78	<b>4QKX</b>	-9.60	<i>fr531</i>	-121.8	<b>3SN6</b>	-10.44
13	<i>fr2231</i>	79.26	<i>fr844</i>	-9.37	<i>fr9</i>	-119.8	<i>fr1648</i>	-10.30
14	<i>fr1479</i>	77.26	<b>4LDL</b>	-9.16	<b>4LDL</b>	-119.7	<i>fr2370</i>	-10.28
15	<b>3SN6</b>	75.59	<i>fr2370</i>	-9.03	<b>4QKX</b>	-118.6	<b>4LDO</b>	-10.18
16	<i>fr210</i>	75.05	<i>fr715</i>	-8.87	<b>4LDO</b>	-117.3	<i>fr1479</i>	-10.00
17	<b>3P0G</b>	72.10	<i>fr1648</i>	-8.84	<i>fr1648</i>	-117.2	<b>3P0G</b>	-9.97
18	<i>fr715</i>	65.97	<i>fr2231</i>	-8.82	<i>fr585</i>	-106.0	<i>fr2661</i>	-9.94
19	<i>fr585</i>	53.95	<i>fr531</i>	-8.76	<i>fr210</i>	-101.1	<i>fr2231</i>	-9.88
20	<i>fr531</i>	40.78	<i>fr585</i>	-8.05			<i>fr210</i>	-9.45
21							<i>fr531</i>	-7.50
22							<i>fr585</i>	-3.61
23								
24								

Table E.10. Binding results of inverse agonist molecule carazolol. Bold characters representing the active states of the receptor, italic characters representing the MD frames.

Rank	ChemPLP		AutoDock		DSX/PDB		Glide	
1	2RH1	93.67	3D4S	-11.05	3D4S	-141.8	2RH1	-12.41
2	3D4S	92.89	2RH1	-11.00	2RH1	-137.7	3D4S	-10.82
3	3NY9	85.27	3NY9	-10.57	3NY9	-134.4	3NYA	-10.65
4	3NYA	84.10	3NYA	-10.41	3NYA	-132.2	3NY9	-10.16
5	<i>fr1365</i>	78.77	3NY8	-10.15	3NY8	-131.6	<i>fr715</i>	-10.05
6	3NY8	77.30	<i>fr1365</i>	-9.49	<i>fr1648</i>	-121.3	<i>fr1648</i>	-10.03
7	<i>fr715</i>	72.98	<i>fr1648</i>	-9.46	<b>3SN6</b>	-113.6	3NY8	-9.93
8	<i>fr1648</i>	72.92	<i>fr715</i>	-9.37	<i>fr715</i>	-112.8	<i>fr531</i>	-8.72
9	<b>4LDL</b>	71.96	<b>3SN6</b>	-9.19	<i>fr9</i>	-111.6	<i>fr1365</i>	-8.40
10	<i>fr9</i>	70.18	<b>3P0G</b>	-9.12	<b>4LDE</b>	-110.1	<i>fr2231</i>	-8.32
11	<i>fr844</i>	70.10	<i>fr531</i>	-9.03	<i>fr210</i>	-109.7	<i>fr9</i>	-8.16
12	<b>3SN6</b>	69.29	<i>fr2231</i>	-9.02	<b>4LDL</b>	-108.8	<i>fr585</i>	-8.01
13	<b>4LDE</b>	69.14	<b>4LDO</b>	-8.96	<b>4QKX</b>	-108.7	<i>fr210</i>	-4.68
14	<i>fr2311</i>	61.63	<b>4LDE</b>	-8.86	<b>3P0G</b>	-105.2		
15	<i>fr210</i>	59.49	<i>fr844</i>	-8.54	<i>fr531</i>	-104.8		
16	<i>fr585</i>	57.79	<i>fr9</i>	-8.39	<i>fr1365</i>	-102.6		
17	<i>fr531</i>	57.35	<i>fr585</i>	-8.13	<b>4LDO</b>	-101.1		
18			<i>fr2311</i>	-7.93	<i>fr2311</i>	-99.46		
19			<i>fr210</i>	-7.80	<i>fr844</i>	-94.67		
20					<i>fr585</i>	-93.45		
21					<i>fr2661</i>	-90.56		
22								
23								
24								

Table E.11. Binding results of agonist molecule salbutamol. Bold characters representing the active states of the receptor, italic characters representing the MD frames.

Rank	ChemPLP		AutoDock		DSX/PDB		Glide	
1	<b>4LDL</b>	69.17	<b>3SN6</b>	-8.33	<b>3SN6</b>	-106.0	<b>4QKX</b>	-10.91
2	<b>3SN6</b>	68.56	<b>4QKX</b>	-8.07	<b>4LDL</b>	-104.5	<b>3P0G</b>	-9.46
3	<b>4LDE</b>	68.22	<b>3P0G</b>	-8.02	<b>4QKX</b>	-99.08	<b>3SN6</b>	-9.45
4	<b>4LDO</b>	66.34	<b>4LDE</b>	-7.82	<b>4LDE</b>	-98.97	3NY9	-9.18
5	<b>3P0G</b>	65.56	<b>4LDO</b>	-7.82	<b>3P0G</b>	-97.41	<b>4LDE</b>	-9.17
6	3D4S	64.64	<b>4LDL</b>	-7.42	<b>4LDO</b>	-96.38	<b>4LDO</b>	-8.76
7	<b>4QKX</b>	64.62	<i>fr210</i>	-7.34	2RH1	-90.76	<b>4LDL</b>	-8.51
8	<i>fr1479</i>	64.42	<i>fr531</i>	-7.10	3D4S	-89.63	2RH1	-7.22
9	2RH1	63.95	2RH1	-7.01	<i>fr9</i>	-88.67	3NY8	-7.15
10	3NYA	63.70	3D4S	-6.97	3NYA	-87.97	<i>fr210</i>	-7.11
11	3NY9	63.64	<i>fr585</i>	-6.96	3NY8	-85.48	<i>fr715</i>	-7.03
12	3NY8	61.46	<i>fr1648</i>	-6.76	<i>fr715</i>	-85.14	<i>fr2311</i>	-7.03
13	<i>fr531</i>	60.59	3NY9	-6.72	3NY9	-84.43	<i>fr1365</i>	-6.90
14	<i>fr1365</i>	60.15	3NYA	-6.59	<i>fr1648</i>	-83.71	<i>fr844</i>	-6.81
15	<i>fr1648</i>	58.40	<i>fr2231</i>	-6.59	<i>fr1365</i>	-83.44	<i>fr9</i>	-6.79
16	<i>fr210</i>	58.29	<i>fr9</i>	-6.02	<i>fr210</i>	-80.65	3NYA	-6.78
17	<i>fr715</i>	57.88			<i>fr531</i>	-78.52	3D4S	-6.69
18	<i>fr585</i>	55.58			<i>fr585</i>	-77.58	<i>fr1479</i>	-6.61
19	<i>fr9</i>	54.72			<i>fr2231</i>	-77.15	<i>fr531</i>	-6.34
20							<i>fr585</i>	-5.85
21								
22								
23								
24								

Table E.12. Binding results of antagonist molecule carvedilol. Bold characters representing the active states of the receptor, italic characters representing the MD frames.

Rank	ChemPLP		AutoDock		DSX/PDB		Glide	
1	<b>4LDL</b>	109.16	2RH1	-12.48	3D4S	-174.1	3NY9	-12.68
2	3D4S	105.43	3D4S	-12.39	<b>4LDO</b>	-171.7	3D4S	-12.51
3	<b>4LDO</b>	105.41	3NY9	-12.16	<b>4LDL</b>	-171.3	3NYA	-11.79
4	2RH1	100.07	3NYA	-12.00	3NY9	-170.1	2RH1	-11.77
5	3NY9	99.05	3NY8	-11.32	3NYA	-170.0	<b>4QKX</b>	-11.45
6	3NYA	98.40	<b>4LDL</b>	-11.08	2RH1	-168.0	3NY8	-11.40
7	3NY8	89.56	<b>4LDO</b>	-11.02	<b>4LDE</b>	-167.1	<b>4LDO</b>	-11.33
8	<b>3SN6</b>	88.61	<i>fr1648</i>	-11.01	3NY8	-157.4	<i>fr2661</i>	-10.93
9	<i>fr1365</i>	86.88	<b>3SN6</b>	-10.73	<b>3SN6</b>	-157.4	<b>4LDE</b>	-10.75
10	<b>4LDE</b>	86.48	<i>fr844</i>	-10.71	<i>fr1648</i>	-145.4	<i>fr844</i>	-10.59
11	<i>fr1648</i>	85.75	<i>fr1365</i>	-10.70	<b>3P0G</b>	-143.4	<b>3SN6</b>	-10.48
12	<i>fr2231</i>	85.65	<i>fr2231</i>	-10.68	<i>fr9</i>	-139.1	<i>fr9</i>	-10.05
13	<i>fr844</i>	85.55	<i>fr9</i>	-10.65	<i>fr844</i>	-134.3	<i>fr1365</i>	-9.70
14	<i>fr9</i>	84.38	<b>4LDE</b>	-10.50	<i>fr210</i>	-133.3	<i>fr2311</i>	-9.09
15	<i>fr2311</i>	84.13	<b>3P0G</b>	-10.31	<i>fr2231</i>	-133.3	<b>3P0G</b>	-8.33
16	<b>3P0G</b>	82.11	<i>fr2311</i>	-9.79	<i>fr1365</i>	-126.9	<i>fr2231</i>	-7.88
17	<i>fr715</i>	74.91	<i>fr210</i>	-9.71	<i>fr715</i>	-112.2	<i>fr531</i>	-7.00
18	<i>fr2661</i>	73.03	<i>fr531</i>	-9.50	<i>fr531</i>	-102.7		
19	<i>fr210</i>	59.62	<i>fr715</i>	-9.36	<i>fr585</i>	-77.95		
20	<i>fr531</i>	54.13	<i>fr585</i>	-6.19				
21	<i>fr585</i>	40.01						
22								
23								
24								

Table E.13. Binding results of agonist molecule epinephrine. Bold characters representing the active states of the receptor, italic characters representing the MD frames.

Rank	ChemPLP		AutoDock		DSX/PDB		Glide	
1	<b>4LDO</b>	64.97	<b>4LDO</b>	-8.09	<b>4QKX</b>	-86.73	<b>4LDO</b>	-11.19
2	<b>3SN6</b>	63.75	<b>4LDE</b>	-7.96	<b>4LDO</b>	-86.10	<b>4LDE</b>	-10.56
3	<b>4QKX</b>	62.44	<b>4LDL</b>	-7.70	<b>4LDL</b>	-85.56	<b>3SN6</b>	-9.95
4	<b>3P0G</b>	60.36	<b>3P0G</b>	-7.53	<b>3P0G</b>	-80.83	<b>4QKX</b>	-9.27
5	<b>4LDL</b>	59.72	<b>4QKX</b>	-7.49	<b>4LDE</b>	-80.49	<b>3P0G</b>	-9.08
6	<b>4LDE</b>	57.89	<i>fr210</i>	-6.88	2RH1	-76.06	<b>4LDL</b>	-9.07
7	3NY8	55.41	<i>fr1648</i>	-6.76	3NYA	-75.57	<i>fr531</i>	-8.87
8	<i>fr210</i>	53.75	2RH1	-6.67	3D4S	-74.07	3NY8	-8.52
9	<i>fr585</i>	52.33	<i>fr531</i>	-6.50	<b>3SN6</b>	-71.29	<i>fr715</i>	-7.92
10	3D4S	51.88	<b>3SN6</b>	-6.45	3NY9	-68.94	<i>fr1365</i>	-7.47
11	3NY9	51.67	3NY9	-6.33	3NY8	-68.62	<i>fr210</i>	-7.45
12	<i>fr1365</i>	49.97	<i>fr2231</i>	-6.32	<i>fr715</i>	-64.34	3D4S	-7.45
q	<i>fr2661</i>	49.91	<i>fr585</i>	-6.26	<i>fr2231</i>	-62.11	3NYA	-7.44
14	<i>fr1648</i>	49.56	<i>fr715</i>	-6.26	<i>fr531</i>	-58.98	3NY9	-7.41
15	3NYA	49.47	3NY8	-6.04	<i>fr585</i>	-53.17	2RH1	-7.37
16	<i>fr531</i>	49.10	<i>fr2661</i>	-5.93	<i>fr1365</i>	-50.13	<i>fr1648</i>	-7.23
17			<i>fr2370</i>	-5.64	<i>fr2661</i>	-47.89	<i>fr585</i>	-6.90
18							<i>fr2231</i>	-6.51
19								
20								
21								
22								
23								
24								



## APPENDIX F

### ROC Curves of MD Frames

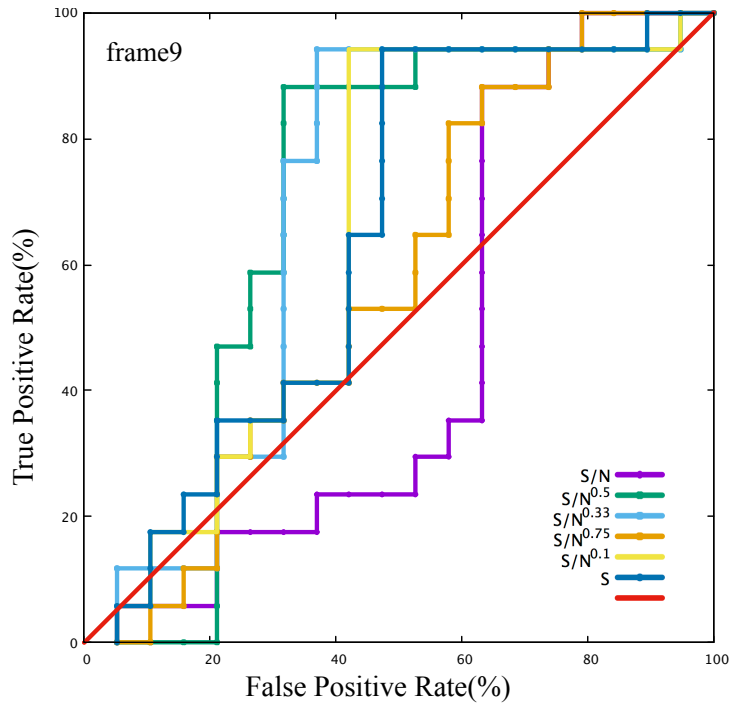


Figure F.1. ROC curves of frame9. AUC values are  $S=0.64$ ,  $S/N^{0.1}=0.64$ ,  $S/N^{0.75}=0.57$ ,  $S/N^{0.33}=0.68$ ,  $S/N^{0.5}=0.69$ ,  $S/N=0.46$ .

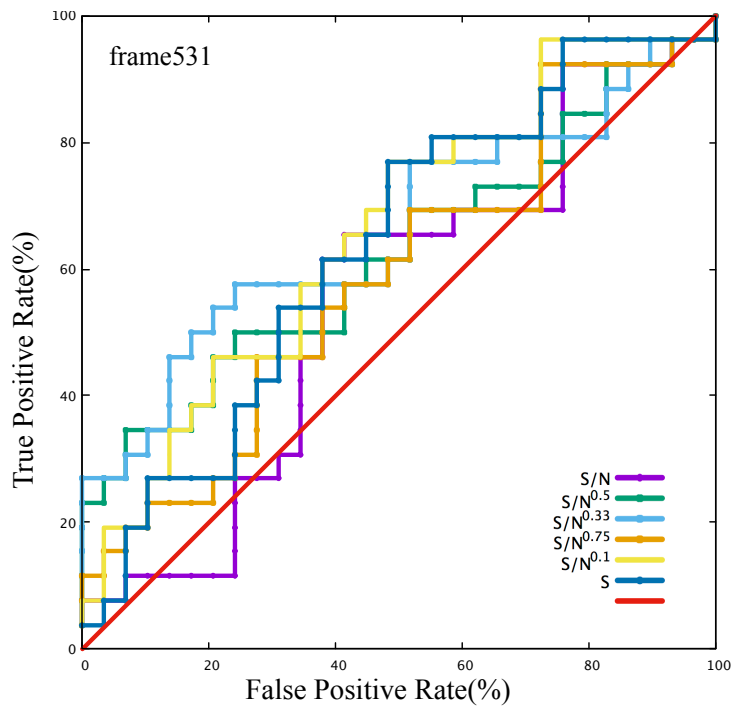


Figure F.2. ROC curves of frame531. AUC values are  $S=0.63$ ,  $S/N^{0.1}=0.65$ ,  $S/N^{0.75}=0.58$ ,  $S/N^{0.33}=0.66$ ,  $S/N^{0.5}=0.62$ ,  $S/N=0.54$ .

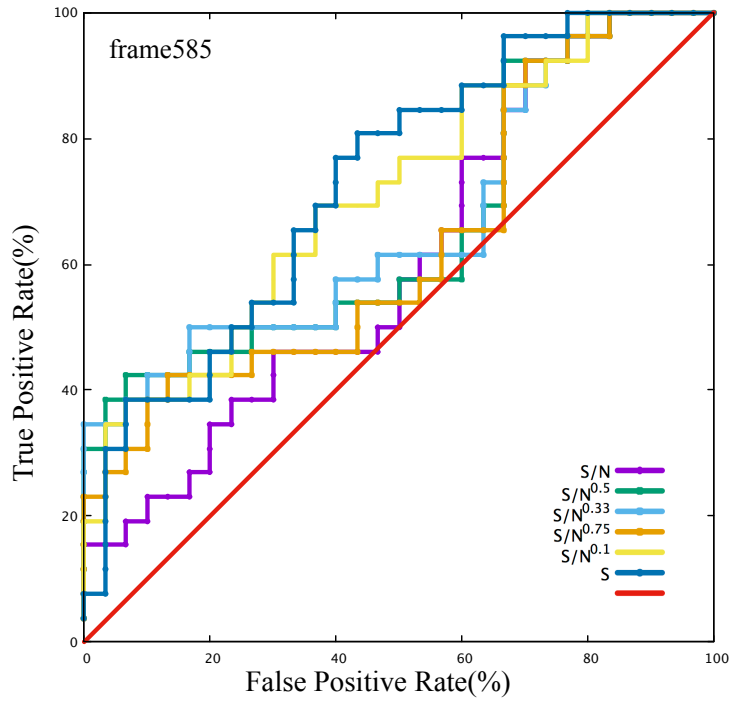


Figure F.3. ROC curves of frame585. AUC values are  $S=0.72$ ,  $S/N^{0.1}=0.71$ ,  $S/N^{0.75}=0.63$ ,  $S/N^{0.33}=0.66$ ,  $S/N^{0.5}=0.65$ ,  $S/N=0.60$ .

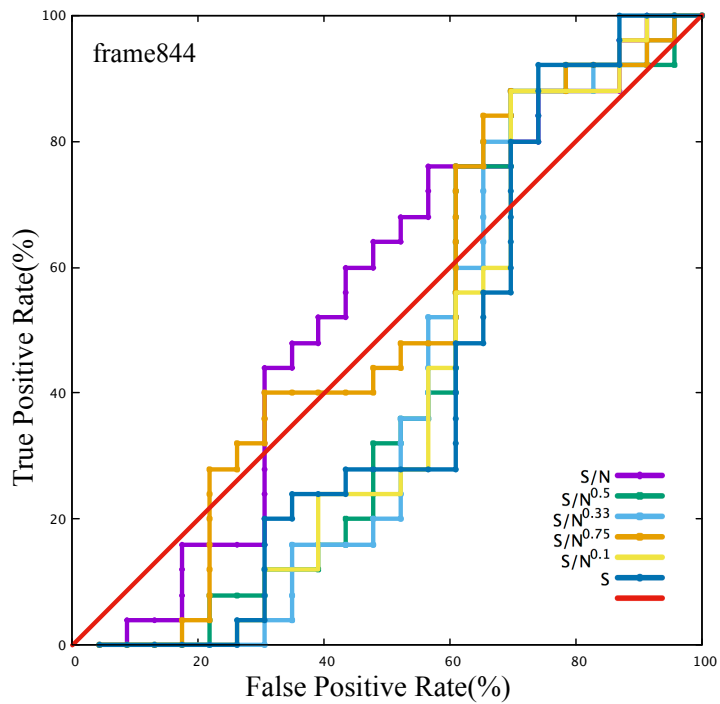


Figure F.4. ROC curves of frame844. AUC values are  $S=0.41$ ,  $S/N^{0.1}=0.40$ ,  $S/N^{0.75}=0.50$ ,  $S/N^{0.33}=0.41$ ,  $S/N^{0.5}=0.42$ ,  $S/N=0.54$ .